SIMPLIFIED DYNAMIC BOUNDARY CONDITIONS FOR NUMERICAL MODELS OF BOREHOLE HEAT EXCHANGERS

SIMPLIFIED DYNAMIC BOUNDARY CONDITIONS FOR NUMERICAL MODELS OF BOREHOLE HEAT EXCHANGERS

By ANDREW HOLMES, B.ENG.

A Thesis Submitted to the School of Graduate Studies in Partial Fulfilment of the Requirements for the Degree Master of Applied Science

Master of Applied Science (2022) McMaster University

(Mechanical Engineering) Hamilton, Ontario, Canada

TITLE: Simplified Dynamic Boundary Conditions for Numerical Models of Borehole Heat Exchangers

AUTHOR: Andrew Holmes

B.Eng. (Mechanical Engineering)

McMaster University, Hamilton, Ontario, Canada

SUPERVISOR: Dr. Marilyn Lightstone

NUMBER OF PAGES: xvii, 199

Abstract

This work describes the development and validation of a computational model for vertical borehole heat exchangers in residential ground-source heat pump energy systems. Due to the size and shape of vertical borehole heat exchangers, their operation thermally impacts a large volume of surrounding soil and thus discretized models have largely been confined to short-term transient simulations, such as the case of a thermal response test. The proposed model employs a computationally efficient physics-based models at variable spatial dimensions which can be used for long-time simulation of the ground heat transfer.

The model can generally be considered as a composition of three separate domains: the borehole domain, which combines one-dimensional, three-dimensional and equations-based physics, the near-field soil domain, which resolves three-dimensional transient heat conduction and the far-field soil domain which is modelled as one-dimensional axisymmetric transient heat conduction. The main purpose of this work is to present each component of the model and validate their behaviours and assumptions through a combination of comparison to experimental data, highly cited published works, and well-known analytical models. The complete composite model ignores the three-dimensional effects of fluid heat transfer, and the axial heat transfer in the far-field in order to reduce the computational effort, and the level of uncertainty introduced by each simplification is explored.

Finally, to support the composite model, a new method determining the thermal impact of the borehole operation mentioned previously was devised and presented alongside the model development and validations. This method, based on the previously defined thermal impacting radius, improves the consistency and theoretical foundation of the value's definition based on a system energy balance, rather than local temperature conditions.

Acknowledgements

I would first like to thank Dr. Marilyn Lightstone for her supervision, guidance and support throughout this research. Without her this work would not have been possible. I have been incredibly fortunate to learn and grow under her supervision.

I would like to thank Dr. Chan Ching, who first provided me the opportunity to do research, and without whose passion and encouragement I would not have pursued graduate studies. Also, to John Colenbrander, whose friendship and mentorship was invaluable during my time at McMaster.

To my colleagues, who have now become friends, thank you. To Chantel Millar, thank you for the constant help, collaboration and problem-solving that occurred over years of socially-distanced video calls. Thank you, and good luck as you continue on your own academic journey. Daniel Deacon and Mohammad Zamanian, I'm immensely appreciative of the discussion and generosity that you both offered during my years of study. Good luck to both of you as you move forward in your careers.

Finally, to my family; my parents, siblings and new siblings; I could not have made it through without your unyielding love and support. Throughout the term of this research, which coincided with the COVID-19 pandemic, I was always able to turn to you for support and stress-relief. Thank you.

Notations and Abbreviations

Nomenclature

$\boldsymbol{A}$	Area [m^2]
$\boldsymbol{C}$	Thermal Capacitance [J/K]
$\boldsymbol{C_A}$	Churchill Coefficient A [-]
$\boldsymbol{C_B}$	Churchill Coefficient B [-]
$\boldsymbol{C_P}$	Specific Heat Capacity [J/kg·K]
$\boldsymbol{d}$	Diameter [m]
$\boldsymbol{e}$	Surface Roughness [m]
$\boldsymbol{E}$	Energy [J]
$\boldsymbol{f}$	Fraction [-]
$\boldsymbol{f_D}$	Darcy Friction Factor [-]
$\boldsymbol{h}$	Heat Transfer Coefficient [W/m^2·K]
$\boldsymbol{h'}$	Integrating Variable [m]
$\boldsymbol{H}$	Overall Depth of Borehole [m]
$\boldsymbol{H'}$	Non-dimensionalized Integrating Variable [-]
$\boldsymbol{hZ}$	Heat Transfer Coefficient per Unit Length [W/m·K]
$\boldsymbol{k}$	Thermal Conductivity [W/m·K]
$\boldsymbol{L}$	Length [m]
$\boldsymbol{M}$	Mass [kg]
$\boldsymbol{\dot{m}}$	Mass Flow Rate [kg/s]
$\boldsymbol{P}$	Heat Rate in CaRM Models [W]
$\boldsymbol{P_o}$	Perimeter [m]
$\boldsymbol{Q}$	Heat Flow per unit Time [W]
$\boldsymbol{q_l}$	Heat Flow per Unit Length [W/m]
$\boldsymbol{q''}$	Heat Flux [W/m^2]
$\boldsymbol{r}$	Radius [m]
$\boldsymbol{r}$	Radial Coordinate (In Cylindrical Systems) [m]
$\boldsymbol{R}$	Non-dimensionalized Radial Coordinate [-]
$\boldsymbol{R}$	Thermal Resistance [K/W]
$\boldsymbol{t}$	Time [s]
$\boldsymbol{T}$	Temperature [K or °C]
$\boldsymbol{u}$	Fluid Velocity [m/s]
$\boldsymbol{V}$	Volume [m^3]
$\boldsymbol{x}$	X-Coordinate (In Cartesian Systems) [m]
$\boldsymbol{y}$	Y-Coordinate (In Cartesian Systems) [m]
$\boldsymbol{z}$	Axial Coordinate (In Cartesian and Cylindrical Systems) [m]
$\boldsymbol{Z}$	Non-dimensionalized Axial Coordinate [-]

Greek Symbols

$\boldsymbol{\alpha}$	Thermal Diffusivity [m^2/s]
$\boldsymbol{\mu}$	Dynamic Viscosity [kg/m·s]
$\boldsymbol{\varphi}$	Non-dimensionalized Temperature Excess [-]
$\boldsymbol{\rho}$	Density [kg/m^3]
$\boldsymbol{\sigma}$	Non-dimensionalized Radial Heat Flow Variable [-]
$\boldsymbol{\tau}$	House Load Time Constant [s]
$\boldsymbol{\theta}$	Angular Coordinate (In Cylindrical Systems) [rad]
$\boldsymbol{\vartheta}$	Temperature Excess [K or °C]

Dimensionless Numbers

$\boldsymbol{Fo}$	Fourier Number
$\boldsymbol{Nu}$	Nusselt Number
$\boldsymbol{Pe_D}$	Péclet Number
$\boldsymbol{Pr}$	Prandtl Number
$\boldsymbol{Re}$	Reynolds Number

Subscript

$\boldsymbol{AHE}$	Accumulated Heat Extracted
$\boldsymbol{AHR}$	Accumulated Heat Rejected
$\boldsymbol{amb}$	Ambient
$\boldsymbol{ave}$	Average
$\boldsymbol{b}$	Borehole
$\boldsymbol{b}$	Bulk, as in Temperature
$\boldsymbol{C}$	Cooling, as in Mode for Heat Pump
$\boldsymbol{diff}$	Difference
$\boldsymbol{exp}$	Experimental Data
$\boldsymbol{ext}$	External
$\boldsymbol{f}$	Fluid
$\boldsymbol{g, load}$	Ground Load
$\boldsymbol{h}$	Hydraulic
$\boldsymbol{H}$	High, as in Upper Limit
$\boldsymbol{H}$	Heating, as in Mode for Heat Pump
$\boldsymbol{h, load}$	House Load
$\boldsymbol{i}$	Inner
$\boldsymbol{in}$	Inlet
$\boldsymbol{int}$	Internal
$\boldsymbol{L}$	Low, as in Lower Limit

$\boldsymbol{lam}$	Laminar
$\boldsymbol{max}$	Maximum
$\boldsymbol{min}$	Minimum
$\boldsymbol{model}$	Numerical Model
$\boldsymbol{o}$	Outer
$\boldsymbol{p}$	Pressure
$\boldsymbol{pipe}$	U-tube Pipe
$\boldsymbol{rad}$	Radial
$\boldsymbol{rtn}$	Return
$\boldsymbol{s}$	Soil
$\boldsymbol{sup}$	Supply
$\boldsymbol{turb}$	Turbulent
$\boldsymbol{t_i}$	Current Timestep
$\boldsymbol{t_{i+1}}$	Next Timestep
$\boldsymbol{und}$	Undisturbed, or Initial
$\boldsymbol{w}$	Wall, as in Pipe Properties
$\boldsymbol{wall}$	Heat Transfer through Outer Wall

Abbreviations

BHE	Borehole Heat Exchanger
CaRM	Capacitance Resistance Model
COP	Coefficient of Performance
EWT	Entering Water Temperature
FEM	Finite Element Model
FLSM	Finite Line Source Model
FVM	Finite Volume Model
GHG	Greenhouse Gas
GSHP	Ground-Source Heat Pump
ICSSM	Infinite Cylindrical-Surface Source Model
ILSM	Infinite Line Source Model
IR	Thermal Imbalance Ratio
PCM	Phase Change Material
TIR	Thermal Impacting Radius
TRCM	Thermal Resistance and Capacity Model
TRT	Thermal Response Test

Contents

List of Tables

List of Figures

Chapter 1 – Introduction and Problem Statement

The emissions from residential and commercial buildings in Canada account for eleven percent of the total greenhouse gas emissions of the country, which includes heating and cooling [1], and are an area that is ripe for decarbonization, due to the unique systems requirements. Unlike fossil-fuel burning vehicles, buildings are stationary and as such energy density is of far less importance to the practicality of sustainable energy alternatives. Additionally, energy loads for heating and cooling are easier to predict than other energy needs, due to the repeatability of weather patterns and as such long-term planning can be more easily made during design.

There is a wealth of thermal energy stored in the Earth's crust that is available for access by geothermal energy systems that, due to its nature, is largely distributed all over the Earth's surface. This thermal energy is replaced by heat flow from the Earth's core to the surface that has been estimated at 44.2 TW [2], and although not all of this energy is recoverable, it currently exceeds all human energy consumption and represents a largely untapped resource. Geoexchange energy systems allow for the use of the stores of energy in the shallow depths of the soil for heating and cooling systems without extensive infrastructure. Figure 1 illustrates the general components of a single geoexchange system, although the geometry should not be considered to scale. By running a circulating fluid through a long borehole, energy can be exchanged, either injected or extracted, with the surrounding soil.

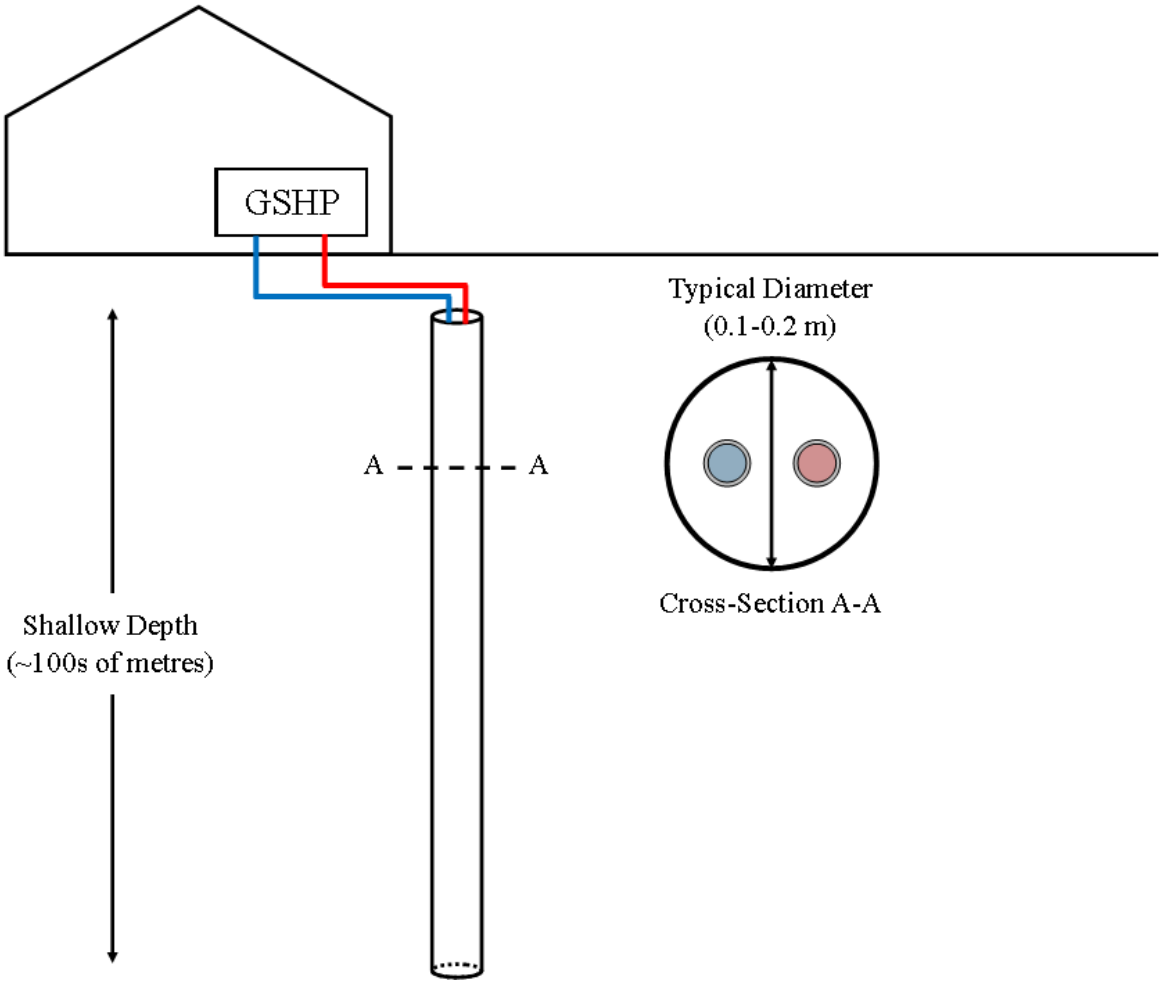

Figure 1: Simple Schematic of Geoexchange Energy System

Computational modelling of borehole heat exchangers is an incredibly varied field; however models are typically able to adhere to one of, but not both of, the following conditions. If the fluid heat transfer and surrounding borehole domain are resolved, the simulation is typically restricted to short time-scales, and if long time-scales are necessary, the borehole behaviour is highly idealized, and often applied as boundary conditions to the soil domain.

This thesis will outline the development and validation of a composite computational model for vertical borehole heat exchangers, which includes portions of lower dimension physics to make the model viable for long time-scale simulation. Additionally, a new method for defining the thermal impact of a borehole operation, in both space and time, is presented, based on an overall system energy balance to improve the method for determining the volume of soil affected by operation.

The following is an overview of the key points of each chapter found within this research. Chapter 2 is a background of the important concepts that inform the following work, including the inspiration for improving and implementing sustainable energy systems and the history of modelling and testing borehole heat exchangers. Chapter 3 is the literature review, which connects the history of modelling to the current topics of research on borehole heat exchanger modelling, particularly in discretized modelling methods. This review has informed the assumptions made in the proposed model. Chapter 4 will focus on developing and validating two of the three sub-components of the mixed-dimension model within the borehole domain, which are the one-dimensional pipe modelling and the surrounding three-dimensional solid modelling; the third sub-component is presented in Appendix A.3. In Chapter 5, the influence of the outer boundary in long time-scale operation is investigated and a new method for determining the thermal impacting radius is proposed. The thermal impacting radius is a function of the operating time of a borehole, and thus for long time-scale simulations, the domain size and assumed boundary condition can influence the results within the domain if not properly scaled. The implementation of the far-field soil simplification is presented in Chapter 6, and the effect of the simplification

is explored by comparing the performance of the composite model to the solutions of two analytical models, the Finite Line Source and Infinite Cylindrical-Surface Source models. Finally, in Chapter 7 the conclusions from the work are presented and recommendations for the use of the composite model and the continued development of the new method for evaluating the thermal impact are made.

Chapter 2 – Research Background

2.1 Climate Change and Decarbonization

Climate change is a global phenomenon that presents a wide range of environmental, socio-political, and economic problems for the current and future populations of the world. A landmark year for the fight against climate change is 2015, when the Paris Agreement [3] was adopted. Greenhouse gas (GHG) emissions will cause an increase in mean global temperature [3], which will dramatically affect the planet and its human, animal and plant populations. The Paris Agreement set the long-term goal of limiting the rise in this mean global temperature to below 2°C above pre-industrial levels, with an ideal target of below 1.5°C [3], which can only be achieved by dramatic reductions in GHG emissions. Despite this ratification in 2015, total GHG emissions continued to rise in the decade between 2010-2019, albeit at a lower rate of growth than the decade previous [4]. As of 2019, the global net anthropogenic GHG emissions were 59 ± 6.6 GtCO2e [4], according to the IPCC and Canada's contributions were equivalent to 1.5% of these emissions [5], despite being about 0.48% of the world population.

As part of the Paris Agreement in 2015, Canada pledged to reduce its greenhouse gas emissions to a level 30 percent below the country's 2005 levels [6] by the year 2030. In 2021, the target was increased to a level of 40-45 percent by 2030 [6], which despite being more ambitious, was still below the 54 percent needed to be compatible with the Paris Agreement. Although these pledges may be seen as moving Canada in the right direction, the current implementation of the necessary policies has largely been insufficient. As of

2019, the country had only achieved a decrease of 1.1 percent [1], and many of the subsequent decreases were a result of the COVID-19 pandemic and cannot be considered permanent decreases. As such, aggressive and targeted policies must be adopted for Canada to do its part in countering climate change.

As mentioned in the introduction, in Canada, residential and commercial emissions, excluding those from electricity, amount to 77.8 Mt of CO2e, or 11 percent of current emissions [1]. These are dominated by space and water heating needs, which are high in Canada due to the dominance of cold weather in the region. There is often an inherent mismatch between the availability of renewable energies, more explicitly solar energy, and the demand for space heating; when solar energy is abundant, the air temperature is typically higher and thus less space heating is needed. This mismatch is not present in most geothermal energy systems, the details of which will be explained further in the next section.

Within the field of possible renewable energy sources, geothermal energy can be seen to have unique attributes that make it attractive when considering the need for secure and consistent energy supply. Since the energy does not rely on external weather conditions, in the same way that wind and solar due, geothermal energy can be better relied on for a constant flow of energy [7], when the systems are designed and sized properly. Rubio et al. [7] carried out a life cycle assessment for the use of geothermal energy in a single-family home in Spain and found incredibly low amortisation periods. The next section will briefly explain and contrast a few of the important concepts within the broad field of geothermal energy.

2.2 Geothermal Energy, Geoexchange and Ground-Source Heat Pumps

Geothermal energy is a broad term that refers to a wide range of technologies that access and interact with the thermal energy in the Earth's crust for human uses. This ranges from the access of high temperature resources, like water or rock raised to high temperatures by depth or high volcanic activity [8], [9], to the exchange and storage of heat in relatively shallow ground, which is found at much lower average temperatures. High temperature resources can be used for both direct heating, which has a relatively high thermal efficiency since no energy conversion is necessary, or more recently geothermal power, which generates electricity using the geothermal energy as the input into a power station in various forms [8]. The locations where high temperature resources are at depths accessible to human's are low, however, and as such it is difficult to scale the existing high-temperature technologies to address decarbonization needs [9]. A more distributed type of geothermal energy system is what is sometimes known as Geoexchange, which can alternatively use more shallow depths of the ground as a heat source, and/or sink, for the exchange of thermal energy. Through a ground heat exchanger and a heat pump, the system circulates a heat carrier fluid for heat transfer into and/or out of the ground. The focus of this thesis will be on closed loop heat exchangers, which continually circulate a fixed mass of fluid and incorporate a heat pump to transfer energy between the building and the ground.

Closed loop ground heat exchangers can largely be categorized into two different configurations: horizontal and vertical (Figure 2). These refer to the orientation of the length of the heat exchanger; a horizontal heat exchanger lies in parallel to the surface of the ground and the vertical heat exchanger lies perpendicular.

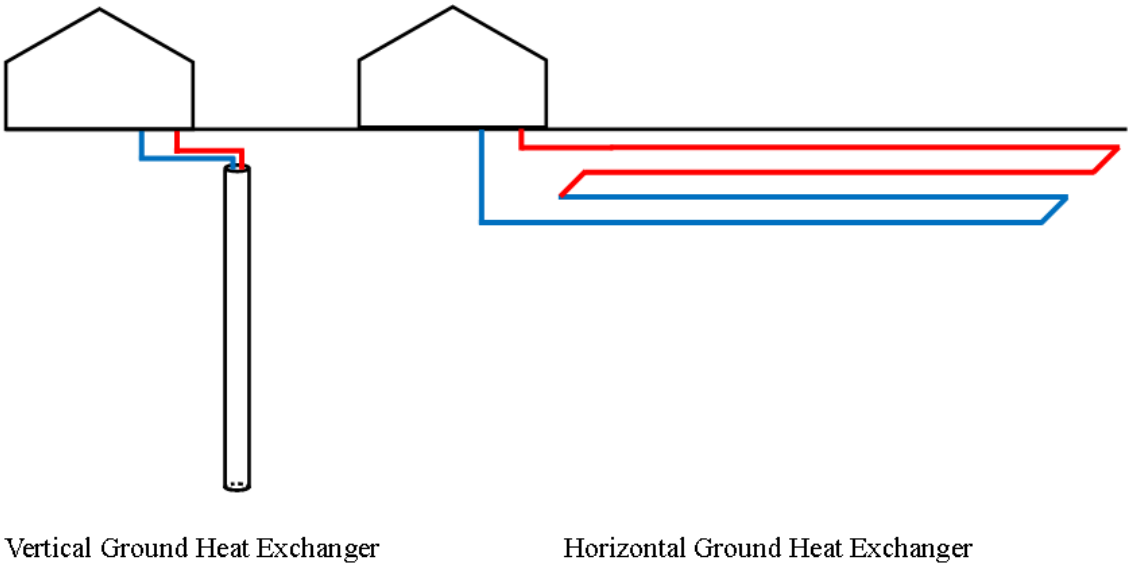

Figure 2: General Orientation of Vertical and Horizontal Closed Loop Ground Heat Exchangers

In horizontal ground heat exchangers, the entire length of the heat exchanger is close to the ground surface, and as such, the ground surface and its interactions with the surrounding air play a much larger role on its performance [10]. This includes, but is not limited to, the seasonal temperature variations of the air, phase changes due to freezing and thawing of the ground near the surface, and the changes in moisture content of the soil surrounding the heat exchanger [10]. Horizontal systems are far less popular than vertical systems and, as such, there is far less literature on the systems when compared to vertical systems ([10], [11]). Claesson and Dunand's fundamental work [11] is often used as a basis of reference for the design of horizontal systems as well as scientific modelling.

This work will focus exclusively on vertical ground source heat exchangers, frequently known as borehole heat exchangers (BHE), for a number of reasons. As previously stated, vertical ground source heat exchangers are much more prevalent than

horizontal ones, which is largely, but not exclusively, due to the fact that borehole heat exchangers are able to access far greater volumes of soil from a relatively small area of disruption to the ground surface [12]. Economically speaking, this means that for a sufficiently large system to be installed, access to large areas of land is not necessary for the installation of high length heat exchangers.

When connected to closed loop systems, Ground Source Heat Pumps (GSHPs) are sometimes referred to as ground-coupled heat pumps. Although they are not the main focus of this work, a general understanding of how heat pumps operate is important for context. Ground source heat pumps use the refrigeration cycle to transfer thermal energy between the borehole heat exchanger and the building, which acts as the load. The efficiency of the heat pump operation is a function of a number of variables (fluid flow rates, entering fluid temperatures, pump power, etc.), with the most important one being the entering fluid temperature at the source (borehole) side [12]. The performance of the heat pump plays a significant role on the overall system energy balance and the conditions in the soil surrounding the borehole heat exchanger. Therefore, any model which assumes there is no variability within the heat pump, only within the borehole heat exchanger itself, is oversimplified and could result in large uncertainties. A simple model for a variable performance heat pump will be proposed and developed in the Appendix of this thesis.

2.3 Thermal Response Tests

Thermal Response Tests (TRTs) are important components of ground source heat pump system design and are used to determine the thermal properties of the borehole and the surrounding soil. Knowledge of the subsurface conditions, including the undisturbed temperature, volumetric heat capacity and thermal conductivity are vital to properly design borehole heat exchangers [13]. Before installation, designers must determine the borehole length required to satisfy the energy load of the local building, and this length is highly dependent on local thermal properties, such as thermal conductivity and the borehole thermal resistance. TRTs continue to be recommended since the local soil properties are highly variable, and thus must be measured in-situ for nearly all cases. Any miscalculation caused by error in TRT measurements will be reflected in the required length, and therefore accurate estimation of the site-specific properties will have a direct impact on the installation cost and efficiency of ground source heat pump systems [14].

A TRT is a simple in-situ test which provides designers with much needed design criteria that is specific to the local site. The test begins with a measurement of the initial, or undisturbed, temperature of the surrounding soil [15], as it is an important design metric. The air in the borehole pipes is purged and the flow increased to a value high enough to sustain transitional to turbulent flow to be representative of the flow conditions that will be used during real borehole operation [15]. Finally, heat is steadily injected into the borehole heat exchanger through the pump connected to an electric heater, at a recommended rate of 50 to 80 W/m and for a period typically between 36 and 48 hrs [16]. More detailed

specifications for TRTs can be found in Kavanaugh and Rafferty [12] as well as in Raymond et al. [15], which reviewed methods to improve TRT analysis.

TRTs and similar tests have been widely explored in the literature surrounding borehole heat exchanger modelling. Beier et al. [17] created a laboratory sandbox in order to produce a set of experimental data explicitly meant to be used to validate the results of computational models. The data has been used extensively for this purpose since its creation ([18]–[22]). Numerical models have proven highly useful in studying the effectiveness of TRTs, by providing additional information on the operating conditions, for example, the temperature gradients within the borehole and/or soil [18] and the effects of a test disturbance [19]. When validated against real experimental data, the additional information can provide researchers with valuable information that could improve predictions and design considerations made by traditional TRTs.

One of the reasons simulations of TRTs are so prevalent in studies of borehole heat exchanger models is due to the time scale on which these studies can be performed. These tests are typically completed in less than 100 hours, which is a much more manageable time scale than attempting to simulate true borehole operation, which occurs over the time scales of years. The reason these TRT validations are more manageable is twofold. Firstly, for a transient simulation, a shorter test time will typically result in faster computation times, since equivalent timesteps will cover the full test time in fewer steps than a test on a longer scale. Secondly, the spatial impact of borehole operation will increase with operation time, since thermal energy will flow into (or out of) farther reaches of the surrounding soil as time increases, due to thermal diffusion. When a constant load is applied to a borehole heat

exchanger, like in the case of a TRT, thermal energy will continually flow in one direction, towards or away from the borehole, so that the heat transfer processes continue to reach farther into the surrounding soil as more energy is constantly drawn to (or deposited into) the borehole from the heat pump. For borehole heat exchanger models, particularly those solved on discretized meshes such as Finite Element Models, this is a great concern since the size of the mesh scales with the size of the soil domain. Therefore, the longer the time of the simulation, the larger the necessary geometry and in turn the higher the computational effort. This challenge will be explored much further within this thesis, with proposals for how to increase computational efficiency.

2.4 GSHPs in Canada

Canada has long been one of the leaders in the world for GSHP usage in the world. In 2004, Canada was a top 5 user of GHSP in the world, producing 435 MWt [23]. Worldwide, geothermal energy in general and GSHP in particular has experienced strong growth (Figure 3) in recent years, due to increased urgency in decarbonization. Between 2005 and 2020, the worldwide GSHP use has increased by over five times. In addition, the number of countries that employ GSHP technology has gone from 26 to 54 between 2000 and 2020 [24].

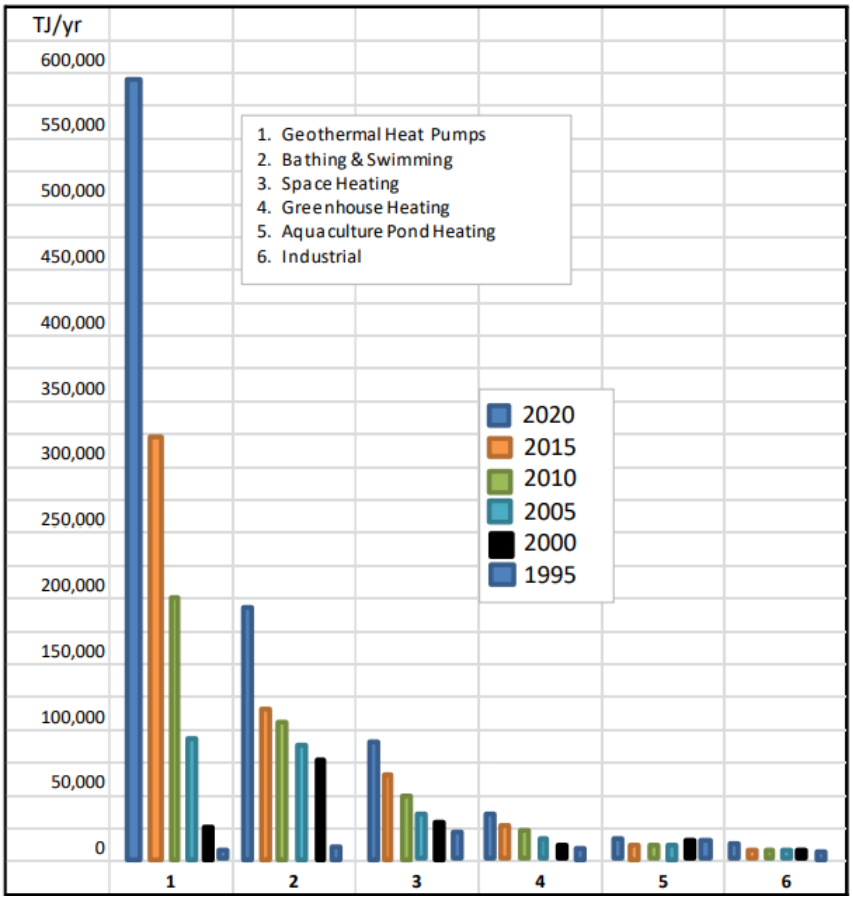

Figure 3: Worldwide Production of Geothermal Energy in the 21st Century [24]

Although GSHP use in Canada has continued to increase during that same time frame, it has not grown at quite the same pace (4.19 times between 2004 and 2020) [23], [24]. There could be many factors for this trailing, which has resulted in Canada falling out of the top ten countries in MWt of geothermal energy installed [24], which includes China and Turkey investing heavily in geothermal technology in recent years, as well as the distribution of geothermal potential within the country. Figure 4 shows the resource potential in Canada, which includes areas of interest of both electrical generation as well as direct heat exchange, which could be used for GSHPs.

The majority of the potential for geothermal energy is in Western Canada, particularly in Alberta, British Columbia and the Northwest Territories [25]. These regions of the country are high producers of natural gas, which may provide an understanding of why Canada's geothermal energy market has not kept up with other world leaders. Not only does Alberta use natural gas for their residential heating, approximately half of their electricity was generated from natural gas. This is an area of great potential to continue Canada's plan of decarbonization while replacing fossil fuels with reliable sustainable energy sources, however political attitudes towards sustainable energy must evolve before this resource is exploited.

Fortunately, in Ontario and Atlantic Canada, there are areas of the country that have potential for GSHP installation (Figure 4). The areas of Figure 4 highlighted by purple, blue and dark grey are regions where Geoexchange systems would be able to be implemented but do not have sufficient resources for electrical generation. These areas include most of Southern Ontario as well much of Atlantic Canada and the remaining territories in Southern Western Canada that do not have greater potential for electrical generation. Although these areas have made strides in reducing fossil fuels in their electricity generation, they are still reliant on natural gas (Ontario) and heating oil (Atlantic Canada) for much of their residential space heating. Residential GSHPs could be a very viable option for these regions as they have relatively balanced load profiles due to cold winters and warm to hot summers.

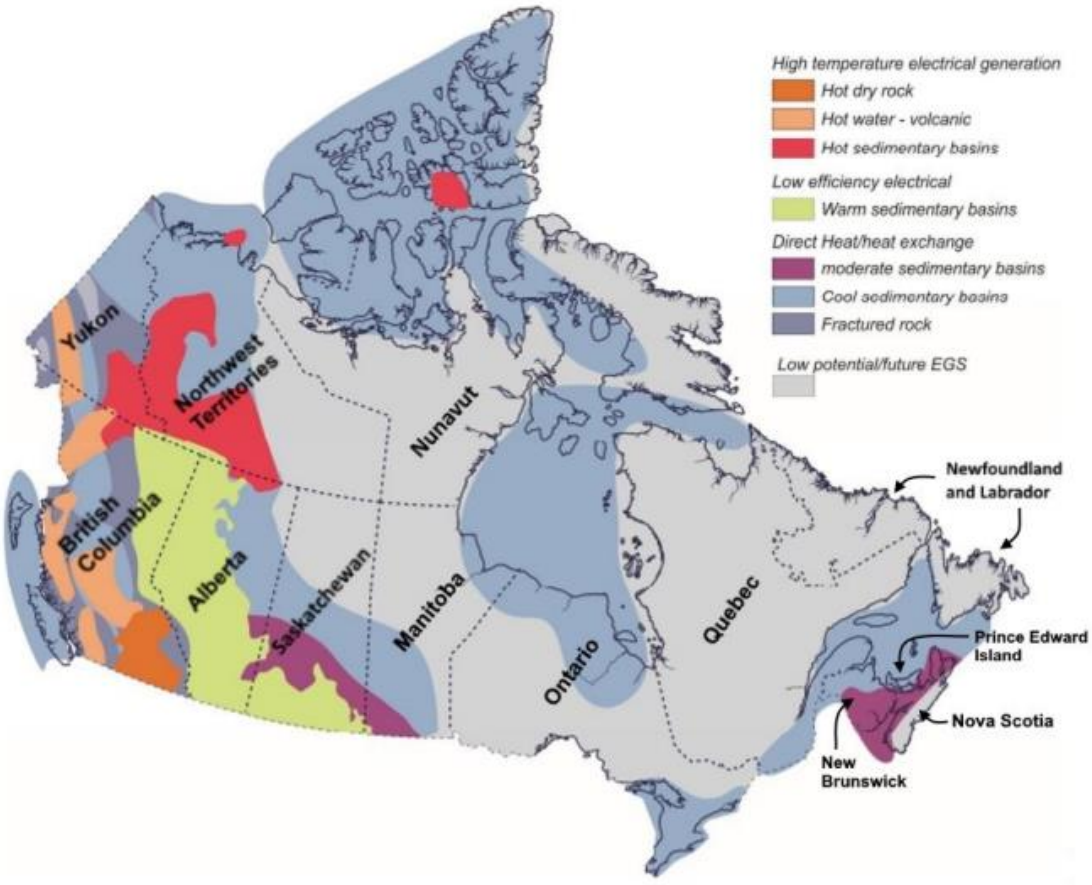

Figure 4: Geothermal Energy Potential within Canada [25]

2.5 History of Models

Modelling is an important concept of any engineering application, and there is a long history of models for vertical borehole heat exchangers. Most conventional borehole heat exchanger models find their roots in the work of Ingersoll et al. [26], who initially developed simple models for heat transfer through an infinite soil domain, with line and cylindrical sources. These problems were not explicitly solved, but methodologies were

proposed for the integration of additional model complexities. Later work continued the formulation of these models, to solve analytical solutions for these problems [27] as well as making it possible to continue increasing the complexity and accuracy of borehole heat exchanger models. Bertagnolio et al. [28] and Cui et al. [29] each completed comprehensive reviews of historical and modern models, many of which include complex formulations of work stemming from Ingersoll et al. [26].

A few of the most important early models for borehole heat exchangers will be laid out below in their mathematical form, as they will be referenced extensively within this thesis in addition to laying the basis for the more complex models in use today.

Infinite Line Source Model

Due to the high ratio between the depth and the radius of the borehole heat exchanger, H/r_b, a reasonable assumption in certain cases is to represent the borehole as a line source that releases (or absorbs) heat to (or from) the surrounding soil domain [30]. When axial heat transfer is assumed to be negligible, the problem can be reduced to one of radial dependence only, which is known as the Infinite Line Source Model (ILSM). This is given mathematically as [30]

$$\begin{cases} \rho_s C_{p,s} \dfrac{\partial T_s}{\partial t} = k_s \left(\dfrac{\partial^2 T_s}{\partial r^2} + \dfrac{1}{r} \dfrac{\partial T_s}{\partial r} \right) \\ r \to 0 \quad -2\pi k_s \lim\limits_{r \to 0} r \dfrac{\partial T_s}{\partial r} = q_l \\ r \to \infty \quad T_s = T_{und} \\ t = 0 \quad T_s = T_{und} \end{cases} \tag{1}$$

This formulation is a transient, heat conduction problem, made to be one-dimensional through the use of an axisymmetric coordinate system. Both boundary conditions are applied at limits, as the solution approaches zero and infinity, which correspond to an applied heat load and the undisturbed temperature, respectively. Furthermore, these correspond to a Neumann and Dirichlet boundary condition, respectively. Relationships have been proposed for solutions to the borehole wall temperature, solved at $r = r_b$. A general solution for temperature throughout the soil domain is typically solved numerically.

Infinite Cylindrical-Surface Source Model

The Infinite Cylindrical-Surface Source Model (ICSSM) is a slight adjustment to the Infinite Line Source Model, which is clear when comparing the mathematics (Equation 2, and 1, respectively). Although the borehole geometry allows for the simplification of the borehole being represented by a line source, this is an assumption that can add error to the solution. Instead of applying the load at $r = 0$ but evaluating the borehole temperature at $r = r_b$, assuming the solution for the domain between is non-physical, the ICSSM restricts the solution to the real soil domain, between the borehole wall and infinity. This is given mathematically as [30]

$$\begin{cases} \rho_s C_{p,s} \dfrac{\partial T_s}{\partial t} = k_s \left(\dfrac{\partial^2 T_s}{\partial r^2} + \dfrac{1}{r} \dfrac{\partial T_s}{\partial r} \right) \\ r = r_b \quad -2\pi r_b k_s \dfrac{\partial T_s}{\partial r} = q_l \\ r \to \infty \quad T_s = T_{und} \\ t = 0 \quad T_s = T_{und} \end{cases} \tag{2}$$

Although the first boundary condition is applied at a real internal radial position, compared to the limit of the ILSM, the solution to the model is actually more complicated than the ILSM, and it is more difficult to incorporate other design factors, such as ground surface conditions, groundwater flow etc. [30]. The G-function for the ICSSM employs Bessel functions, unlike the exponential integrals of the ILSM [30], which can explain some of the high complexity. Similarly, to the ILSM, a general solution for the soil domain is typically solved for numerically.

Finite Line Source Model

Both the previous models are able to reduce the problem to one of radial heat transfer only, due to the infinite formulation in the axial direction. However, this is a significant model simplification since the effects of the ground surface and the end effects of the borehole can have considerable impacts on the overall soil temperature distribution.

The Finite Line Source Model (FLSM) applies a line source, similar to the ILSM, but applies it to a semi-infinite soil domain, instead of an infinite domain [31] and it allows for axial heat diffusion. The line source is of a finite length, which starts at the ground surface, $z = 0$, and extends vertically into the domain to a depth of $z = H$. The borehole heating load is constant with the axial position, however due to the application of the boundary condition at $z = 0$, of a fixed undisturbed temperature, and the region of soil below $z = H$, the soil temperature is dependent on axial position as well as the radial

position. Just as in the radial direction, the external boundary condition at $z \to \infty$ is also the undisturbed temperature.

The full formulation of the FLSM can be found in Zeng et al. [31], but the real solution for the temperature excess at any given point within the soil domain can be given as

$$\vartheta = \frac{q_l}{4k_s\pi}\int_0^H \left\{ \frac{erfc\left(\frac{\sqrt{r^2+(z-h')^2}}{2\sqrt{\alpha t}}\right)}{\sqrt{r^2+(z-h')^2}} - \frac{erfc\left(\frac{\sqrt{r^2+(z+h')^2}}{2\sqrt{\alpha t}}\right)}{\sqrt{r^2+(z+h')^2}} \right\} dh' \qquad (3)$$

This can further be nondimensionalized using the variables, $Z = z/H$, $H' = h'/H$, $R = r/H$, $Fo = \alpha t/H^2$ and $\varphi = 4k_s\pi(T - T_{und})/q_l$. This is expressed in the dimensionless form

$$\varphi = \int_0^1 \left\{ \frac{erfc\left(\frac{\sqrt{R^2+(Z-H')^2}}{2\sqrt{Fo}}\right)}{\sqrt{R^2+(Z-H')^2}} - \frac{erfc\left(\frac{\sqrt{R^2+(Z+H')^2}}{2\sqrt{Fo}}\right)}{\sqrt{R^2+(Z+H')^2}} \right\} dH' \qquad (4)$$

Once again, the transient solution is typically solved for numerically, however an analytical solution for the steady-state distribution is presented in the original paper. This solution will appear later in this thesis as a point of comparison. Due to the incorporation of axial heat transfer and the axial boundary conditions, the FLSM can actually reach a steady-state solution, unlike the two infinite models above, which will continue to extend its thermal impact into the surrounding infinite domain without constraint [31]. There have

been further attempts to reformulate the FLSM in order to improve its performance, as well as decrease the computational effort [32].

When solving problems with complex, or non-standard boundary conditions, geometries, or other model inputs, there is often no other option but to solve the problem numerically, through the use of Finite Element or Finite Volume Models (FEM and FVM). Just a few of the most noteworthy models include the work of Al-Khoury et al. [33], Al-Khoury and Bonnier [34], Marcotte and Pasquier [14], Lamarche et al. [35] and Ozudogru et al. [36]. Although these models have many similarities, one important way in which they differ is how they incorporate the borehole domain itself into the numerical model. These range from a modified discretized heat pipe element ([33], [34]), effective borehole thermal resistances ([14], [35]) and a 1D energy equation [36]. These models range in accuracy, computational effort and other factors which are outside the scope of this thesis.

One significant way to simplify these numerical approaches is to remove the borehole domain entirely and apply a boundary condition at the surface of the borehole, similar to the approach of the ICSSM. This boundary condition has been prescribed as both a temperature value [37] and a heat flux ([38], [39]), typically varying with time. It is important to note that, like the FLSM, although axial heat transfer is typically resolved in these numerical models, the boundary condition at the borehole is often constant with the axial position.

The simplest fluid temperature distribution to assume is a linear profile which, when applied to a U-tube borehole design means the average fluid temperature, between the supply and return portions of the U-tube, would be a constant for each axial position. However, Marcotte and Pasquier [14] proved this to be an oversimplification, that overestimates the borehole thermal resistance which will have a great effect on borehole heat exchanger design. Instead, they defined a new solution based on a power average, known as the *p*-linear estimator [14], to improve the assumed fluid temperature distribution. The results of this study will be investigated further in this thesis.

The common thread in these models is the need to reduce the computational effort for the borehole domain. Since the borehole, which is both asymmetric for a U-tube design and is the location of heat injection and extraction, there are high temperature gradients within the domain. In FEM models, this means that the mesh needs to be highly dense, which increases the computational effort. Additionally, the equations that must be solved for a fluid domain are much more complex than in a solid domain. Therefore, finding a simpler way to resolve the borehole domain is of great interest to improving model efficiency.

Chapter 3 – Literature Review

3.1 Borehole Sizing Tools

During the design of borehole heat exchangers, engineers must determine the appropriate bore field length based on situation-specific data. There are a variety of sizing tools that have been developed over the years, with varying complexities, however they all rely on similar input parameters. Ahmadfard and Bernier [40] listed these parameters in tabulated form, recreated here in Table 1.

Table 1: Typical Input Parameters for Borehole Sizing Tools [39]

Required input parameters for most sizing tools
Building or ground loads and peak load duration
Target temperature limits for heat pumps ($\boldsymbol{T_L}$ and $\boldsymbol{T_H}$)
Bore field geometry (number of boreholes and location)
Ground thermal properties ($\boldsymbol{k_s}$, $\boldsymbol{\alpha_s}$ and $\boldsymbol{T_{und}}$)
Borehole characteristics (geometry, thermal properties)
Heat pump characteristics ($\boldsymbol{COP_H}$ and $\boldsymbol{COP_C}$)
Flow rate
Design period
Starting month of operation

The authors identified five levels of complexity (*L*0 to *L*4) to categorize these sizing tools, which are explained and paired with example tools in Ahmadfard and Bernier [40].

*L*0 and *L*1 tools are simply rule-of-thumb and two pulse tools, respectively, and are outdated methods which do not capture the true behaviour of borehole heat exchangers. For instance, *L*1 tools, which use the peak heating and cooling loads, are ineffective in properly predicting the long-term estimations of the system [40]. Among other sources of error, this can be understood as the effect of the absence of any data on the thermal imbalance, which will be explored further in the next section, which can be understood as the balance of the heating and cooling building/ground loads over one year of operation. The peak heating and cooling values may not properly capture the environmental conditions, as they carry no information on the time periods that the BHE will be used for heating and cooling, or the ratio of the peak load to the average load during these periods. Although these tools are, generally, no longer in use, it is important to recognize the limitations of any design tool which does not include more detailed information of the load profiles, as the heat accumulation or degradation that is caused by a thermal imbalance is being ignored.

As part of their review, Ahmadfard and Bernier [40] did an inter-model comparison of tools ranging from *L*2-*L*4. The most pertinent test was a cooling dominated load (due to the high thermal imbalance) and it was found that the tools that do not account for borehole thermal interaction estimated much lower values of borehole length minimums than the other tools. These two tools, both level *L*2, are the Classic ASHRAE sizing equation [16] and the GHX design tool box [41], [42]. In scenarios with high thermal imbalance, the effects of the past imbalance on the surrounding soil propagate through the system operation which increases the intensity of borehole interaction. In reality, these tools would calculate insufficient borehole lengths that would result in system deterioration after years

of operation, which may lead to increases in the unguaranteed heating time as well as reducing the economic viability of the GSHP system. The unguaranteed heating time ([43], [44]) is the time when the GSHP system cannot keep the building temperature above the allowable minimum temperature, which can result in homes in cold settings operating at dangerous conditions, which could lead to the illness or death of vulnerable people.

Flow charts within the review show the iterative nature of calculating the borehole length for the sizing tools [40]. A better understanding of how the local thermal imbalance is affected by the length, due to the increased soil volume and effective soil volume 'surface area' could be employed to improve sizing tools accuracy. Tools that do not account for the borehole interaction underestimate borehole lengths, whereas overestimating could result in economic unviability, therefore more detailed understanding of this relationship could widen the scope of implementation of GSHPs and reduce the chance for design error.

3.2 Solid Heat Transfer and Properties

There are many factors to consider in the heat transfer through the solid domains that determine the performance of BHEs. Some of these factors are decided on by design engineers, while others are predetermined. GSHP technology takes advantage of the local surroundings and therefore the thermal properties of the soil surrounding the BHE must be measured for each case, not determined through design. This accounts for the importance of TRTs in GSHP design. However, there is still discussion on appropriate modelling of the soil domain for numerical studies of BHEs and GSHPs systems.

Although the thermal properties of the soil like thermal conductivity and specific heat capacity are predetermined, as previously mentioned, the distribution of these values within the soil field are still a topic of debate for numerical studies. It is well understood that the thermal properties of soil are heterogenous, both at a local level as well as within the stratified nature of sub-surface organic and inorganic materials. The effect of this heterogeneity on overall system performance is, however, up for debate.

The geology below ground level is naturally stratified with layers of differing types of soil and rock, with a wide range of thermal properties, that have historically been lumped into a homogeneous continuum for modelling or sizing purposes ([26], [27], [31]). When accounted for, they are typically represented by horizontal layers of varying thickness ([45]–[47]). The significance of the homogeneous soil assumption is still a matter of debate, with many researchers attempting to quantify the amount of error caused by this simplification. In a study using TRNSYS, Lee [48] analyzed the effect of multiple ground layers on the analysis of a thermal response test and a long-term simulation. In the dynamic ten-year simulation, the difference in the total power consumption of the heat pump is negligible, 0.13% higher with multiple ground layers, suggesting the overall system performance is not highly sensitive to local differences in soil composition.

This confirms that the homogeneous soil assumption is sufficient for the circulating fluid conditions, however it does nothing to investigate the effects of heterogeneity on the temperature distribution within the actual soil. Also, Lee [48] does make the assumption of no groundwater flow, which has been seen to interact with the heterogeneity of the soil [38], [49]. Tiwari and Basu [49] observed the presence of vortices in the groundwater flow

when multiple layers were used in their model, particularly in the high permeability layers, which likely enhances the effective ground thermal conductivity. This was observed in soil layers with permeability greater than 10^{-9} m^2 and the interaction with adjacent low permeability layers. These vortices are a result of the changes in axial and radial groundwater flow caused by the layers of variable permeability.

Others believe the effect of groundwater flow on the heat transfer through the soil domain can be significant due to the directional nature of the flow, even within homogenous soil conditions. In a study of 2D fields, ignoring the axial direction, [50] the heat transfer between the BHE and the surrounding soil was much improved, as the groundwater flow enhanced the movement of heat away from the BHE wall, effectively increasing the thermal conductivity in the soil, albeit only in the direction of the flow.

Despite the understanding of groundwater flow's effects, and heterogeneous soil properties, the vast majority of studies simplify their models by ignoring both ([43], [51]–[54]), in favour of an effective thermal conductivity of the surrounding soil, determined by a TRT. Lazzari et al. [52], which is a highly cited study within the field of BHE simulation, concurs that the groundwater flow may improve the overall heat transfer of the BHE, but a long-term study can be conducted without taking into account its effects, and still provide useful data. To understand these conditions at potential site locations, much more in-depth experimentation is necessary, which increases surveying costs. As such, this data is not typically available for design, and therefore is not considered in this model.

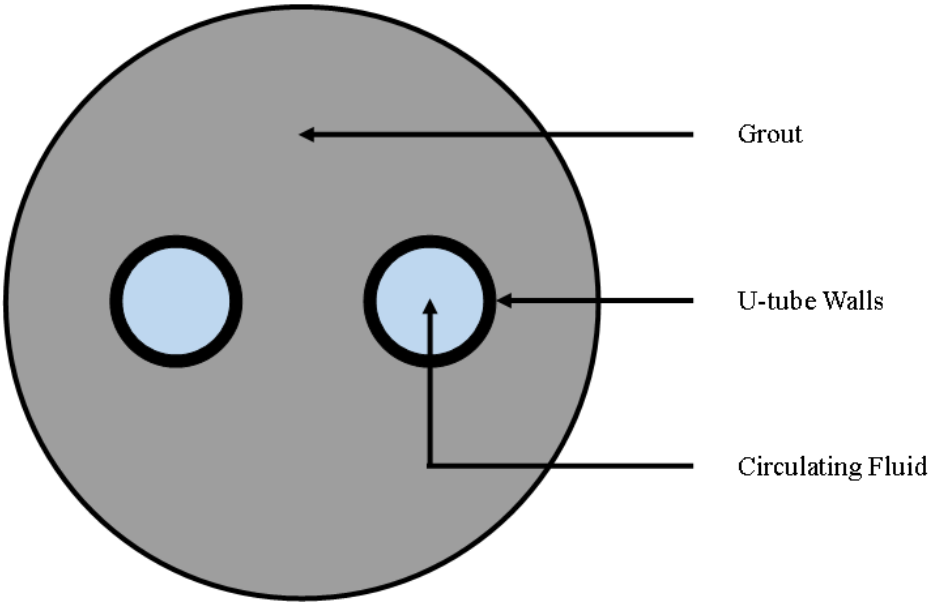

Figure 5: Cross-Section of a Borehole Heat Exchanger

The BHE thermal properties that can be controlled by engineers are the properties of the grout that is used to fill the boreholes. The grout is the intermediate material between the heat carrier fluid passing through the BHE and the GSHP, and the surrounding soil, shown in Figure 5, which means its effectiveness will have significant effects on the transient heat transfer, the radial temperature gradients within the soil, and the temperature recovery during intermittency. In addition to the thermal properties, practical considerations for the installation and operation of BHEs must be made. To be effective, engineers have stated that grout materials should satisfy the following conditions [55]:

(1) High thermal conductivity for efficient heat transfer

(2) Low hydraulic conductivity for control of groundwater movement

(3) High workability for ease of injection into the borehole

Thermal conductivity's effect on BHE effectiveness has been well-established in literature. However specific heat capacity, another thermal property, has historically received less focus. Kim et al. [55] investigated these thermal properties in a study of cement-based grouts, both experimentally and numerically. In continuous operation, analogous to a thermal response test, the study found that thermal conductivity was the sole property determining the mean heat exchange rate, and that specific heat capacity was negligible in these tests. However, in intermittent operation, both the thermal conductivity and specific heat capacity determined the mean heat exchange rate. This may explain the imbalance in focus on the two properties since many prediction models have been based on results from continuous operation tests. With improved computing power, long-term intermittent simulations of BHE operation are becoming more common, and as such the specific heat capacity is becoming a more important factor in design considerations. High specific heat capacity must be paired with high thermal conductivity to improve the BHE performance [55], however this is dependent on the properties of real materials and as such performance must be optimized based on available materials.

In an effort to solve this dilemma, some researchers have begun exploring the use of phase change materials (PCMs) within the borehole ([56], [57]). Phase change materials have been used in applications of long-term thermal energy storage to reduce thermal energy loss due to temperature gradients within storage materials, and it has been considered in GSHP design to reduce necessary land use and reduce the thermal wave into the surrounding soil [58]. When PCMs were used as the entire backfilling material, the heat injected into the borehole was much more localized near the borehole axis than with simple

soil, which was used as a control case. This was evident in the transient, radial temperature measurements, which show almost no rise in the temperature at 200 or 300 mm radii [56]. The thermal energy is used in the melting of the PCM, and so a much lower temperature is reached, both within and outside, the borehole. This allows for a more densely packed borehole field to be created, as they will not be subjected to conventional thermal interaction. However, due to the lower thermal conductivity of the PCM, when compared to traditional soil or grouting, the heat transfer rate is lower for all PCM materials than the control case. This would reduce the peak load of the GSHP for a given borehole length, and would require longer boreholes in extreme climate regions, like Canada's north.

When adding micro-encapsulated PCM to conventional grout, small reductions in borehole length can be achieved [57]. The peak performance of the PCM observed by Aljabr et al. resulted in a 7% reduction, due to the combination of conventional conductivity of the grout, to transfer heat to and from the surrounding soil, as well as the latent heat storage of the PCM capsules, smoothing the thermal load that must be transferred at any time. However, the performance was extremely sensitive to the PCM thermal properties in relation to the grout, so the applicability of the technique was still in question. In Canada, where population density is much lower, land use is less of a factor in GSHP design. As such, typical BHEs use conventional grouting techniques, to minimize installation cost and improve the payback period of the GSHP investment. Aljabr et al. [57] concluded that enhancing the thermal conductivity of the grout would be more cost-effective than adding PCM.

3.3 Thermal Imbalance

One of the most difficult design considerations in GSHP systems is the effect of a thermal imbalance on the soil surrounding the BHE. A thermal imbalance occurs when the required heating and cooling loads of the building or buildings which the GSHP system services are unequal, due to the local environmental conditions over the course of one year. This imbalance can be due to an overreliance on heating or cooling. In Canada, however, load profiles tend to be heating dominated due to the cooler climate. A useful metric for this imbalance is the Thermal Imbalance Ratio (IR) [59], which is defined as

$$IR = \frac{E_{AHR} - E_{AHE}}{max(E_{AHR}, E_{AHE})} \times 100\% \quad (5)$$

where E_{AHR} and E_{AHE} are the accumulated heat rejected and extracted, respectively, as defined by the building load profile and the heat pump performance. IR is a useful index, not only because it gives a quantitative value for the degree of the severity of the imbalance, but also an explicit statement of whether the system is heating or cooling dominant; with a positive IR indicating cooling dominant and a negative IR indicating heating dominant. The IR is of interest, because of the implications that it will have on the long-term performance of the GSHP.

The reason thermal imbalance is a design concern is due to the potential for the long-term changes to the soil surrounding the BHE. When the value of the IR is large (in magnitude), the overall energy balance on the soil plug is changing not only seasonally, but annually. These changes generally have negative effects on the efficiency of the GSHP system and either need to be considered in the economic analysis of the system or mitigated

through system modifications [44]. In heating dominated climates, like much of Canada, You et al. [44] reviewed many cases of thermal imbalance and found long-term ground temperature degradation, which led to lower outlet fluid temperatures, lower heat pump Coefficient of Performances (COPs), and therefore lower system efficiencies. One example found in this review is shown in Figure 6, where the soil temperature decreases during each yearly period, which is coupled to local fluctuations due to the instantaneous time-of-year operation.

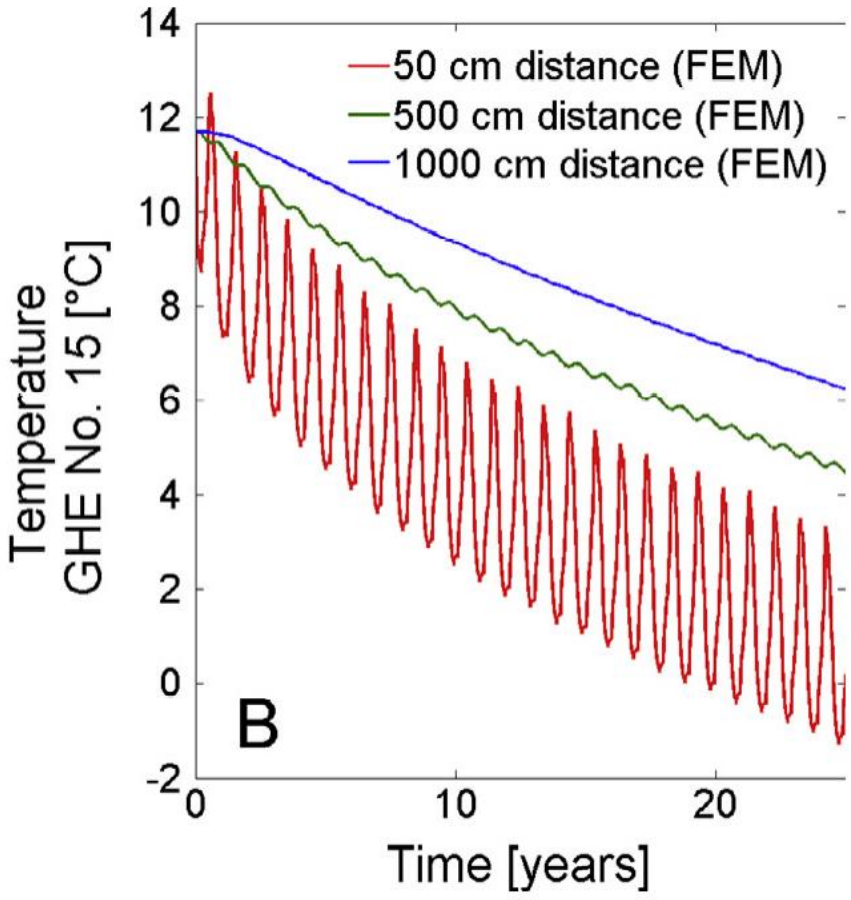

Figure 6: Example of Soil Temperature Degradation due to Thermal Imbalance [60]

Multiple recent studies ([61]–[64]) have attempted to characterize and mitigate this thermal imbalance effect in cold- and hot-dominated regions of China and Korea. Both experimental [63] and numerical studies [64] found that connecting multiple boreholes in parallel exhibited superior heating performance. When systems were studied holistically, including considering the effects of the heat pump and water separator, Chen et al. [64] found a borehole field installed in parallel will 'self-adjust' to maximize the thermal capacity of the soil surrounding the entire BHE. It is beneficial to create as uniform a temperature field as possible within the BHE, to reduce the chance of adverse temperature gradients near the individual borehole walls, which may hamper heat transfer during one or more operations. The numerical simulation was completed two-dimensionally, so the axial interaction with this 'self-adjustment' is not known and would be of interest.

In You et al. [44]'s review, the cases of drastic thermal imbalance in cold-dominated China are summarized. Liu et al. [65] found that for a case in Qiqihar, China, with an IR of -76.5%, showed an average soil temperature decrease of nearly 5°C over a ten-year period. Qiqihar is in a Köppen climate classification of a humid continental climate (*Dwa*). The majority of Canada, including nearly all of Ontario, are also in subcategories of the humid continental climate. It is clear that in substantial portions of the country, modifications will need to be made to mitigate this thermal imbalance to ensure system efficiencies stay within acceptable ranges. For BHE specific solutions, these modifications may include increasing borehole spacing, increasing borehole length, modifying borehole field layout, or improving the BHE thermal properties. For system specific solutions, it may include integrating fossil fuels, integrating solar energy or other green energy sources, or using an

absorption heat pump rather than an electric heat pump [44]. As found in You et al.'s review, researchers [44] found an increase of borehole depth from 80 to 100 to 120 metres decreases the average soil temperature decrease from 8.4 to 7.3 to 6.5°C. Unfortunately, the initial investment of borehole per unit depth increases with overall length due to increasing drilling difficulty [44], therefore this solution becomes increasingly expensive for scenarios with high IR values. A more complete understanding of the result of increasing depth on the overall soil energy balance is important for scenarios where increasing length is the only design solution, including locations with limited surface area or hostility to additional system components such as solar.

Some work has been done on thermal imbalance in Canada ([21], [66]). Law and Dworkin [21] studied the long-term effects of four real buildings, however, the load profiles were varied and did not include a highly heating dominant scenario. It was still noted that without balanced loads, the ground temperature will change, which has a negative impact on system efficiency. Shukla et al. [66] studied the thermal imbalance and attempted to mitigate the problem through the use of phase change materials, however the system was not a traditional GSHP, but rather a novel 'caisson-based' thermal storage system in the buildings foundation, similar to energy piles.

3.4 Mixed Dimension Models

In order to complete a long-term study of GSHP systems and investigate the implications of thermal imbalance on the soil volume and the resulting temperature

gradients, a three-dimensional model of the soil is necessary. Particularly in scenarios with multiple boreholes, the temperature gradients both in the radial and axial direction have implications on the BHE performance and can only properly be resolved numerically due to model complexities.

Bauer et al. [67] highlights how it is impractical to solve large numerical models on discretized meshes, using methods such as FVM and FEM, to assess the uncertainty of TRTs due to the high computational effort required for full three-dimensional models. Instead, they created 3D models based on thermal resistance and capacity (TRCMs) networks in an effort to reduce said computation time. The models generally agreed with the fully discretized ANSYS model, except at early times when the temperature front moved through the U-tube, with significant reductions in computational time. However, Bauer et al. [67] did not report any data on the soil temperatures. It can be assumed that, like the fluid nodes, there were very few nodes within the soil domain, and as such detailed temperature gradients were not available. When the model in the soil domain is complex, due to specific boundary conditions or system components, for example a buried tank [37], the complete data provided by three-dimensional models is of great interest and cannot be omitted without significant loss of accuracy to the solution.

Ozudogru et al. [36] took the step to model the fluid using one-dimensional line elements using the commercial software COMSOL to greatly reduce this computation effort without sacrificing solution accuracy. In Ozudogru et al.'s model [36], the fluid domain is modelled using a one-dimensional energy equation and the solid domain remains in three-dimensions, solving transient heat conduction in the grout and soil. This approach

proved highly effective and has been adopted by multiple subsequent authors ([18], [68]). The computational time can be found to be much shorter without solving a three-dimensional model of the fluid, however this time reduction has not often been the main topic of studies found in the literature.

It is important to note that in Cerfontaine et al. [68], the authors disagreed with the initial approach of giving the pseudo pipe domain, which replaces the U-tube walls, its own heat capacity value. They claimed it avoids a non-physical transient phase within the pipe when the temperature should be constant and correspond exactly to the temperature of the line element. However, the paper makes no mention of the error in the amount of heat energy dissipated to the surrounding grout, as this approach would overestimate how much passes through the U-tube walls. Fortunately, due to the thin walls of the U-tube, it may be negligible compared to the overall borehole volume. The Ozudogru et al. [36] model will be used in the following work, and a more complete explanation of the model will be provided in a later section.

Resolving an accurate fluid temperature distribution is essential for extracting the full benefit of a 3D finite element model. This allows the axial distributions within the soil to be captured by the modelling, and the interaction between the variable fluid temperature and the soil boundary conditions, particularly the surface and ‘deep ground’, which may have significant effects on the soil temperature gradients. Marcotte and Pasquier [14] developed the *p*-linear estimator, which is an analytical solution that better predicts the fluid temperature distribution within the U-tube. The motivation for the work was that the assumption of a constant heat flux along the borehole, with an average temperature based

on the inlet and outlet temperatures, overestimated the borehole thermal resistance. This overestimation has a significant economic impact, as the necessary length of the borehole is artificially raised, which increases installation costs. Marcotte and Pasquier [14] found that in the case of a borehole resistance miscalculation of $R_b = 0.15\ mKW^{-1}$ instead of the true value of $R_b = 0.10\ mKW^{-1}$R would result in an extra cost of $63,900 over a ten-year period, an increase of 10.7% for the total cost of the project. It should be noted that this study was completed in 2008, and both the installation cost of the borehole and the energy cost of electricity are subject to change, however oversizing the BHE due to miscalculation would still result in economic inefficiency. Ensuring the fluid temperature distribution of a numerical study aligns with the *p*-linear estimator will provide confidence in calculated results and their applicability to real-life scenarios.

There is some uncertainty in what the value of *p* should be to properly estimate the fluid temperature distribution. Marcotte and Pasquier [14] suggested that $p \rightarrow -1$ should be used, however they acknowledged that the real solution was time dependent, and that *p* should decrease with time to remain accurate. Gordon et al. [69] verified this value in their own results, also acknowledging that $p \rightarrow -1$ was most successful when used to validate short-term operation. ([70], [71]) have made multiple attempts to improve upon Marcotte and Pasquier's model, by proposing methods which estimate *p* based on time, called the p(t)-linear method. Unfortunately, the time dependent solution requires knowledge of a known soil temperature profile to be initialized. In a real-life setting, this may not be possible without significant experimental apparatuses, which makes the improved model

unfeasible. The original *p*-linear method is sufficient for assuring the model is working during short-term operation, which can be used as validation for the fluid domain.

It is clear from the literature, that there is a history of mixed physics and mixed dimension models in studies of borehole heat exchangers. Methods such as reducing the spatial dimensions, using effective borehole thermal resistances and average fluid temperature, solving CaRM or TRCM equations instead of discretized methods, and others are regularly employed to improve computational efficiency. However, it is imperative that these simpler models still resolve the proper borehole heat exchanger performance, or else the uncertainties may result in error that could cause significant economic impacts.

3.5 Effect of Borehole Length and Axial Heat Transfer on GSHP Systems

Fewer studies than would be expected investigate the effect of length on GHSP system performance, as analytical models predict the necessary borehole length based on a series of other environmental factors, rather than using the length to calculate other quantitative factors. Overall, optimization in BHE design is typically interested in minimizing the length of the BHE while providing the necessary thermal loads ([40], [46], [72], [73]) due to economic concerns, although if designed incorrectly, more unguaranteed heating time is observed at shorter lengths [43], [44]. The dominant path of heat transfer is in the radial direction, and so there is variation in the literature on if axial heat transfer within the ground needs to be included to properly optimize borehole lengths.

The Taguchi method is an optimization method that has begun to appear more often in engineering studies ([47], [73]) as a new method of determining appropriate borehole lengths. Pandey et al. [73] used the method to optimize BHE design, however, it is only able to be applied to cooling and heating separately. In studies where the interest is on an annual thermal imbalance, and how thermal recovery occurs annually, as well as during off-seasons (spring and autumn, namely), this style of optimization is less useful. One major difference in these two studies is the way in which they handle the axial component of heat transfer. Pandey et al. [73] employed an ILS model, which completely eliminates axial heat transfer from the model's mathematics. Zhou et al. [47], on the other hand, solved a three-dimensional FEM model which clearly resolves the heat transfer in all directions. It would seem that ignoring axial heat transfer when explicitly studying the effect of axial (borehole) length would be an oversimplification which could result in model error, but this highlights the insignificance of axial heat transfer in comparison to radial heat transfer.

A major factor in determining borehole length is the cost of installation, as economic viability is paramount for GSHP systems to compete with traditional, fossil fuel-based heating systems. Economic unviability of GSHP systems relies heavily on cheap fossil fuel access, particularly natural gas [54], however as measures are put in place to combat climate change, the price of these products may rise. For vertical BHE, the cost of drilling is typically considered as a function of the diameter and depth ([72], [74]), however the borehole depth is much more important to the final value. As such, the continued increase in borehole depth in an effort to combat soil temperature degradation should be carefully considered, and its effectiveness studied thoroughly, to determine the viability of

this method of system improvement. As stated in the ASHRAE Handbook, GSHP boreholes tend to be drilled to between 70 and 130 m in depth, and so any study of the effect of length should reside somewhere within that range [16]. Although this thesis will not have an explicit economic analysis, engineering work should be done with economic viability in mind to ensure applicability.

The necessary borehole length is closely related to the borehole thermal resistance [47], which is a model simplification that measures the overall resistance that the heat transfer encounters from the circulating fluid and the surrounding soil [17]. The borehole thermal resistance combines the fluid convective resistance, the U-tube wall resistance and grout resistance. Although this overall resistance is not a component of the model used in this study, instead the individual material properties are independently set, the relationship between the length and this value cannot be ignored.

In a study of the effect of total borehole length on GSHP performance Naldi and Zanchini [43] found that the general performance, which included heat pump COP and the Energy Efficiency Ratio, reached a steady state after approximately 40 years of operation. This suggests systems will reach a balance between the imbalanced load through the borehole and the heat flow through the fictional boundaries that surround the volume of soil that is affected by the presence of the BHE. Although studies of this time scale are largely untenable when detail within the soil domain is of interest, in shorter time scales the trends of the long-term performance can be determined. Naldi and Zanchini [43] ultimately determined the longer the length of the boreholes, the better the system performance, however the studied cases were often in different configurations, which

changed the affected soil region. Many studies have attempted to maximize the heat flux per unit depth of BHE ([46], [53], [72], [75]) in an effort to maximize heat transfer without calling for further drilling which would lead to diminishing returns at the expense of increasing drilling costs ([72], [74]). The phenomena of diminishing returns in this context are seen repeatedly, as Batini et al. [45] observed increase the Aspect Ratio of the borehole, H/R, by increasing the height, from 10 to 20 resulted in an increase of thermal energy extraction between 152% and 170%, while increasing from 20 to 40 increases only from 87% to 100%. Li et al. [53] and Noorollahi et al. [72] both observed non-linear increases in the fluid temperature differences while increasing the borehole depth, and Chen et al. [46] used this maximum value of heat flux per unit depth to determine an optimal borehole depth.

A complication in the analysis of BHE modeling is the presence of or simplification of the heterogeneity of soil. When included in numerical modeling, heterogeneity is typically employed in layers as a function of depth ([46], [47], [75]). This model simplification, discussed in a previous section, is uniquely connected to the sensitivity of system performance to borehole length, as changing the overall length will also change the average soil properties that surround the borehole. Although Lee's [48] findings concluded that the same simulation using average and stratified soil properties resulted in negligible differences in the performance, this study does not result in any change in soil composition. When average soil properties are employed in numerical modeling, as opposed to variable properties, it is important to contextualize the changes in borehole length in relation to other important parameters rather than simply optimizing strictly for length.

Despite these complexities that arise when studying borehole length, axial heat transfer is typically of less concern than the average heat transfer between the borehole and the surrounding soil. This is highly reflected in much of the literature presented here, with many studies omitting axial heat transfer altogether ([43], [53], [72], [73]) and others including it in the model physics but neglecting to analyze the data through the lens of axial heat transfer ([46], [47], [53], [75]). Batini et al. [45] and Chen et al. [46] are two studies which did investigate certain heat transfer processes as they varied with depth, however neither investigated axial heat transfer to determine its significance in relation to other heat transfer processes. It can reasonable be assumed that the effects of axial heat transfer are more significant when the soil is represented as heterogeneous layers, since thermal diffusivity will no longer be isotropic, which may explain for the slight increase in attention in studies that employ a heterogeneous soil domain.

3.6 Thermal Impacting Radius

One of the many benefits from the designs of vertical borehole heat exchangers is the ability to access a large volume of soil by installing a deep borehole of a relatively small radius. As a reminder, the high ratio between the depth and radius of the borehole is the basis for the assumption that allows for models that employ a line-source, such as the infinite and finite line source models [31]. Although the radius of the borehole is small, the borehole is able to access and store energy in a cylinder of soil of a much greater radius. This assumption can be made due to the high favourability of radial heat transfer over the

heat transfer in the angular and axial dimensions, which is evident by the early one-dimensional models being radial models only.

Exactly how far the thermal impact of the borehole extends into the soil domain is an important area of study for borehole heat exchanger operation. This is important, not only for determining the heat transfer in and around a single borehole, but in how the operation of a borehole will interact with other heat transfer activities in its vicinity. The thermal process of interacting boreholes is a very complex phenomenon but is one that has been studied extensively ([32], [37], [43], [76], [77]). Geothermal heat pump systems which employ borehole fields are common, in order to supply a greater energy load, either to large, high-use buildings [43] or to interconnected, multi-building energy systems [37]. Eskilson and Claesson [76] developed a method that uses the superposition technique, which was also adopted by Li et al. [77], who employed superposition to study the performance restoration under intermittent operation in borehole fields. However, these methods are typically built on the assumption that although there are multiple boreholes, they exist within a single system. These studies rarely focus on multiple systems of singular boreholes, which may be of interest if there is to be wide-scale adoption of geothermal heat pump systems in typical suburban Canadian neighbourhoods.

One method of quantifying the volume of soil that is affected by single borehole operation is known as the thermal impacting radius [78]. The thermal impacting radius is defined, by Luo et al. [78], as the greatest distance from the borehole's central axis in the radial direction that has been affected by the application of the borehole load. At any fixed time value, the location of the thermal impacting radius is determined by a minimum soil

temperature excess, θ, which is the difference in the local soil temperature from the undisturbed temperature. Figure 7 simply illustrates the measurement of the thermal impacting radius from a temperature versus radial position graph. The dotted line in Figure 7 represents the undisturbed soil temperature plus (or minus in the case of heat extraction) the minimum soil temperature excess. The red line is the radial soil temperature distribution, and the intersection of these two lines represents the thermal impacting radius. The thermal impacting radius is known by other names as well, like the impact scope or radius ([79], [80]), or thermal effect radius [81] , however the physical definition of these values is the same.

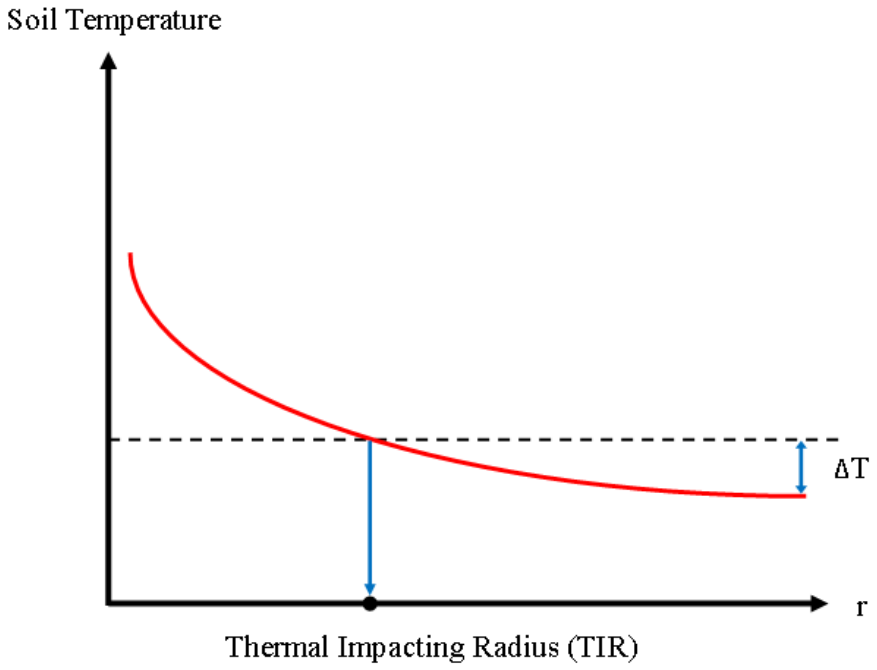

Figure 7: Illustration of the Thermal Impacting Radius Definition

This method for defining the thermal impacting radius is incredibly simple, which means that it can be easily applied to any FEM solution. However, this may be an

oversimplified way of determining the thermal impact of borehole operation. This definition uses only one factor for any fixed time value, the temperature excess, which is arbitrarily determined by the researcher. Additionally, the method does not contextualize the local temperature excess values with any other model inputs, or borehole operating conditions. Most importantly, the local temperature excess is not enough information to determine the overall system energy balance.

These concerns highlight the problem of an inconsistent definition of the thermal impacting radius with limited theoretical basis. The appropriateness and efficacy of the current definition is to be investigated within this thesis and an alternative method will be proposed.

3.7 Modelling Summary

The review of the current state of research as found in the literature will inform the model proposed within this thesis. Homogeneous soil properties are used widely in discretized modelling of BHEs and are found to be sufficient to resolve overall system performance. Additionally, the amount of effort, and therefore investment, that system designers would require to determine the heterogeneous soil composition is much greater than determining the average thermal properties, and therefore increases complexity without greatly improving the model performance. Groundwater flow is also highly specific to site conditions and studies have found that a great amount of useful data can be obtained without its inclusion in the study.

It has been found that for BHE modelling, it is a waste of resources to resolve a fully three-dimensional model since it provides little information, in certain domains, at high computational cost to the overall model. This model will reduce the model complexity where possible, using justifications found in analytical solutions and research found in literature. The literature shows that axial heat transfer should be considered, but it is also clear that in many processes radial heat transfer is more dominant. This understanding will inform the current work and the proposed three-dimensional model.

Portions of the model's physics will be taken from previous, highly cited works, and will be validated along with other model components developed and presented within this work. The proposed model will include domains governed by physics that can be described as: 3D transient heat conduction, 1D axisymmetric transient heat conduction, 1D fluid energy equations and modified CaRM equations.

Chapter 4 – Mathematical Modelling of Borehole Heat Exchangers using COMSOL Multiphysics

4.1 Validation of COMSOL's Heat Transfer in Pipes

COMSOL's *Heat Transfer in Pipes* is a physics interface used to model heat transfer by conduction and convection in one-dimensional pipe segments, with user-prescribed flow conditions like fluid velocity and pressure [82]. COMSOL solves an energy balance equation for 1D pipes, represented by the equation

$$\rho A C_p \frac{\partial T_f}{\partial t} + \rho A C_p \boldsymbol{u} \cdot \nabla T_f = \nabla \cdot Ak \nabla T_f + f_D \frac{\rho A}{2 d_h} |\boldsymbol{u}|^3 + Q + Q_{wall} + Q_p \qquad (6)$$

where $f_D \frac{\rho A}{2 d_h} |\boldsymbol{u}|^3$ corresponds to friction heat dissipated due to viscous shear, Q represents a general heat source, Q_{wall} represents external heat exchange and Q_p represents an optional pressure work term, to be used if the fluid is compressible and pressure drop is expected to be significant.

The solving of a 1D energy equation can save considerable computational time, when compared to three-dimensional computational fluid dynamics software, such as ANSYS CFX, however it is necessary to verify and validate the results of a 1D solution with analytical and experimental data, respectively. The COMSOL solver is verified by comparison with three simple analytical solutions, with corresponding theoretical development, and then a fourth case to verify the use of the 'Pseudo Pipe' method developed by Ozudogru et al. [36], discussed further below. The four verification test cases are as follows:

1. Constant Heat Rate

2. Constant Heat Transfer Coefficient and Wall Temperature

3. Transient Heat Accumulation

4. Pseudo Pipe Conduction

The analytical proofs of each solution are laid out in full in the Appendix, along with the corresponding COMSOL model equations. It should be noted, these verifications are focused solely on the fluid and pipe domains, and not the external solid domains. The appropriate theoretical justifications can be found there, as well. The final analytical solution, along with figures comparing the solutions to the results of each simulation are presented within this section.

1. Constant Heat Rate

The case of a simple pipe with a fixed inlet temperature and a constant heat flux at the pipe wall is an appropriate solution to be used as the first verification. The full derivation of the analytical solution can be found in the Appendix, of which the result is the equation

$$T_{f,b}(z) = \frac{2q_o''}{\rho r_o u C_p} \cdot z + T_{in} \tag{7}$$

where $T_{f,b}(z)$ represents the bulk temperature, or 1D temperature as a function of the position within the pipe. Figure 8 compares a specific analytical solution to the results from COMSOL for a constant applied heat rate.

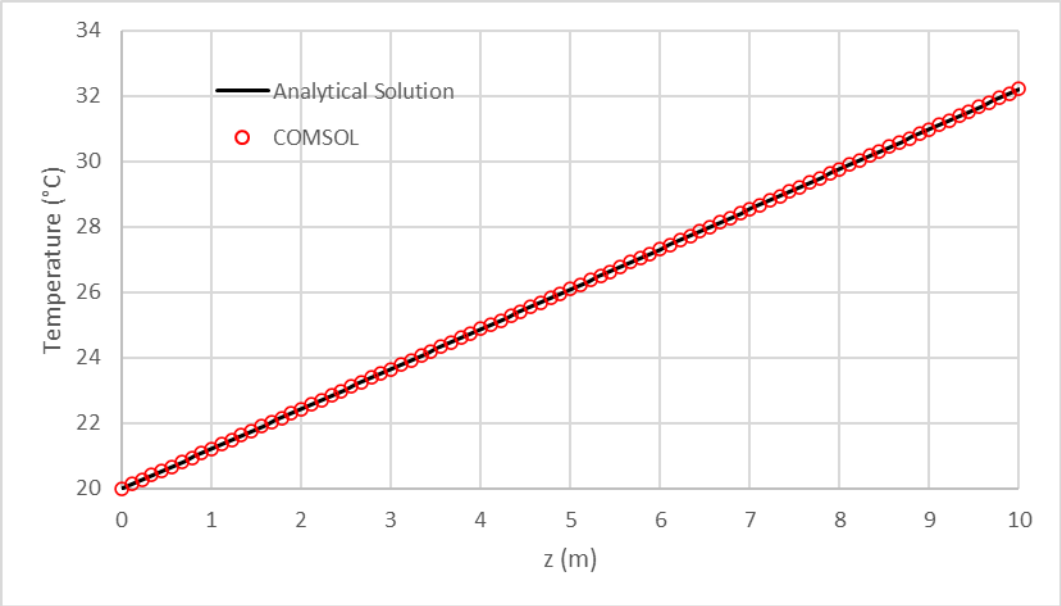

Figure 8: Results of the Constant Heat Rate Test Verification

2. Constant Heat Transfer Coefficient and Wall Temperature

In contrast to the previous case, in this case the heat rate applied to the fluid is a function of the position within the pipe. This is achieved by holding the heat transfer coefficient and external temperature constant, which therefore causes the heat flux to diminish in magnitude from the inlet to the outlet, due to the reduction in the temperature difference between the bulk fluid and external temperatures. The analytical solution is governed by the equation

$$T_{f,b}(z) = (T_{in} - T_{ext})e^{\left(-\frac{hP_o z}{\dot{m}C_p}\right)} + T_{ext} \quad (8)$$

and is compared to the COMSOL results in Figure 9.

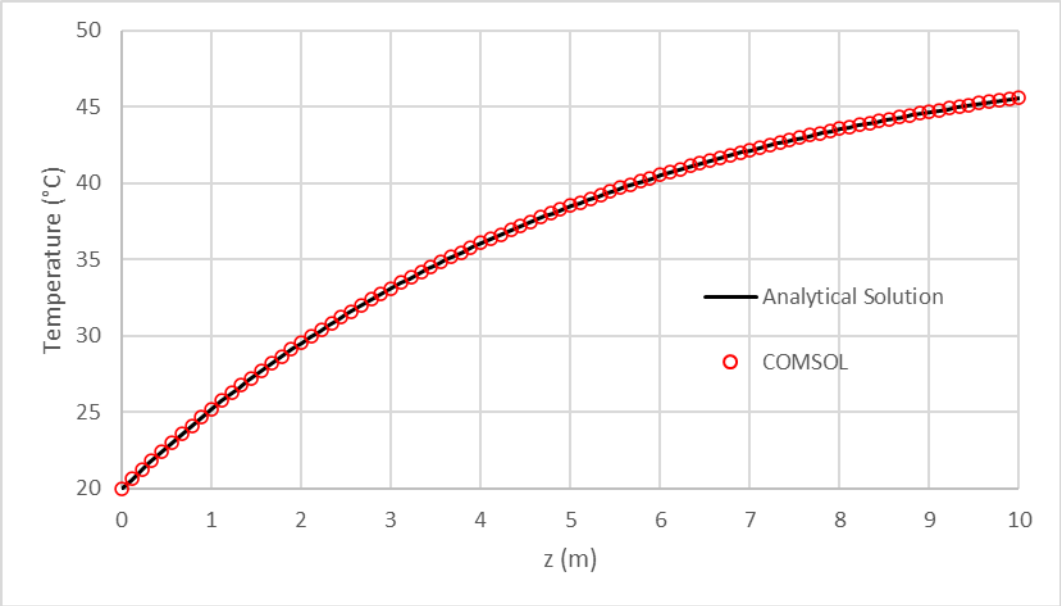

Figure 9: Results of the Constant Heat Transfer Coefficient and Wall Temperature Verification

3. Transient Heat Accumulation

The two previous solutions were both steady state problems and explored the spatial temperature distributions. BHE modelling is typically done for transient problems, and as such, it is important to ensure the transient term properly resolves the thermal mass of the circulating fluid despite the 1D elements lacking a volume, and therefore mass as defined by the three-dimensional geometry. To reduce the problem to one of only time and not also of space, the fluid velocity was set to zero to allow the fluid to respond only to heat transfer from the pipe walls. The equation

$$T_{f,b}(t) = (T_{in} - T_{ext})e^{-\frac{hA}{MC_p}t} + T_{ext} \quad (9)$$

governs the analytical solution to the response of the bulk fluid temperature with boundary conditions that follow the same definition as the constant heat transfer coefficient and external temperature as the second verification. The results are found in Figure 10.

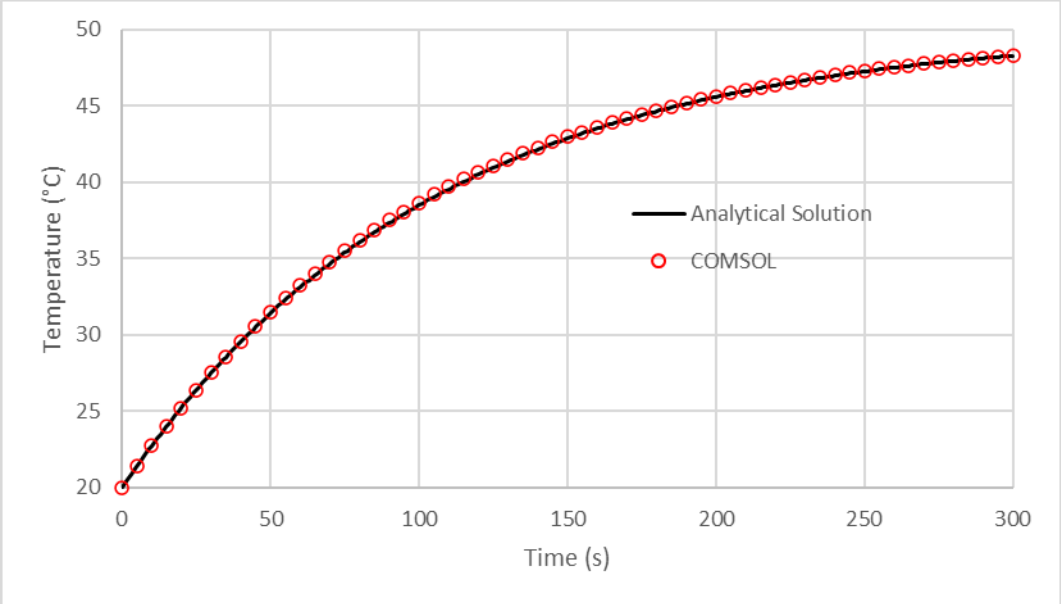

Figure 10: Results of the Transient Heat Accumulation Verification

4. Pseudo Pipe Conduction

Finally, a major component of the model that will be validated later in the thesis is the pseudo pipe, which will be explained further along with the pseudo pipe approach in the next section. To ensure it does not introduce non-physical thermal resistances, the COMSOL solution is compared to an analytical solution of the thermal resistance analogy, that includes internal convection, conduction through the pipe wall and conduction through a surrounding medium, such as soil in BHEs. An illustration of the cross-sectional geometry for the verification and the real-world counterpart are shown in Figure 11.

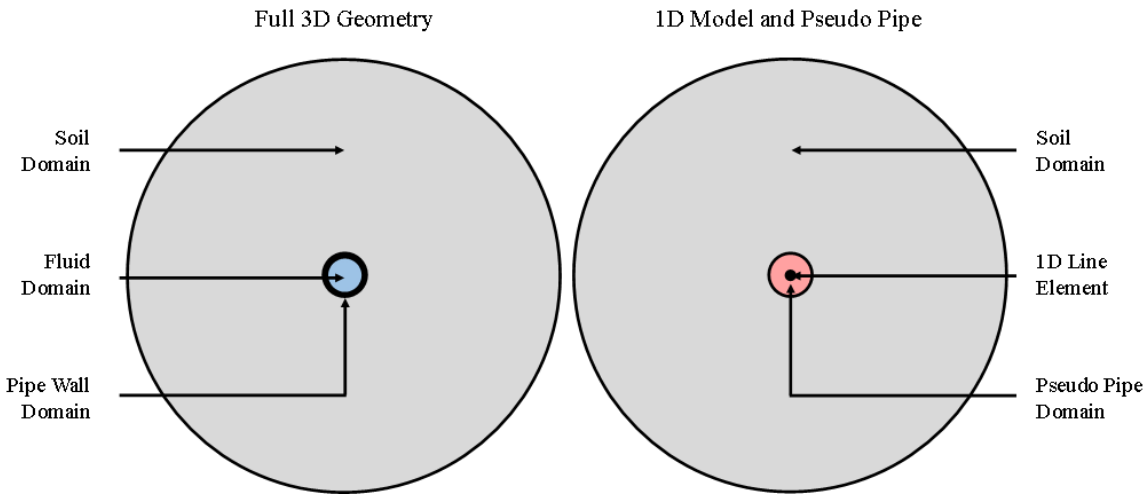

Figure 11: Cross-Sectional Geometry of Pseudo Pipe Verification and Corresponding Full 3D Geometry

The temperature difference between the fluid temperature and the outer edge of the soil domain of the model is compared to a solution using the thermal resistance analogy. The radial temperature distribution of the solution at one axial location is shown in Figure 12 and the analytical solution for the temperature difference can be expressed as the equation

$$\Delta T(z) = q'' A_o R_{Total} = q'' A_o \left(\frac{1}{h A_{w,i}} + \frac{\ln\left(d_{w,o}/d_{w,i}\right)}{2\pi k_w L} + \frac{\ln\left(d_{s,o}/d_{s,i}\right)}{2\pi k_s L} \right) \qquad (10)$$

and is compared to the COMSOL solution in Figure 13.

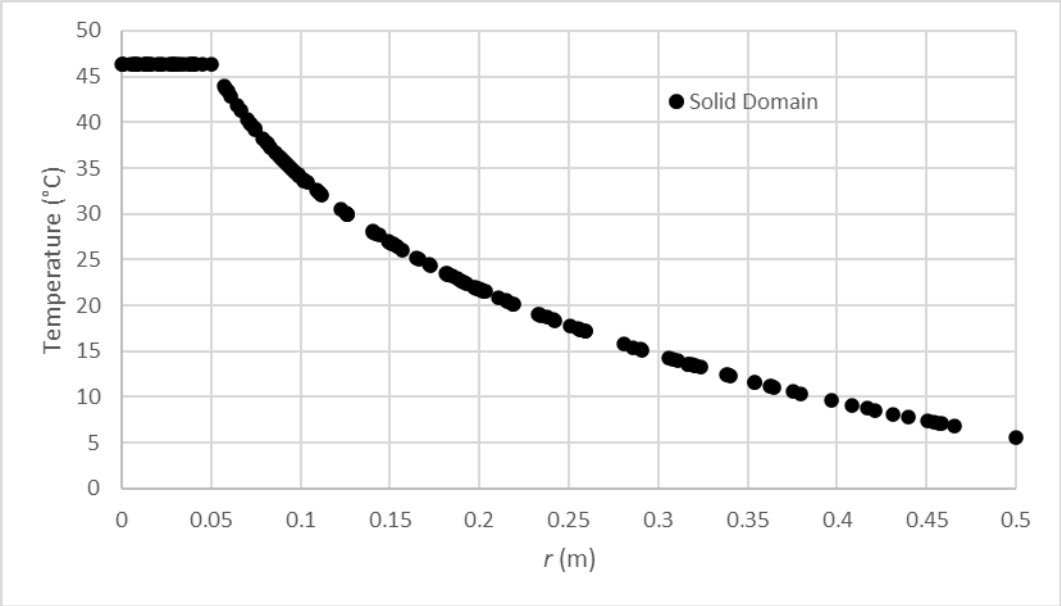

Figure 12: Radial Temperature Distribution at z = 5 m

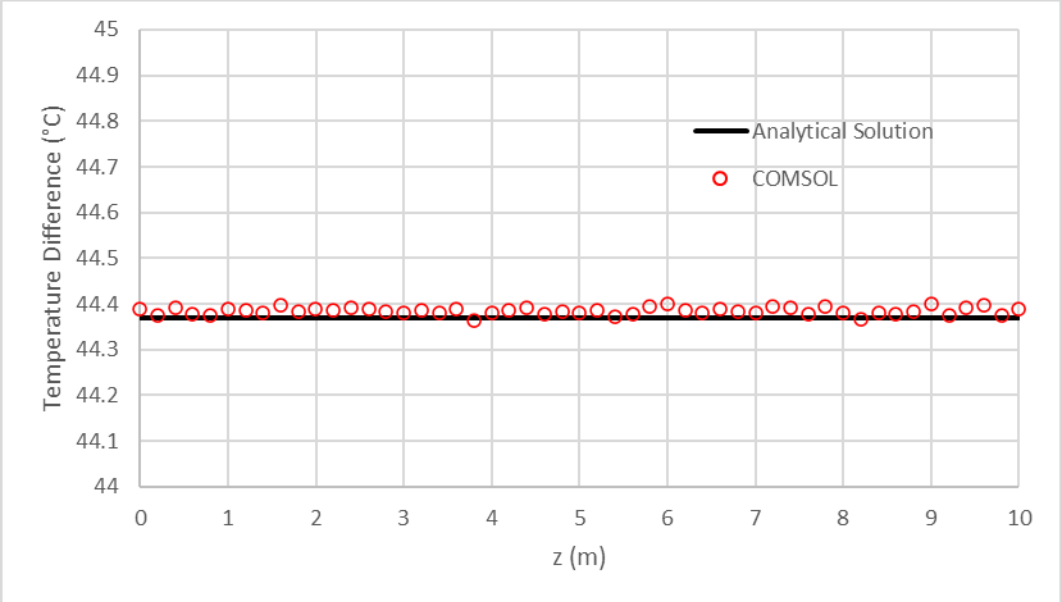

Figure 13: Results of the Pseudo Pipe Conduction Verification

Conclusions

COMSOL's *Heat Transfer in Pipes* interface is shown, through Figures 8-13, to accurately solve a 1D energy equation, analogous to bulk temperature analytical solutions for fluid flow heat transfer. Additionally, it has been shown that the 'pseudo pipe' method accurately couples the 1D pipe elements to the true 3D geometries. The interface can now be combined with the 3D *Heat Transfer in Solids* interface to model borehole heat exchangers in both the fluid and solid domains.

4.2 Description of Pseudo Pipe Approach for Borehole Heat Exchanger Modelling

4.2.1 One-Dimensional Numerical Model for Pipe Flow

Ozudogru et al. [36] proposed a numerical model for vertical U-tube BHEs, which reduces the computational effort of a traditional 3D FEM solution, by coupling a 3D finite element mesh in the solid domains with 1D linear elements for simulating the BHE U-tubes and the internal fluids. The proposed model used the COMSOL software with the *Heat Transfer in Pipes* and *Heat Transfer in Solids* physics. The model uses the principles established in Section 4.1 and increases the overall complexity by incorporating the 1D energy equation for the fluid into a three-dimensional U-tube BHE design. The following section will present additional details of the fluid model as well as the particular boundary conditions utilized by the model.

As presented in Equation 6, the *Heat Transfer in Pipes* physics solves a 1D energy equation within the fluid domain, represented by the equation [82]

$$\rho A C_p \frac{\partial T_f}{\partial t} + \rho A C_p \boldsymbol{u} \cdot \nabla T_f = \nabla \cdot A k \nabla T_f + f_D \frac{\rho A}{2 d_h} |\boldsymbol{u}|^3 + Q_{wall} \tag{11}$$

for incompressible flow with no internal heat generation. The radial heat transfer between the fluid domain and the surrounding solid domain is calculated by the following two equations

$$Q_{wall} = (hZ)_{eff}\left(T_{ext} - T_f\right) \tag{12}$$

$$(hZ)_{eff} = \frac{2\pi}{\frac{1}{r_i h_{int}} + \frac{\ln\left(\frac{r_o}{r_i}\right)}{k_{pipe}}} \tag{13}$$

when there is fluid flow through the centre of a circular, hollow pipe with a single wall material embedded within the solid borehole. The internal film resistance is calculated using

$$h_{int} = Nu \frac{k_f}{d_h} \tag{14}$$

For internal turbulent flow, the Nusselt number is estimated using the correlation developed by Gnielinski [83] as follows:

$$Nu = \max(Nu_{lam}, Nu_{turb}) \tag{15}$$

$$Nu_{lam} = 3.66 \tag{16}$$

$$Nu_{turb} = \frac{(f_D/8)(Re - 1000)Pr}{1 + 12.7(f_D/8)^{1/2}(Pr^{2/3} - 1)}, \qquad \begin{matrix} 0.5 < Pr < 2000 \\ 3000 < Re < 6 \times 10^6 \end{matrix} \tag{17}$$

The friction heat dissipation due to viscous shear, represented by the second term on the right-hand side of Equation 11 is governed by the Darcy friction factor, f_D, which is a function of the Reynolds number and the relative roughness

$$f_D = f\left(Re, \frac{e}{d_h}\right) \tag{18}$$

where

$$Re = \frac{\rho_f u d_h}{\mu} \tag{19}$$

The Darcy friction factor is estimated using the Churchill [84] equation as follows:

$$f_D = 8\left[\left(\frac{8}{Re}\right)^{12} + (C_A + C_B)^{-1.5}\right]^{1/12} \tag{20}$$

where C_A and C_B are factors given by the relationships:

$$C_A = \left[-2.457 \ln\left(\left(\frac{7}{Re}\right)^{0.9} + 0.27(e/d_h)\right)\right]^{16} \tag{21}$$

$$C_B = \left(\frac{37530}{Re}\right)^{16} \tag{22}$$

The Churchill equation, Equation 20, is valid for both laminar and turbulent flows. The symbol, e, is the absolute surface roughness of the inner pipe wall, which is given as 0.0015 mm for thermoplastic pipes.

In this model, specifically Equation 12, the external temperature, T_{ext}, corresponds to the temperature computed in the surrounding solid domain, which couples the pipe flow, treated as a line heat source or sink, to the three-dimensional domain. This method has its limitations, as addressed by Ozudogru et al. [36], which is accounted for in the pseudo pipe approach that is used, explained further in the next section.

The *Heat Transfer in Solids* physics is governed by the equation

$$\rho C_p \frac{\partial T_s}{\partial t} + \nabla \cdot \boldsymbol{q} = 0 \tag{23}$$

$$\boldsymbol{q} = -k \nabla T_s \tag{24}$$

for the case of transient heat conduction without generational heat source or groundwater flow. T_s is the temperature resolved within the solid domain. This physics governs the heat transfer in the solid domains of the borehole and the surrounding soil field.

4.2.2 Pseudo Pipe Approach

The one-dimensional fluid model presented above, despite its vast advantages, presents a few sources of error when connected to an external three-dimensional borehole and soil model, as is. These issues were addressed by the pseudo pipe approach, developed by Ozudogru et al. [36], which connects the 1D linear elements, positioned at the centre axis of the real U-tube, to the 3D borehole domain that exists at the outer boundaries of the U-tube pipe walls. The two main issues that the 1D approximation introduce will be

highlighted here and followed by an explanation of how the pseudo pipe approach removes them from the overall model.

First, although the 1D energy equation considers the contribution of the U-tube pipe wall conduction to the effective heat transfer coefficient, it does not account for the thermal mass of the pipe wall, since it has no method for incorporating the volumetric heat capacity into the energy model. Secondly, the 1D elements transfer heat with the surrounding 3D domain at the position of the linear elements, however the external temperature in the coupling equation, T_{ext}, is the temperature that corresponds to the outer diameter of the hollow pipe, $d_{p,o}$, in the real geometry.

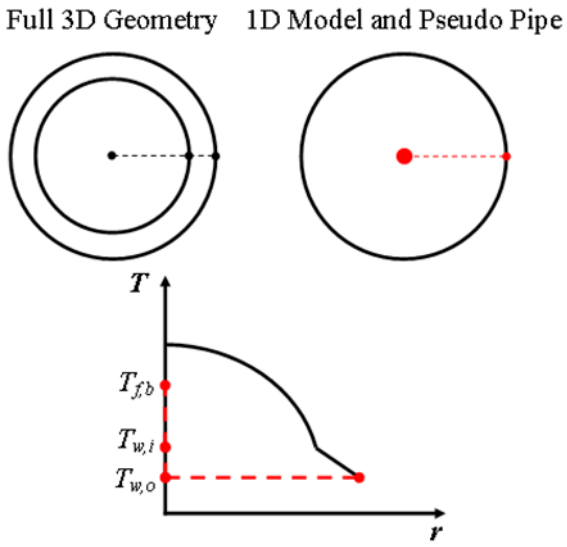

Figure 14: Spatial Distribution of Real and Model Temperatures within a Single Pipe

Figure 14 provides an illustration of the temperature versus radial position within a single pipe for the real geometry and the pseudo pipe model. The temperatures resolved within the 1D model, $T_{f,b}$, $T_{w,i}$ and $T_{w,o}$, refer to the bulk fluid, inner pipe wall and outer

pipe wall temperatures, respectively. The pseudo pipe approach introduces a method which accounts for both the thermal mass of the U-tube and corrects the geometric and temperature coupling error of the 1D pipe elements. The pseudo pipes are solid cylinders that replace the volume of the two separate geometries of the hollow cylindrical pipe walls and the internal fluid domain. Since the solid cylinder is used to represent the thermal mass of the hollow pipe, the density is adjusted to ensure the proper volumetric heat capacity is calculated, by using the effective density

$$\rho_{w,eff} = \rho_w \left(\frac{d_{w,o}^2 - d_{w,i}^2}{d_{w,o}^2} \right) \tag{25}$$

An illustration of the geometry of the borehole and pseudo pipe adjustments can be seen in Figure 15. In addition, the pseudo pipes are given a high anisotropic thermal conductivity (1000 W m^{-1} K^{-1}) in the *x*- and *y*-direction, and zero in the *z*-direction. This corrects the temperature coupling error, since the external temperature calculated at the centre axis of the 1D element, T_{ext}, is immediately conducted to the radial position of the outer diameter of the pipe wall for each axial position, creating a 2D boundary with the exact temperature distribution of the calculated external temperature of the 1D elements.

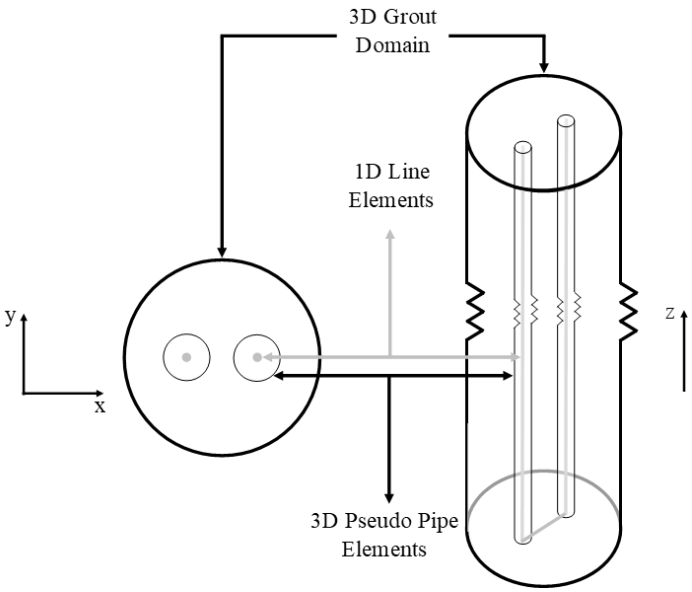

Figure 15: Illustration of Pseudo Pipe Model within a Single U-tube BHE Geometry

Due to the simplified geometry of the *Heat Transfer in Pipes* physics, the temperatures of the fluid and U-tube wall domains are characterized as transient and one-dimensional (varying with axial location z). The application of a high thermal conductivity in the radial direction allows for the pseudo pipe temperature to be reduced to a one-dimensional transient function. This is achieved without causing unphysical thermal conduction in the direction of the flow, by reducing the thermal resistance of the pseudo pipes to a negligible value. The correct heat transfer from the fluid to the exterior of the pipe wall is ensured through the application of Equations 12 to 17.

4.3 Proposal of Model Adjustments using Symmetry Boundary Condition

In FVM and FEM simulations, the application of symmetry, where appropriate, can significantly reduce the necessary computational effort. Since these methods of modelling rely on solving a distributed solution on a discretized mesh, the geometric size is an important contributing factor to the overall computational effort required for each simulation. Symmetry in the overall domain allows for the opportunity to reduce the size of the mesh, and thus the number of nodes, without negatively affecting the resulting solution. A practice common to FV and FE modelling is employing a symmetry plane, which constrains the solution to have a zero gradient at the boundary, so that the solution reflected outside of the final mesh would result in a symmetrical solution for the two domains (the real and the reflected) together. The following section outlines how to apply symmetry to a model that employs the pseudo pipe approach as the one above, inspired by Ozudogru et al. [36], does.

The pseudo pipe approach presents a unique challenge to the use of symmetry planes in FEM simulations, due to the varying dimensions in which the model resolves its equations. Since the U-tube, and its internal fluid domain, are resolved using a 1D energy equation, and is represented physically as a series of line sources which lie within the 3D solid borehole domain, the U-tube has no volumetric component. Since BHE behaviour is symmetric along a plane that lies congruent with the central axes of the U-tube legs, the 1D linear elements are also congruent with the location of the symmetry plane which presents the challenge, since the linear elements have no volumetric component that can be divided in two, like the overall domain. This is illustrated in Figure 16. This model limitation was

acknowledged by Ozudogru et al. [36] in the initial proposal, and it was recommended that a symmetry plane only be used when the symmetry plane does not intersect with the pseudo pipe itself, like in the case of a double U-tube. This is shown in Figure 17, where the cross-sections of a single and double U-tube are compared. The observation was accepted by other researchers who have cited the initial work and incorporated the pseudo pipe approach into their own work [18], [68]. What follows is a method for incorporating a symmetry plane into a single U-tube model without altering the 1D fluid behaviour.

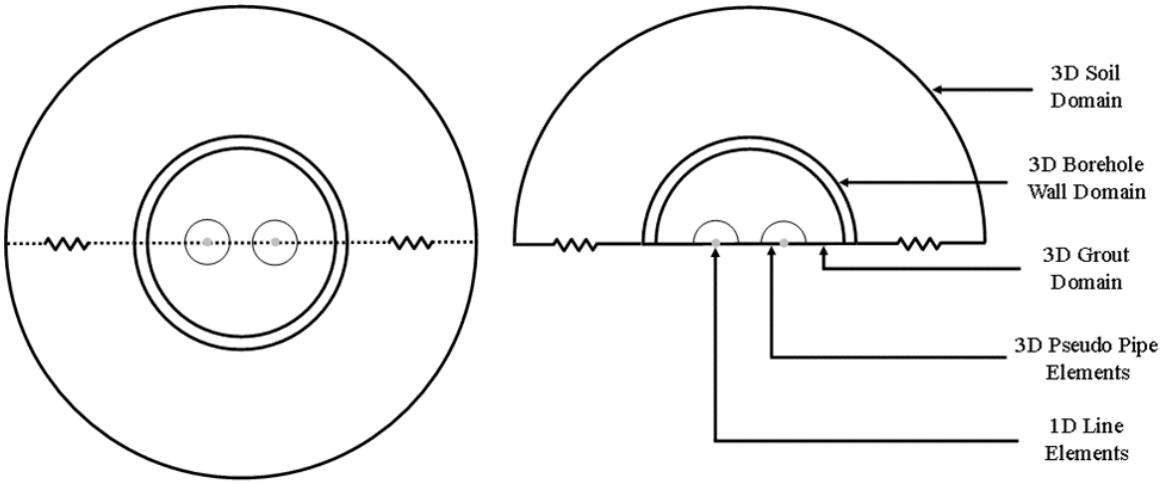

Figure 16: Location of the 1D Linear Elements on the Plane of Symmetry within the Numerical Model

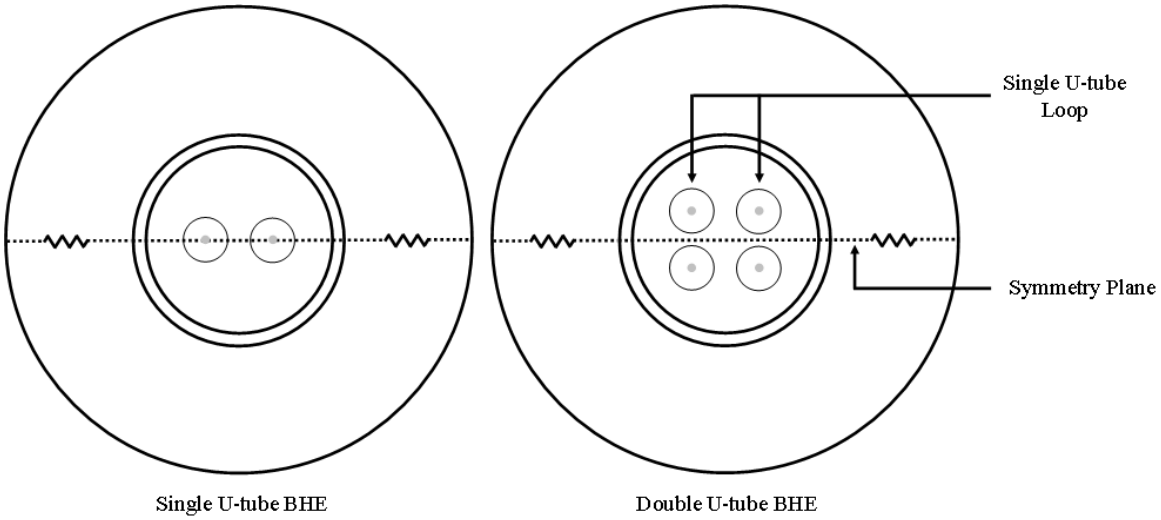

Figure 17: Location of Symmetry Plane in Respect to U-tubes for Single and Double U-tube BHEs

Since the application of a symmetry plane has no effect on a linear element, the portion of the model governed by the *Heat Transfer in Pipes* physics must be independently adjusted to correctly scale the strength of the linear elements by a factor of 0.5. However, the fluid's heat transfer and energy equations are based on prescribed geometry, which is prescribed since the 1D element represents a 3D domain, and therefore it is important to consider the geometric ratios when adjusting the model as to not alter the governing relationships.

The magnitude of the conductive and convective heat transfer terms within the energy equation are both functions of the hydraulic diameter, however only the conductive term scales linearly with the hydraulic diameter and therefore scaling the hydraulic diameter by a factor of 0.5 would cause not only an error in the ratio between the heat transfer terms but also in the magnitude of the overall heat transfer. It is important to scale

each term of the energy equation equally, by a factor of 0.5, to ensure that the same temperature distribution within the fluid is resolved for the half domain as for the full domain, while reducing the radial heat transfer from the 1D element to the surrounding 3D domain by a factor of exactly 0.5. With this in mind, the model was constructed to calculate the correlations found in Equations 12-22 for a full, circular geometry, and then for each term to be properly scaled to ensure consistency with the original pseudo pipe approach. These particular variable adjustments can be found within the Appendix.

4.4 Validation of Pseudo Pipe Approach

4.4.1 Introduction to Experiment

Beier et al. [17] created an experimental data set to be used by researchers as a validation tool for BHE models. In order to control the experimental data, and collect spatially accurate soil temperature data, a large ‘sandbox’ was created in a laboratory, containing a borehole with a U-tube. Two tests were published in the original work [17], and both will be used to validate the pseudo pipe approach, in its original form and with the model adjustments proposed in this work to apply symmetry to a single U-tube BHE model.

The first test replicates a TRT, applying a constant heat input to the circulating fluid for a period of 52 hours. Although it was intended that the sand begin the test at uniform temperature, it was revealed in a later paper by Beier [85] that there was enough variation in the initial temperature to warrant consideration. The fluid in the U-tube is circulated

through the length of the borehole as well as the electric heater, which applied the nearly constant heat input to the system. Thermistors were placed at twenty-two locations throughout the system to monitor the temperature response to the constant heat input. Two thermistors measured the fluid temperature, at the supply to, and the return of, the BHE. Twenty thermistors were spread through out the sand at specified axial and radial locations to accurately map out the resulting temperature field. Average temperatures at the radial locations were calculated in the experimental work and will be compared to the numerical model's results in this thesis. A more in-depth illustration of the location of these thermistors was found in the original work, and is provided here in Figure 18 [17].

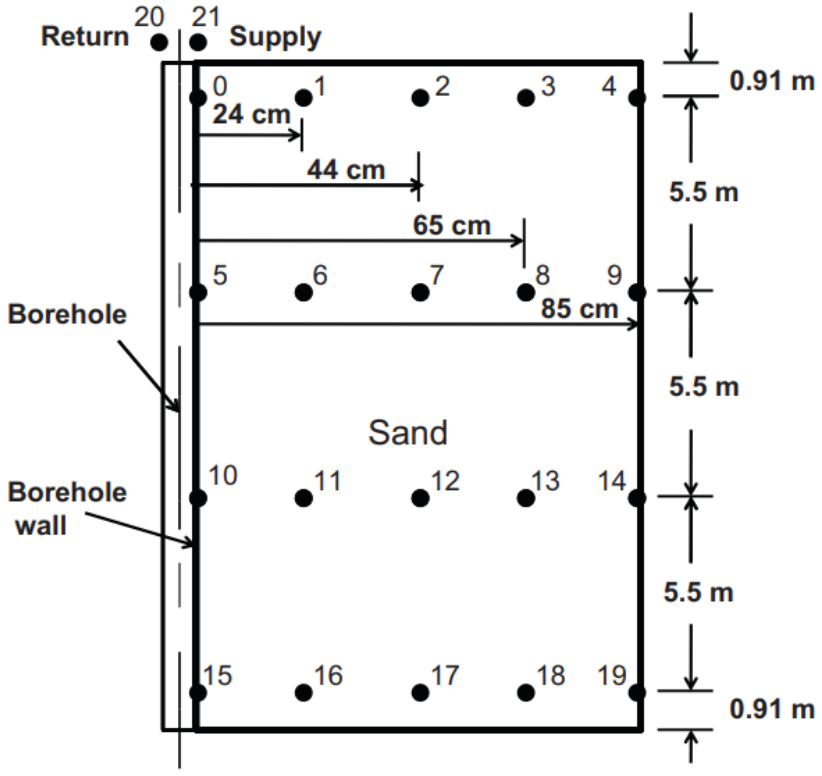

Figure 18: Locations of Thermistors in Beier et al.'s Experimental Sandbox [17]

The second test simulated the case of a TRT which is interrupted by a power outage to the external pump and heater [17]. An interruption to normal conditions occurs after 9 hours of operation and lasts for 2 hours before the heating is once again applied for the remainder of the 52-hour test. The purpose of this scenario was to establish whether experimental data that is gathered with a period of interrupted flow and heating could still be used for the purposes of a TRT. The data, however, is useful to validate the correlations used in the 1D fluid model of the pseudo pipe approach.

The geometric properties and the material properties of the sandbox are summarized in Tables 2 and 3. The geometry was replicated in the numerical model and the material properties were used as the model inputs. Although the thermal conductivity of each material was given in the original work [17], the volumetric heat capacity was not explicitly published until the work by Beier [85]. Just as the uncertainty of the initial sand temperature was explored in the later paper by Beier [85], uncertainties for the geometric and material properties were also given.

Table 2: Geometric Properties of Experimental Sandbox

Parameter	Unit	Value	Description
Borehole inner Diameter	cm	12.6	Aluminum pipe
Borehole pipe thickness	cm	0.2	Wall thickness of aluminum pipe
U-tube length	m	18.3	SDR 11 (1-in.)
U-tube outer diameter	cm	3.340	SDR 11 (1-in.)

U-tube pipe inner diameter	cm	2.733	SDR 11 (1-in.)
Distance between centers of pipe	cm	5.3	High density Polyethylene

Table 3: Material Properties of Experimental Sandbox

Material	Unit	Value	Description	Reference
Pipe Wall Thermal Conductivity	W/(m·K)	0.39	Centre of U-tube pipes	Beier et al. [17]
Soil thermal conductivity	W/(m·K)	2.82	Wet sand	Beier et al. [17]
Soil Density	kg/m^3	1789*		
Soil Specific heat capacity	J/(kg·K)	1789*		
Soil Volumetric heat capacity	kJ/(m^{3}K)	3200		Beier et al. [85]
Grout Thermal conductivity	W/(m·K)	0.73	Bentonite	Beier et al. [85]
Grout Density	kg/m^3	1949*		
Grout Specific heat capacity	J/(kg·K)	1949*		
Grout Volumetric heat capacity	kJ/(m^{3}K)	3800		Beier et al. [85]

* Individual values used to ensure volumetric heat capacity was equivalent to source

4.4.2 Sandbox Boundary Conditions

The external boundary conditions of the numerical model were set to estimate the real conditions of the experimental set-up. Figure 19 is an illustration of the boundaries of the sandbox with relevant information provided in the work [17]. The sandbox was constructed with a wood frame to enclose the sand, with the dimensions of

18m×1.8m×1.8m. In Beier et al. [17], it is stated that the ends of the wooden sandbox were insulated, and so Neumann boundary conditions were applied to set the axial heat flow at the ends of the sandbox to be 0,

$$q^{"} = 0 \tag{26}$$

Stated in the reference data set [17], was that air at a constant temperature was circulated throughout the laboratory that housed the sandbox. Without any further information, an assumption was made that natural convection could be applied, governed by a constant external temperature and a constant heat transfer coefficient. At the four outer boundaries of the sand domain, labelled as the wooden frame in Figure 19, a heat flux condition was applied which can be expressed

$$q^{"} = h(T_{ext} - T) \tag{27}$$

$$\left.\begin{array}{l} h = 5\,W/m^2K \\ T_{ext} = 22.1\,℃ \end{array}\right\} \tag{28}$$

The entire system is initially set to the constant room temperature of 22.1°C. As previously stated, the real initial sand temperature for the experiment was found to be 22.1 ±0.2 °C, as reported in Beier [85].

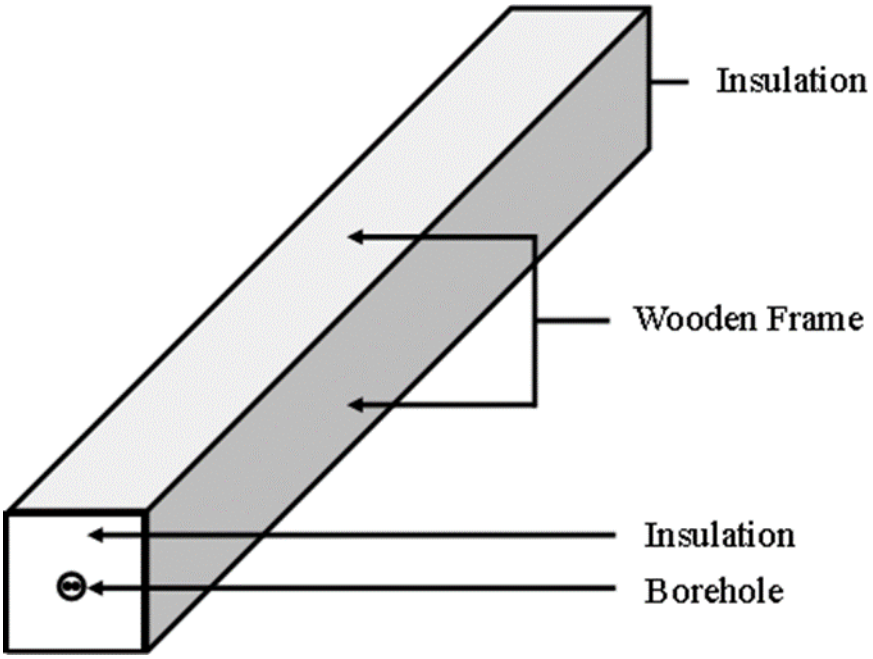

Figure 19: Description of Beier et al.'s [17] Experimental Set-Up

4.4.3 Fluid Boundary Conditions

A unique boundary condition was applied to the fluid domain for each of the two tests. For the constant heat input test, the inlet fluid temperature and the volumetric flow rate of the experimental data were provided to the author by Beier [86] in tabulated form and were applied as a variable boundary condition at the BHE inlet. Figure 20 shows how these values fluctuated with time. Although the target of the flow rate was a constant, in order to reduce fluctuations in the instantaneous heat input, it took approximately 20 hours to reach a nearly steady value. The temperature, however, rose much more steadily due to the heat capacity of the fluid decreasing the impact of these high frequency fluctuations.

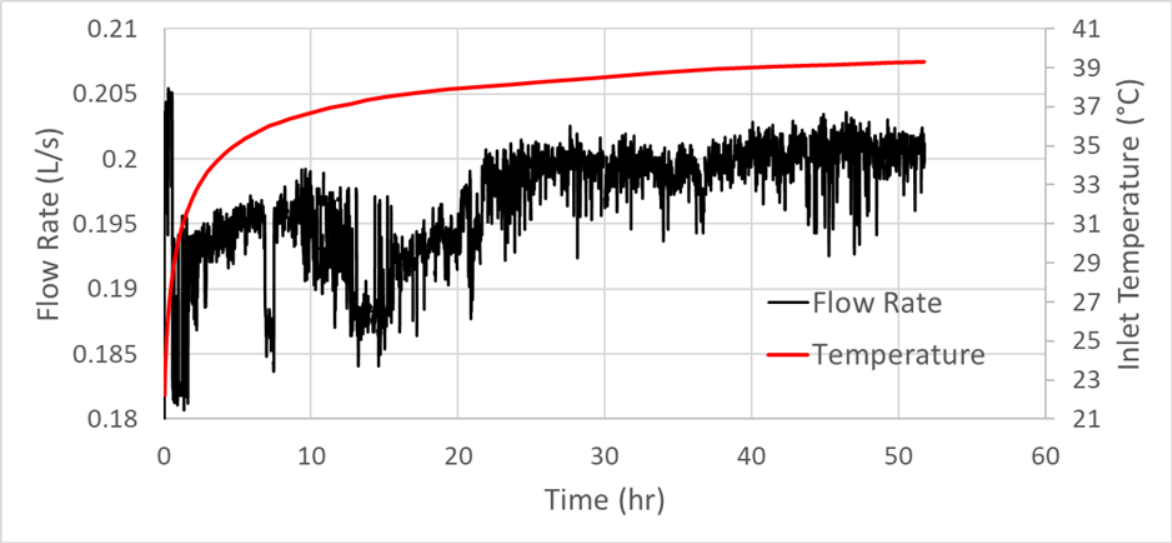

Figure 20: Simulation Fluid Inlet Conditions as Found in Experimental Data

The raw data for the interrupted test was less readily available, as the only figures provided in the original work displayed the electrical power to heater, the flow rate of the pump and the normalised temperature rise of the average loop temperatures. As such, the boundary conditions were adjusted to apply a constant heat input to the fluid between the return and supply of the BHE at each timestep, instead of an explicit temperature profile at the supply side. As the test includes a period of interruption, a constant heat input was applied between the time periods of 0-9 hours and 11-52 hours, with no heat applied from 9-11 hours. The same time periods were applied to the variable flow rate. As stated in the original work [17], the heat input rate was decreased from 1056 W in the constant heat input test to 600 W in the interrupted test, and so the value of 600 W was applied as the external heat source. The effective heat input rate will be investigated in the same manner as the constant heat input rate to ensure the boundary conditions were appropriately adjusted.

4.4.4 Meshing

Appropriate meshes were necessary to validate both the original model and the proposed symmetrical model. These meshes were created to reflect the method described by Marcotte and Pasquier [14], who developed a computationally efficient mesh based on knowledge of BHE operation. The local size of the mesh elements, and the relative size in the radial and axial directions, reflect the approximate temperature gradients that must be resolved in order to increase computational efficiency while maintaining mesh independence. The size of the elements is largest in the axial direction, particularly within and near the borehole itself, due to the low axial gradients in relation to the radial gradients. Additionally, these radial gradients reduce as the radial position increases.

Although Marcotte and Pasquier [14] developed the mesh for a fully 3D solution, including the fluid domain, the basic principles can be applied to a mesh for the pseudo pipe approach, as made evident by its use in Ozudogru et al. [36]. The same techniques that were used in the 3D solution are used in this validation, however the mesh within the pseudo pipes and in the 1D fluid domain is much coarser due to the 1D energy equation approximation.

Table 4 provides information on the mesh nodal values for each solution, and Figures 21 and 22 show the resulting distributions. The blue circles were added to highlight the border between the pseudo pipes and the grout, since the total mesh could seem to be a single geometry. The slight differences in the full and symmetrical geometries' meshes is due to the mesh accommodating the flat plane at the central axis of borehole; otherwise the

meshing techniques were identical. Although the technique by Marcotte and Pasquier [14] called for a much coarser mesh in the axial direction, the density was slightly increased to ensure a mesh independent fluid temperature distribution. Mesh independence testing was completed to ensure the highest accuracy when comparing to the experimental data.

Table 4: Meshing Statistics for Beier Validation

Domain	Original Mesh Elements	Symmetric Mesh Elements
Soil	62,744	45,356
Borehole Wall	8,280	5,060
Grout	19,373	14,863
Pipe U-Tube	-	-
Fluid	946 (1D)	940 (1D)
Pseudo Pipe	1,288	1,656
Total	92,631	67,875

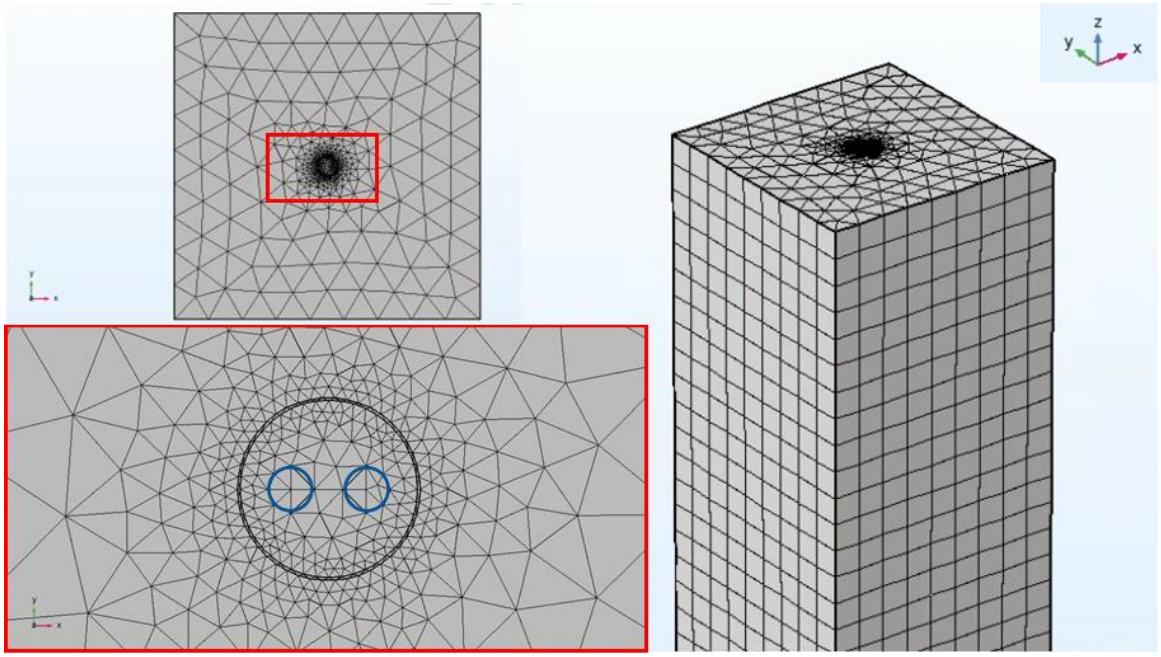

Figure 21: Finite Element Model Mesh for Full Geometry

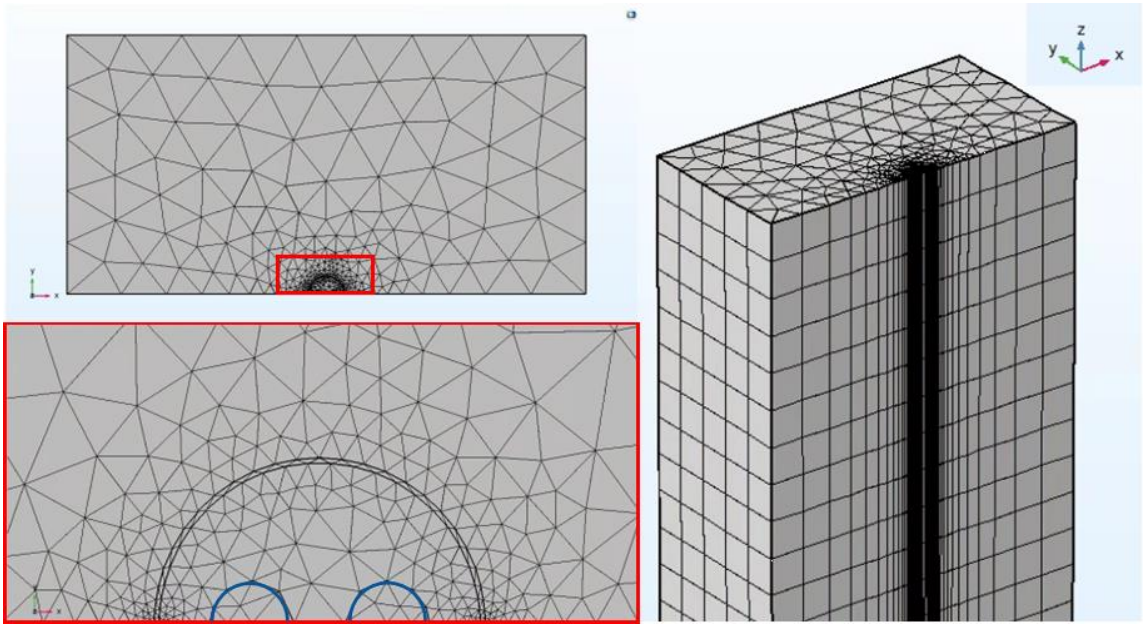

Figure 22: Finite Element Model Mesh for Symmetry Geometry

4.4.5 Validations

4.4.5.1 Constant Heat Rate Test

The performance of the original model and the proposed improvements can now be compared to the experimental data presented in Beier et al. [17]. Figure 23 a) shows the response of the return fluid temperature to the imposed inlet boundary temperature profile and compares it to the experimental data of the reference data [17]. Due to the small scale of difference, the model difference is also displayed in Figure 23 b), calculated as

$$T_{rtn,diff} = T_{rtn,model} - T_{rtn,exp} \tag{29}$$

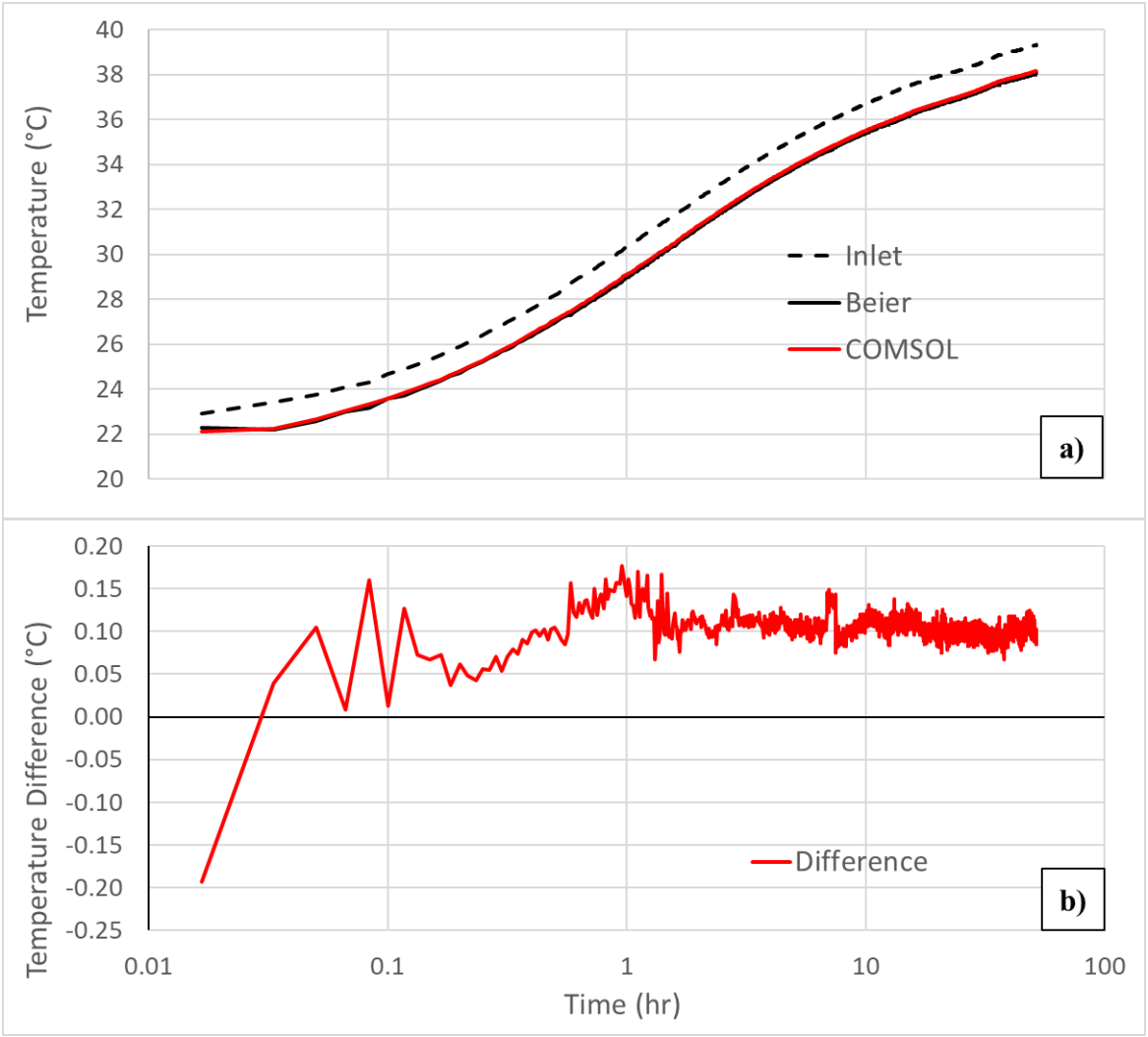

Figure 23: Fluid Temperatures (a) and Return Temperature Difference (b) for Numerical Model

The largest difference occurs at the first timestep, revealing the uncertainty of the initial conditions for the experimental data. Although it was stated that the system was initially at the undisturbed room temperature of 22.1°C, there is already a gradient within the fluid temperature, that reflects the uncertainty of the surrounding sand temperatures [85]. This difference is quickly reduced once the heat transfer occurs between the borehole and the sand as the fluid residence time, the time that it takes for the fluid to circulate

throughout the whole BHE, is 112 seconds. The difference converges to a consistent value of approximately 0.1°C after 1-2 hours of operation (Figure 23 b)). This remaining disagreement between the model and experimental data is within the experimental uncertainty that is extensively explored with the later work of Beier [85]. This paper investigated sources of uncertainty in the original reference data set, including publishing the uncertainty of material properties, geometry, heat input rates, and the undisturbed sand temperatures. The uncertainty of the initial sand temperature is ±0.2 °C, which is greater than the nearly steady difference of the model return temperature.

The fluid temperature difference can be used to estimate the heat input rate, as it was in the experimental work, using the mass flow rate through the heater

$$Q = \dot{m} c_p \left(T_{sup} - T_{rtn} \right) \tag{30}$$

The calculated heat input rates for both the model and the experimental data are provided in Figure 24. The average heat input rate for the model, 966 W, is lower than the experimental average, 1056 W, due to the slightly higher return fluid temperatures of the model seen in Figure 23. This, in turn, reduces the temperature difference through borehole at the same mass flow rate, lowering the heat input rate. The high frequency fluctuations are due to the variable mass flow rate which was applied to the model as a boundary condition, explaining their presence in both the experimental and model solutions.

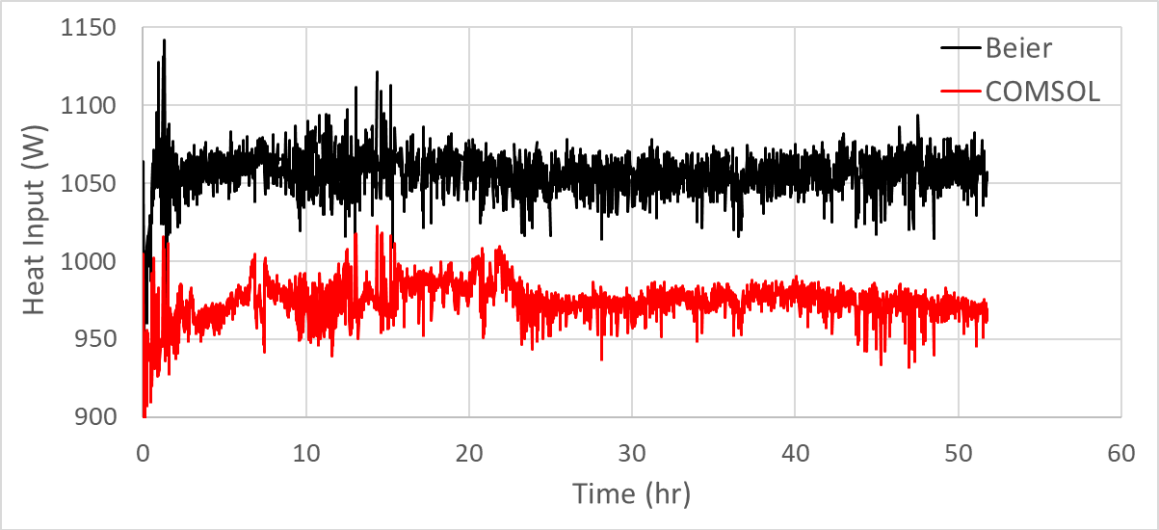

Figure 24: Comparison of Calculated Heat Input Rates for Experimental and Numerical Data

The average sand temperatures for five radial locations from the borehole wall are compared in Figure 25. It can immediately be seen that the initial temperature distribution in the sand is not uniform for the experimental data. Like the fluid temperature, the difference between the model and measured temperatures within the sand is calculated using the equation

$$T_{s,diff} = T_{s,model} - T_{s,exp} \tag{31}$$

where $T_{s,exp}$ is the average temperature of the experimental data at discrete radial locations as measured by the thermistors. Despite the initially higher temperatures in the model solution, the error tends to the opposite trend in the later tests, with negative temperature errors accompanied by negative slopes. This divergence from the experimental data is largely in the region of the semi-log plot that is linear, which occurs at different time values for each radial position and suggests a constant uncertainty that is causing a different in the

thermal resistances that govern the heat transfer. This is well explained by the uncertainties revealed in Beier [85], particularly in the material properties, which alter the overall thermal resistance of the borehole, sand or both. This would result in a different slope in the linear portions of Figure 25 a), causing the ever-increasing error seen in Figure 25 b). Despite all this, the errors seen in both the fluid and sand domains (Figures 23 and 25, respectively) are within the uncertainty values of the initial sand temperatures, of ±0.2 °C.

Although the authors of the original data set reported incredibly low temperature measurement uncertainties (±0.03 °C) [17], this value seemed unrealistic and was further clarified in multiple later works. This value appeared once again, in another paper by Beier et al. [87], which represented the standard deviation of the undisturbed ground temperature measured over a three-day period, rather than the uncertainty of the instantaneous temperature measurement itself. Instead, in this source the uncertainty of the thermistor was reported as the more realistic value of ±0.1 °C [87]. This value was deemed more reasonable, and appeared in additional research done by Beier et al. [88]. Since this uncertainty is applied to both the supply and return temperatures, this represents approximately 1% of the overall temperature difference through the borehole at the end of the test, which is a significant value. Unfortunately, this temperature difference is a function of the overall borehole length, which is constrained due to the size of the indoor sandbox.

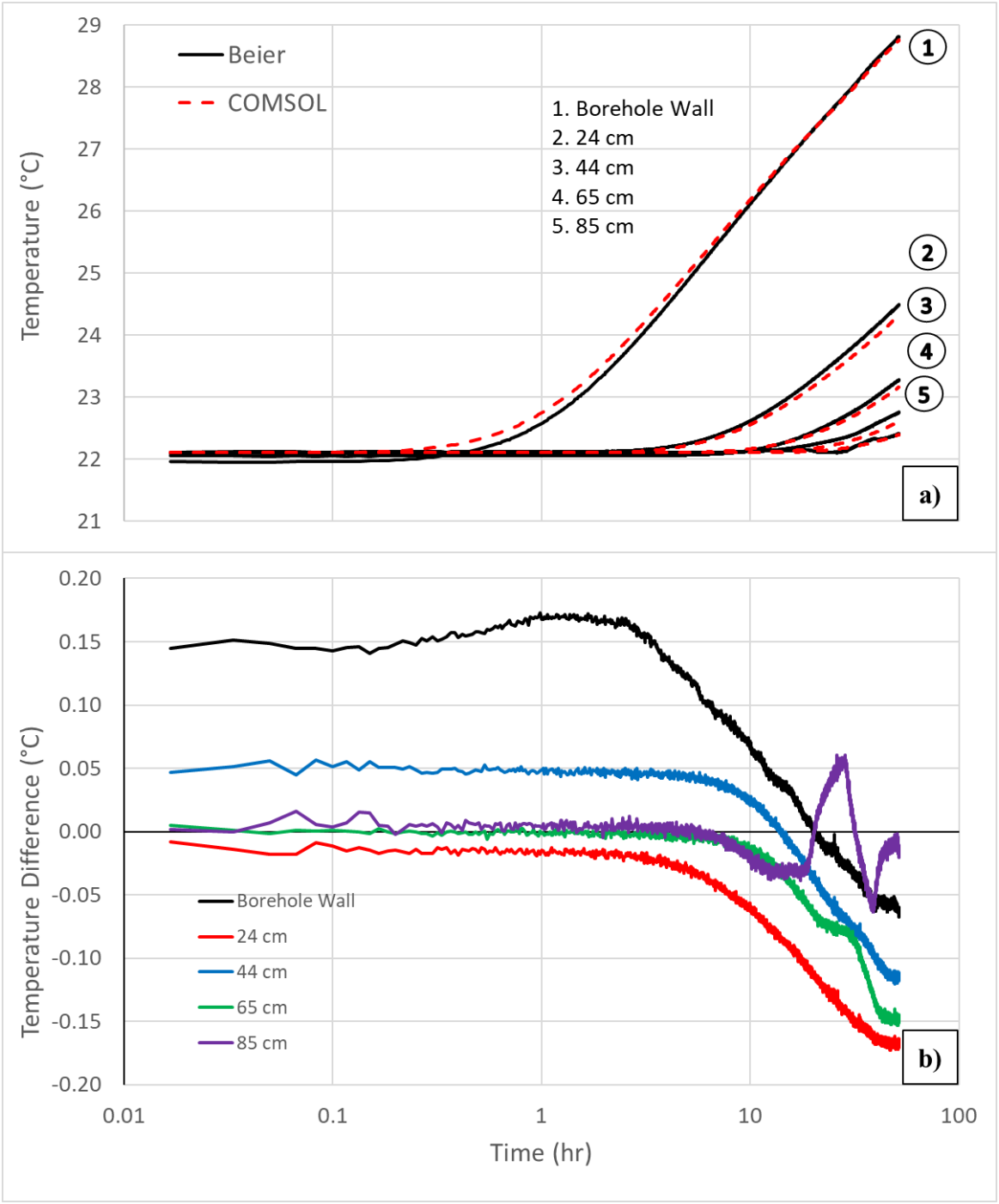

Figure 25: Soil Temperatures (a) and Temperature Errors (b) for Numerical Model

The borehole thermal resistance, a common value used in BHE modelling, can be independently estimated using the fluid temperature, the borehole wall temperature, and the heat input rate. This is calculated by

$$R_b = \frac{\Delta T}{q} \tag{32}$$

$$\Delta T = T_{f,ave} - T_{borehole\ wall,ave} \tag{33}$$

and is a quantifiable metric of the total resistance of the entire borehole composition. $T_{borehole\ wall,ave}$ is the average borehole wall temperature, and the heat rate per unit length, q, is a nominal value based on the average heat input rate, not an instantaneous heat injection value based on supply and return temperatures. This heat input rate is evaluated when the borehole has achieved a steady temperature difference, as seen in Figure 26 a). This temperature difference, and subsequently the borehole thermal resistance, begins to reach a steady value around the 20-hour mark, which is consistent with the experimental data presented in Figure 12 of Beier et al. [17]. The difference between the model and experimental solutions is also presented in Figure 26 b), which plots the difference

$$\Delta T_{diff} = \Delta T_{model} - \Delta T_{exp} \tag{34}$$

for each timestep. The highest error occurs at the start of the test, due to the previously discussed non-uniformity of the initial experimental sand temperature. However, the overall trend of the error is increasing for the majority of the test, suggesting a systemic cause for error in the borehole domain. The error present in the borehole temperature difference suggests at least a portion of the model error previously discussed is due to

uncertainty in the borehole thermal resistance, which is governed by the material properties of the borehole grout and the U-tube walls. However, this error represents approximately 1% of the total borehole temperature difference, and so the combination of the 1D fluid domain and 3D grout domain can be considered a successful method for resolving a transient borehole thermal resistance.

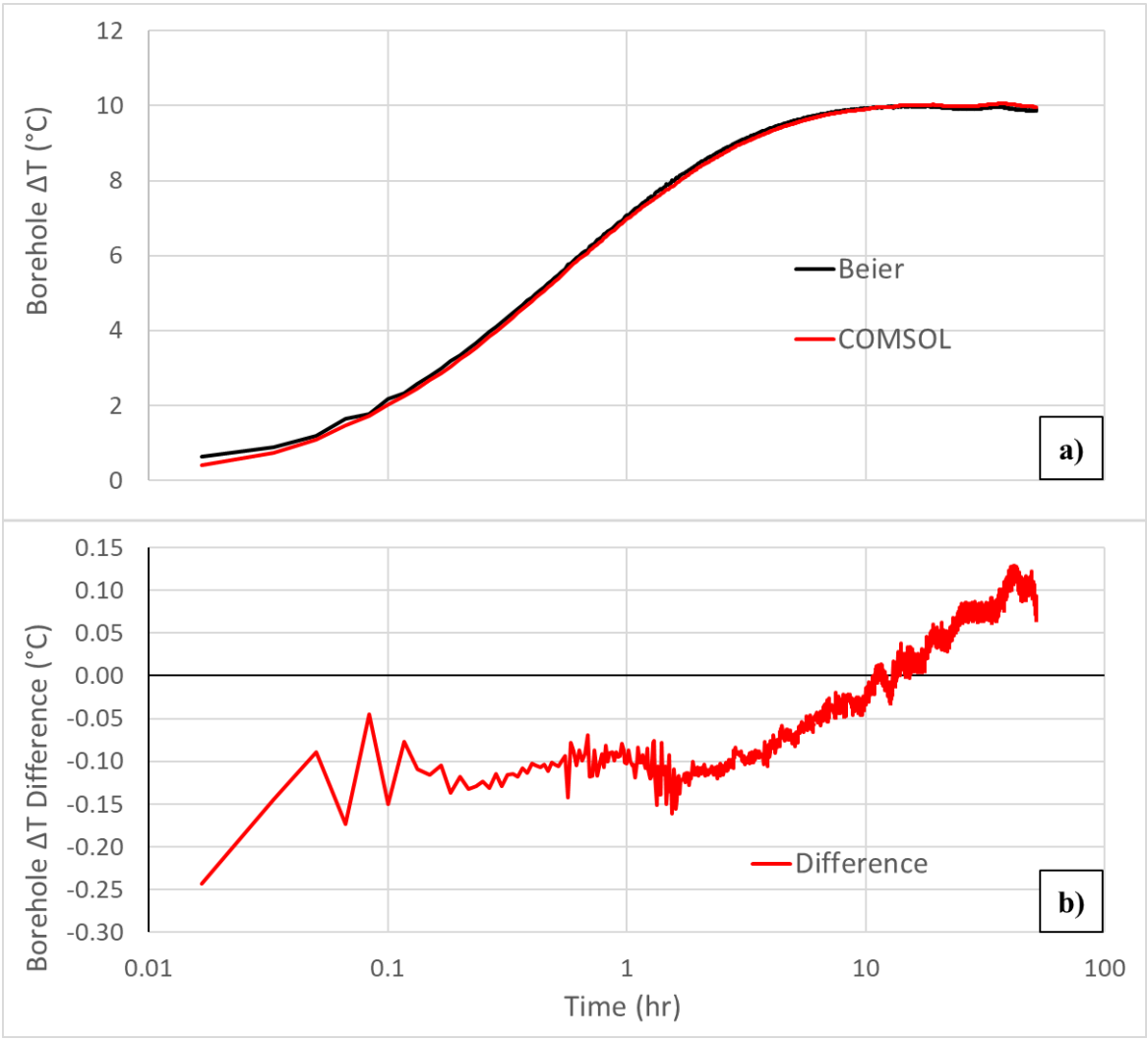

Figure 26: Borehole ΔT between Fluid and Borehole Wall (a) and Difference Between Predicted and Measured Value (b) for Numerical Model

Figures 27 and 28 show a comparison between the fluid and soil temperatures of the full and half domains, respectively. The solutions are nearly colinear, with some round-off errors caused by small differences in the respective meshes. This proves the adjustments to the pseudo pipe method to apply symmetry have ensured the correct magnitude of energy is transferred between the 1D elements and the 3D solid domains despite the U-tube's location on the symmetry plane. This allows for the reduction of the computational effort using a symmetry plane for a single U-tube model, in addition to the double U-tube model, while employing the pseudo pipe approach.

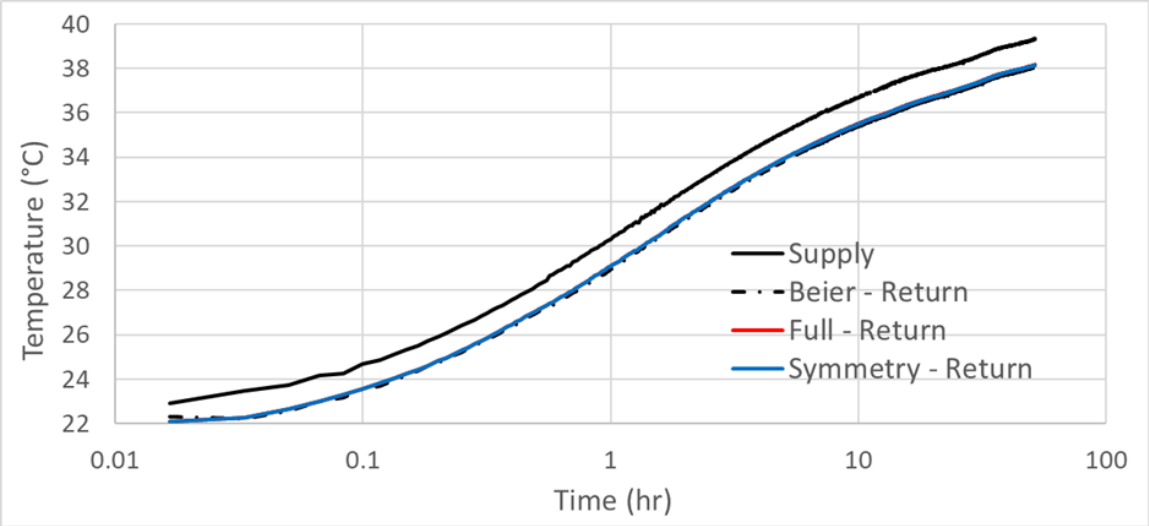

Figure 27: Comparison of the Fluid Return Temperatures for the Full and Symmetry Geometry Solutions

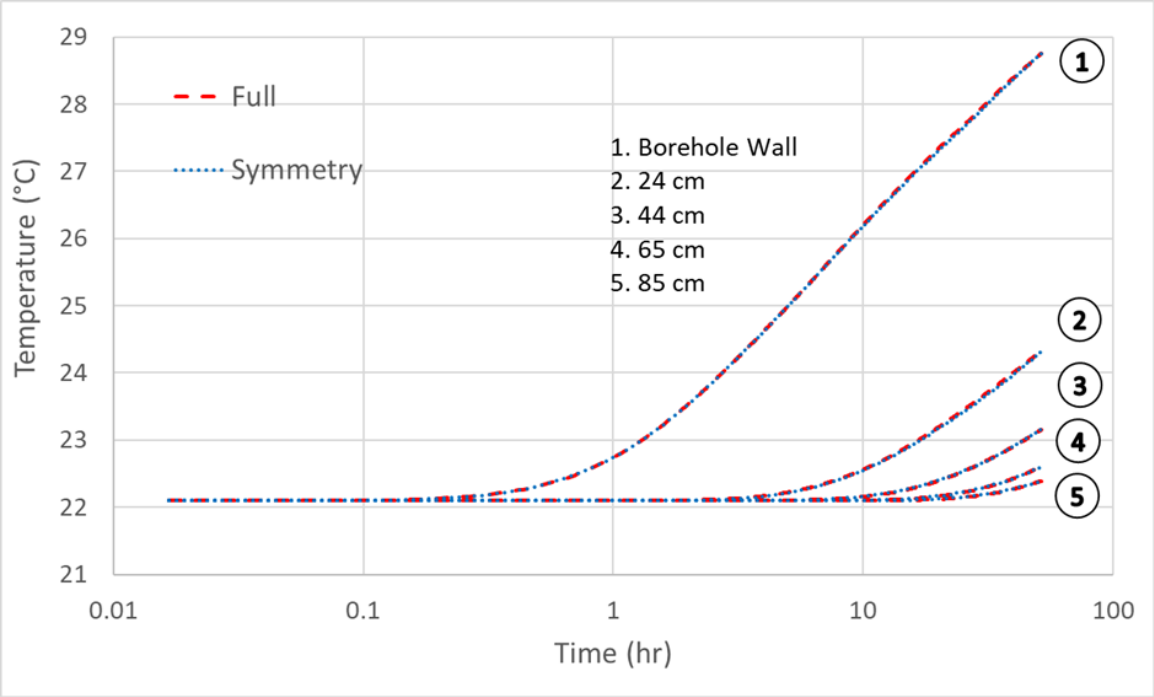

Figure 28: Comparison of the Soil Temperatures for the Full and Symmetry Geometry Solutions

4.4.5.2 Interrupted Flow Test

When correlations are used in lieu of direct numerical analysis, there is the possibility that the model will fail to properly resolve specialized operating conditions that conflict with the empirical relationships and/or assumptions made by simplified models; in this case, the 1D energy equation of the fluid. A specific condition of interest is when the circulating fluid stops flowing, whether the pump shut-off is intentional or nor. This may be due to intermittent GSHP use or due to power failure, respectively. For the model to be considered robust and capable of complex, long-term GSHP simulation, its important that the model can properly resolve the heat transfer when flow has been driven to zero.

Just as in the case of the constant heat input test, the measured heat input for the interrupted flow case was calculated using Equation 30, which well reflected the model input. The heat input and the applied flow rate are shown in Figure 29. The normalized temperature rise, as described in Beier et al. [17], allows for the comparison of results for different heat input rates, and is the change in temperature from the undisturbed value multiplied by the ratio of the heat inputs. The temperature rise of the interrupted case is normalized to compare to the temperature rise from the constant heat rate test, and can be described using the equation

$$\Delta T_{Normalized} = \frac{q_{uninterrupted}}{q_{interrupted}} \Delta T_{interrupted} \tag{35}$$

A comparison between the normalized temperature rise of the two tests is shown in Figure 30. The fluid temperature response to the flow interruption is incredibly consistent between the model and the experimental data. In both solutions, there is a sudden decrease in the average fluid temperature, which recovers to the original curve of the uninterrupted once the power is reintroduced.

It should be noted that there was no available experimental temperature data during the power interruption, between hours 9 and 11, and therefore the linearly decreasing section in the experimental data is not populated by data points, but only connects the experimental values on either side of the disruption. During the test interruption, the power to the heating unit is cut off and the water stagnates, but due to the large temperature difference between the fluid and surrounding borehole, the heat transfer continues, despite the loss of the convective forces. As outlined in Equation 15, COMSOL sets the lower limit

of the heat transfer to be $Nu_{lam} = 3.66$, which is shown to be a reasonable value to mimic the heat transfer in pipes driven by natural convection, when the pump is shut off and flow has been driven to zero.

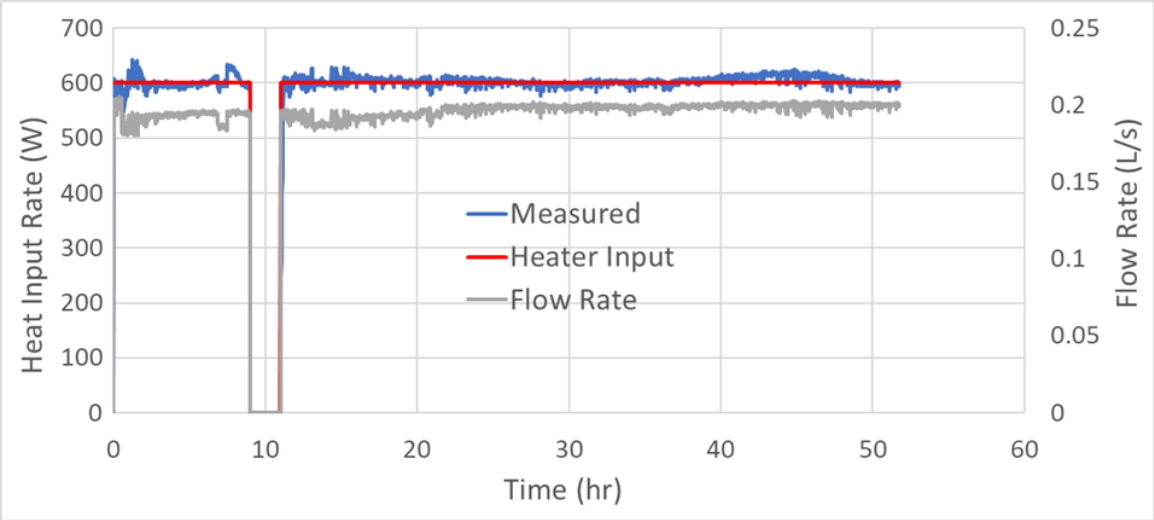

Figure 29: Heater and Pump Conditions for the Interrupted Heat Test Validation

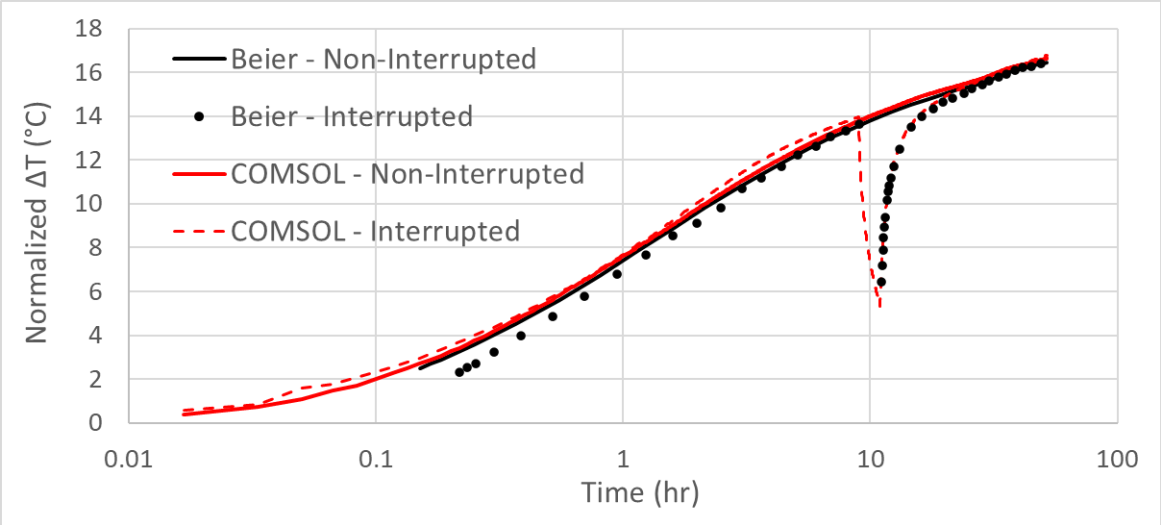

Figure 30: Normalized Temperature Rise of Constant and Interrupted Heat Tests

4.5 Conclusions

With these validations, it becomes clear that the pseudo pipe approach is a robust method for BHE modelling, which can accurately recreate experimental results in a variety of situations. In BHE applications, the flow details within the U-tube are of little importance compared to the bulk temperature of the fluid at each axial location, and therefore is a misallocation of computational effort. Despite the original findings of the authors [36], it is possible to successfully apply a symmetry plane to a single U-tube BHE model using the pseudo pipe approach. This is possible with a few small adjustments and will reduce the three-dimensional domain of the model used in this thesis by a half. Finally, the model still properly resolved heat transfer without active fluid flow through the U-tube, and thus can be used in long-term simulation for a wide range of load profiles, which may include seasonal system shutdown. The section that follows will describe how to apply variable load profiles to the model validated here.

The above validations employed an imposed, transient temperature profile at the inlet, since the information was available from the experimental data of Beier et al. [17]. However, this data is not available in every case that may require simulation, and therefore a method for employing a variable COP heat pump model into the overall fluid model was developed. The details of this model are presented in Appendix A.3.

Chapter 5 – Effect of the Far-Field Conditions on the Solutions of BHE Models using FEM Approaches

5.1 Introduction

FEM (and FVM) approaches to research are increasingly common across many areas of engineering due to the increased efficiency and computational power of modern computers. In the context of borehole heat exchangers, these approaches allow for much more freedom in the model complexities, including boundary conditions and borehole geometry, than the analytical methods. FEMs require discretized meshes, however, which typically require much higher computational effort than other modelling approaches, and the computational cost is sensitive to the domain size. The domain size, in turn, can be influenced by the extent which the presumed boundary conditions influence the solution on the interior of the domain and the time duration of the simulation. This contrasts with typical analytical BHE models, which often apply boundary conditions at infinite limits, and can also be shown to place limits on the possible time duration of transient solutions for BHE modelling.

A version of the composite model that only employs the three-dimensional domains for the soil region can be used to illustrate the need for a model with flexible far-field soil conditions. A solution was employed using the heat pump model and load profile developed in Appendix A.3, and an overview of the results can be used to illustrate the problem with long-term simulation. Figure 31 displays the radial temperature distributions at various times throughout the solution that range from $t = 0$ and 5 years. It can be seen, in Figure

31, that for all points during simulation, with a fluctuating load that has a period of 1 year, the radial temperature distributions quickly develop to equivalent values that are only a function of the time of year, and not of the overall time that the borehole has been operating. The cause of this can be further clarified by looking at a specific point along this radial line, which is displayed in Figure 32. A point at $r = 4.5\ m$ was chosen due to its proximity to the outer boundary. It can be seen that between 1 and 2 years the solution has already reached a pseudo steady-state where, as previously stated, the temperature is only a function of the time of year and not of the overall time of operation. For the true operation of a borehole with a thermal imbalance ratio of -82.71% (Appendix A.3.3), the soil temperature around the borehole would be degrading as more energy is extracted than injected on a yearly basis. Due to the temperature constraint at the edge of the 3D domain, the thermal energy is replaced from the external boundary at magnitudes far higher than in true borehole operation. This is due to two limitations to this type of simulation, since the thermal mass of the surrounding soil is too low, due to the small volume represented in the geometry, and the temperature constraint at the boundary causing higher temperature gradients to be resolved in the interior of the soil domain, increasing the thermal energy flow at the external boundary.

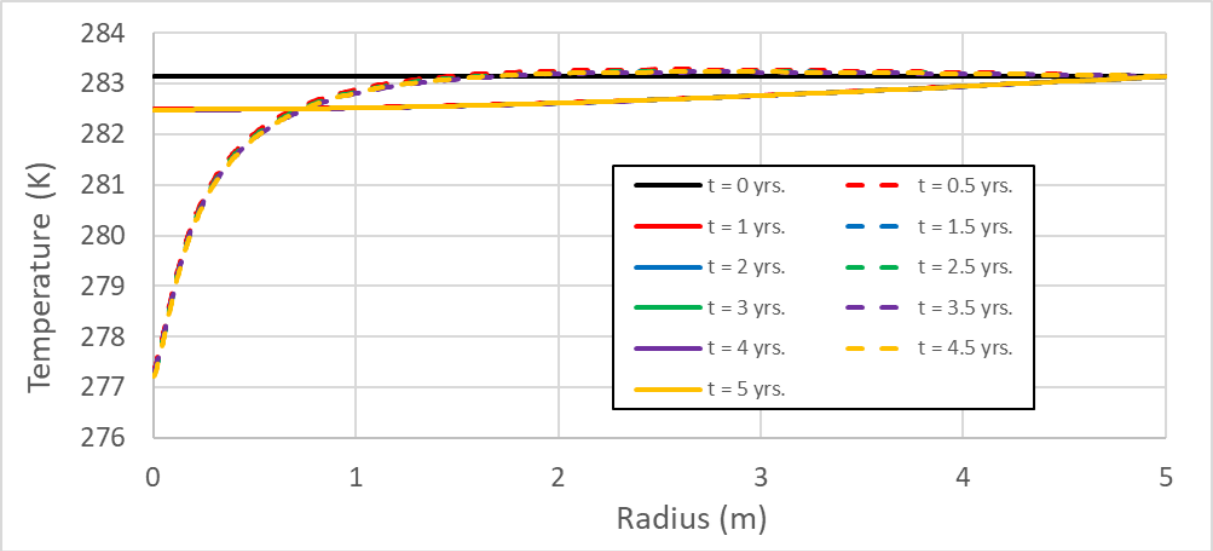

Figure 31: Radial Temperature Distributions for Composite Model with Only 3D Soil Domain

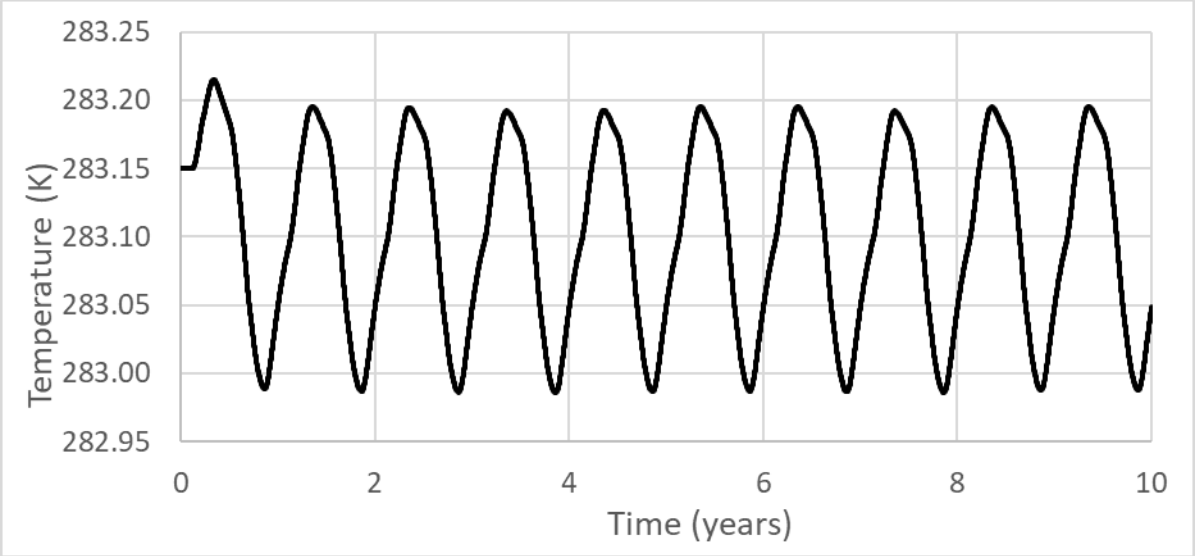

Figure 32: Transient Temperature Data at r = 4.5 m for Composite Model with Only 3D Soil Domain

This error causes a wide variety of problems with the model, the most important of which is illustrated by the data shown in Figure 33. The BHE outlet temperature is a major driver of the COP of the heat pump, and thus the efficiency of the entire GSHP system. Since the soil temperature surrounding the borehole has been driven to a false pseudo steady state, the fluid temperature within the borehole remains a function of the time of year, but not the overall operation time. Therefore, the GSHP system would not experience any change in the system behaviour or efficiency, which would appear in real borehole operation due to the thermal imbalance of the load. Therefore, the model becomes of little use to long-term studies, since the change in soil conditions each year, and its effects on efficiency, is what is of primary interest.

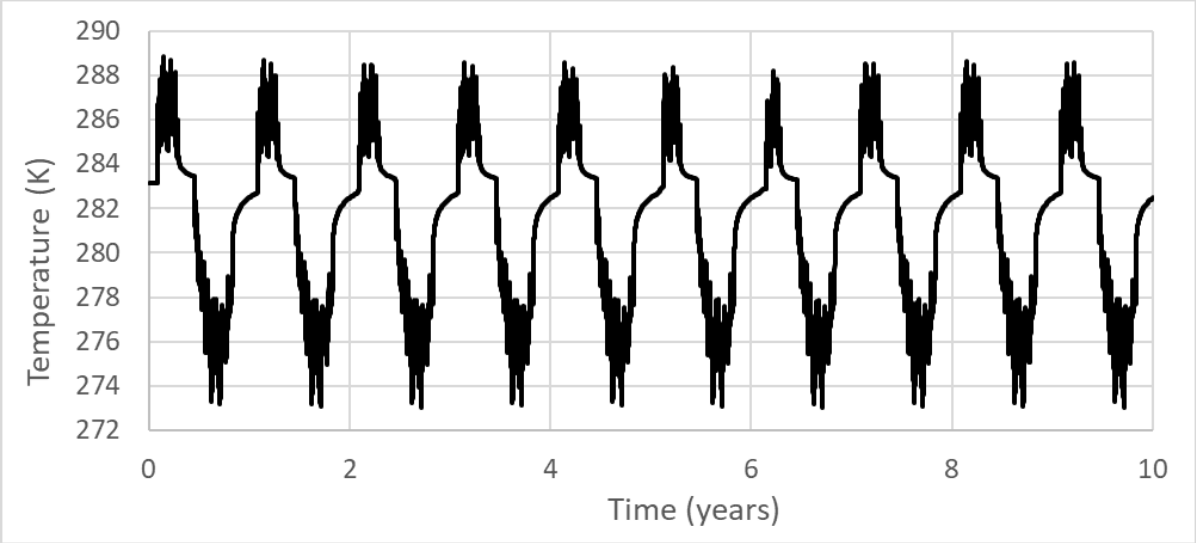

Figure 33: Transient Borehole Fluid Outlet Temperature Data for Composite Model with Only 3D Soil Domain

In summation, it is important to ensure the outer boundary condition does not affect the model for the borehole. Increasing the domain size for three-dimensional heat transfer would cause intensely high computational costs, and therefore an alternative method was developed in this work. The following section will develop a method for considering system performance in the context of heat balances, the effect of a superficially imposed far-field boundary condition and a proposal for a new method of determining the thermal impact of borehole operation, which can help to ensure model independence of outer boundary conditions.

5.2 Development of Radial Heat Flow Variable

The Infinite Cylindrical-Surface Source Model (ICSSM), outlined in the thesis introduction, will be used as a basis for the development of the radial heat flow variable, due to the convenience of the way in which the mathematical formulations are defined. The ICSSM is entirely dependent on radial heat transfer, which allows for the domain to be conceived of as a series of hollow cylinders of infinitesimal thickness. The benefit of this will become clear in the following section.

When a model becomes enclosed within a control volume, as it does in finite element models, an energy balance can be applied. For the ICSSM, there is no mass transfer through the boundaries of the model, as there is no borehole domain and no groundwater flow, and therefore the energy balance can be expressed as:

$$\frac{dE}{dt} = \sum_i \dot{Q} \tag{36}$$

where $\frac{dE}{dt}$ is the change of the energy within the system in time and $\sum_i \dot{Q}$ is the sum of the boundary heat flows. Due to the geometric size and the dramatic temperature gradients within the system, this cannot be treated as a lumped system and must be discretized. Since the ICSSM is a radial model and neglects axial heat conduction (Equation 2), there is zero heat transfer through the ends of the hollow cylinder that encapsulates the domain between the borehole radius, r_b, and the outer radius, r_o. The heat flow is a set boundary condition at the inner radius, r_b, but as previously mentioned (Equation 2) the outer boundary condition is a set temperature.

Since the variable for the finite element model is temperature, T, and it is the heat flows, $\dot{Q}$, that are of interest for the energy balance, we can devise an equation to calculate the radial value as a function of radius and time, $\dot{Q}_{rad}(r,t)$. Since there is no axial or angular heat transfer, the heat flow per unit length can be calculated as the heat flux through a circle of radius, r

$$\dot{Q}_{rad}(r,t) = 2\pi r \cdot \dot{q}_{rad}(r,t) = -2\pi r k_s \frac{\partial T}{\partial r} \tag{37}$$

with the same form as the Neumann boundary condition at $r = r_b$. This variable is a useful metric when discussing borehole heat exchanger models as it contextualizes the relationship between the temperature gradients within the soil and the energy balance in an axisymmetric context. Even in simplified mathematical models, such as the ILS, FLS and

ICSSM, a simple analytical function for the temperature cannot be defined due to the reliance on various Bessel functions [26], and therefore a function for the derivative is also not possible. However, in FEM solutions the temperature derivatives can easily be resolved numerically.

5.3 Influence of the Boundary Location on Radial Heat Flow Variable

Since the mathematical formulation of the ICSSM sets the boundary condition at the limit of infinity, which is not possible within an FEM solution, the effect that the location of the external boundary has on the solution should be investigated. Through investigating the effects of the external boundary location in the solution to even a simple case study, it will become clear that it is imperative that the solution to borehole heat exchanger simulations must be independent of the far-field boundary condition.

This can be done using a simple model such as the ICSSM. Four different domain sizes were employed, with external boundary radii of 10, 50, 75 and 150 m, and Equation 38 was applied as the load for each iteration

$$Q_{load}(t) = -\frac{(Q_{max} - Q_{min})}{2}\sin\left(\frac{\pi}{182.5}t\right) + \frac{(Q_{max} + Q_{min})}{2} \tag{38}$$

where t is the time in days, Q_{max} is the peak heating load and Q_{min} is the peak cooling load.

The dimensionless temperature excess and heat flow are calculated using the equations

$$\varphi = \frac{4k\pi(T - T_{und})}{q_l} \tag{39}$$

$$\sigma = \frac{-2\pi r k_s \frac{\partial T}{\partial r}}{q_l} \tag{40}$$

respectively. The radial temperature distributions at the end of the transient solution, ten years, is compared for each solution in Figure 34. In Figure 34 a), it can be seen that the solution for the smallest domain is incredibly dependent on the location of the boundary. The influence of the borehole operation has reached far past the location of the boundary, and thus there is a high amount of error in the temperature distribution. The error is smaller, but still visible for the 50 m domain, shown clearly in Figure 34 b), and the error between the 75 and 150 m solutions is negligible, comparatively. Additionally, the domain size is influencing the interior temperatures, not only the temperatures at the outer boundary, as it can be seen in Figure 34 b), that the divergence in the solutions extends back into the interior, to at least 35 m. How far back, and by what percentage, this error extends is a function of not only space, but time and therefore it is of interest to isolate the solutions for particular radial positions and compare the temperature distributions in time as well.

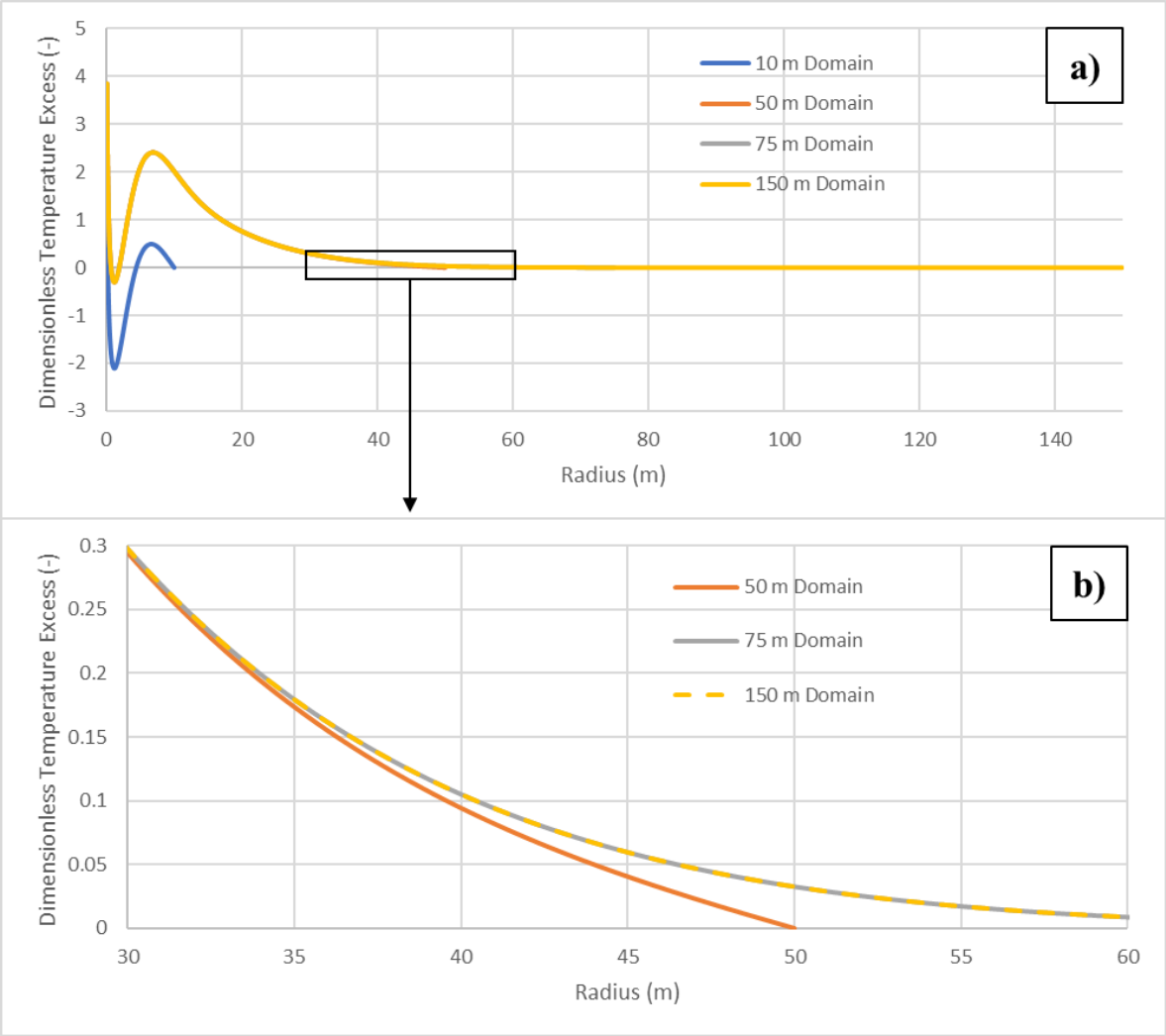

Figure 34: Radial Distribution of Dimensionless Temperature Excess a) Entire Domain b) Point of Divergence

First, the dimensionless temperature excess and heat flow are compared at the smallest external radii value, in Figure 35. Since the external boundary condition is set to the undisturbed temperature, Figure 35 a) shows that the temperature response in the larger domains cannot be replicated in the minimum domain size. Additionally, the fluctuations in the dimensionless heat flow are much higher in the 10 m domain than in any of the larger domains (Figure 35 b)). The larger domains have much larger thermal masses due to the

increased soil volume, which allows for the absorption or rejection of much higher magnitudes of energy with significantly lower temperature responses. Thermal mass has a dampening effect on the heat flow since the temperature gradients are lower for the same energy imbalance when the soil volume increases.

The heat flow at 10 m (Figure 35 b)), while fluctuating, has also reached a pseudo steady-state for the 10 m domain, while the average heat flow is still in the transient phase for the three larger domains. For the 10 m domain, the dimensionless heat flow begins to fluctuate around the value of 1.0 after only a few years, with the maximum heat flow occurring at the peak of the first year. This diverges significantly from the other solutions, which clearly shows the average heat flow value increasing yearly with a diminishing rate of change, roughly in the same fashion as a logarithmic function. This decrease in the time it takes to reach the pseudo steady-state would have dramatic effects on soil temperature distribution and, in turn, the overall system performance of a realistically operating borehole heat exchanger.

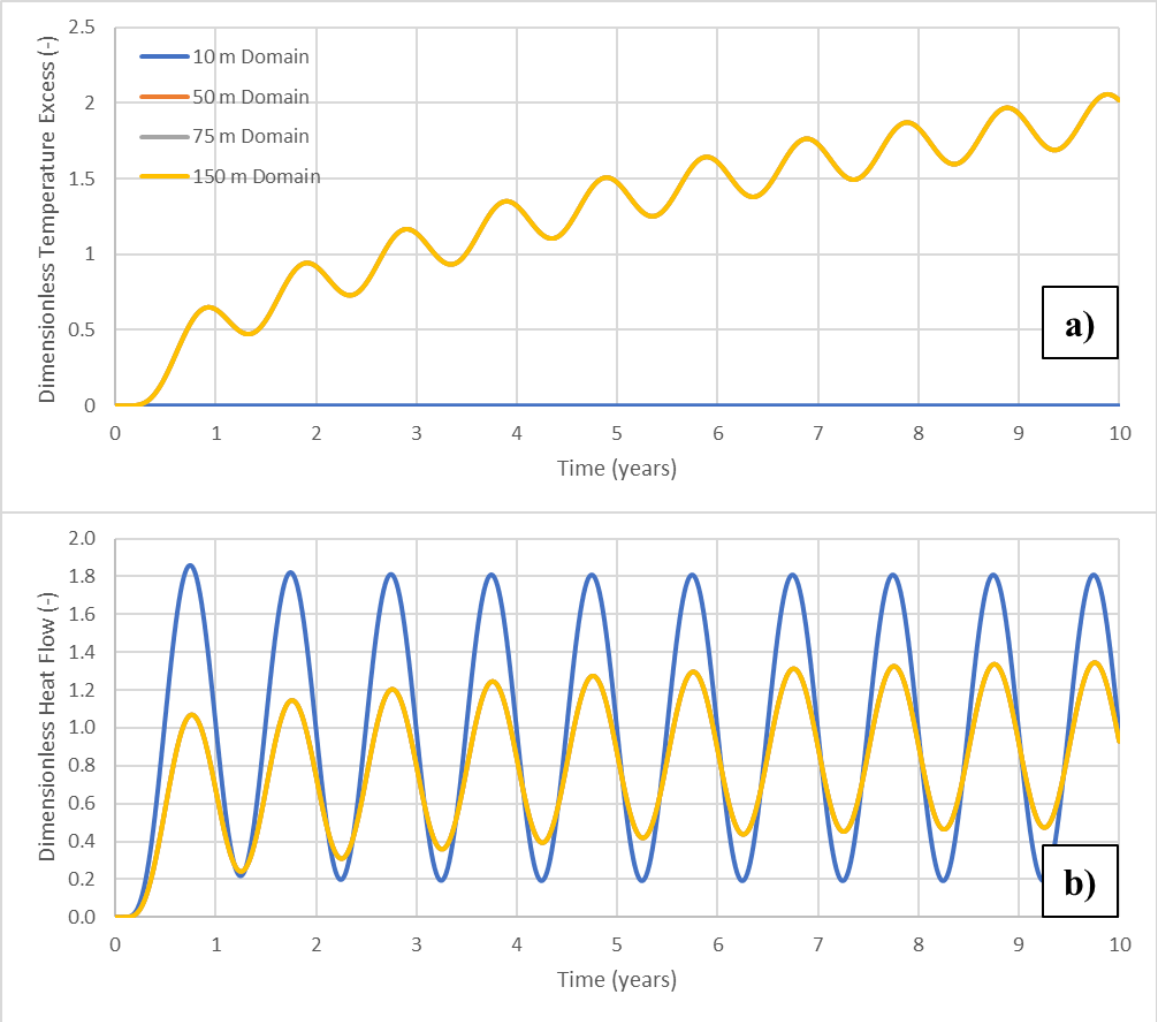

Figure 35: Dimensionless Temperature Excess (a) and Heat Flow (b) at r = 10 m

Previously the radial temperature distributions were compared, but the radial heat flow distributions are also of interest. Presented similarly to Figure 34, the dimensionless heat flow distribution for each solution is shown in Figure 36.

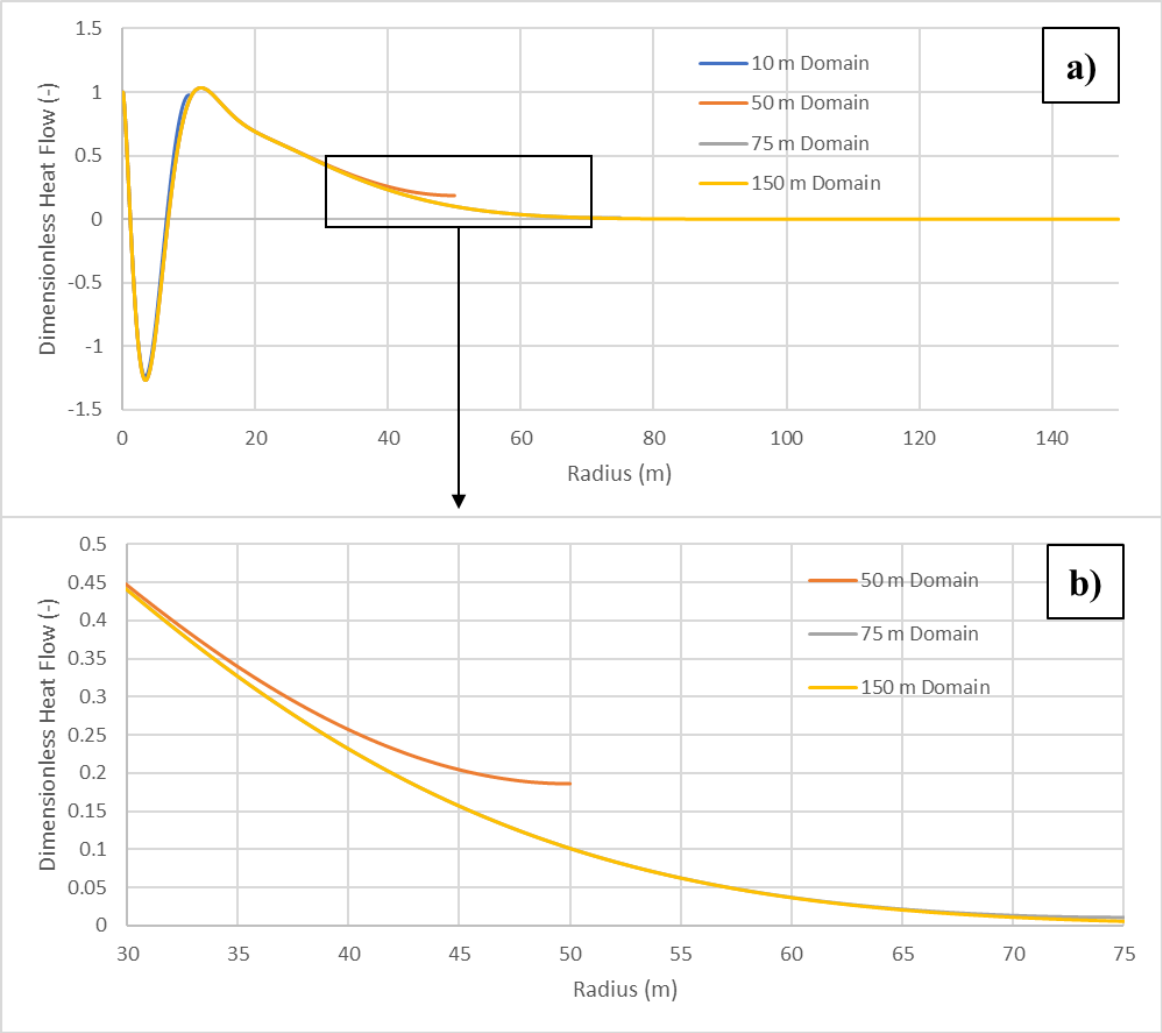

Figure 36: Radial Distribution of Dimensionless Heat Flow a) Entire Domain b) Point of Divergence

Consistent with the previous observations, the solutions for the 50 m solution and the larger domains diverge once the heat flow reaches the external boundary of $r = 50\ m$. As the temperature excess is constrained at this point, the temperature gradients within the far-field begin to increase in magnitude at a faster rate than the boundary independent solutions, which results in higher dimensionless heat flow when the radial location is the boundary, rather than within the solution domain (Figure 37). Similar to the decrease in

time it takes to reach a pseudo steady-state that was seen in the soil near the borehole (Figure 36), higher heat flow values are found at the boundary of smaller domains. This value will approach the dimensionless value of 1.0 much faster than boundary independent solutions which, when combined with the undisturbed temperature restraint, results in a pseudo steady-state solution.

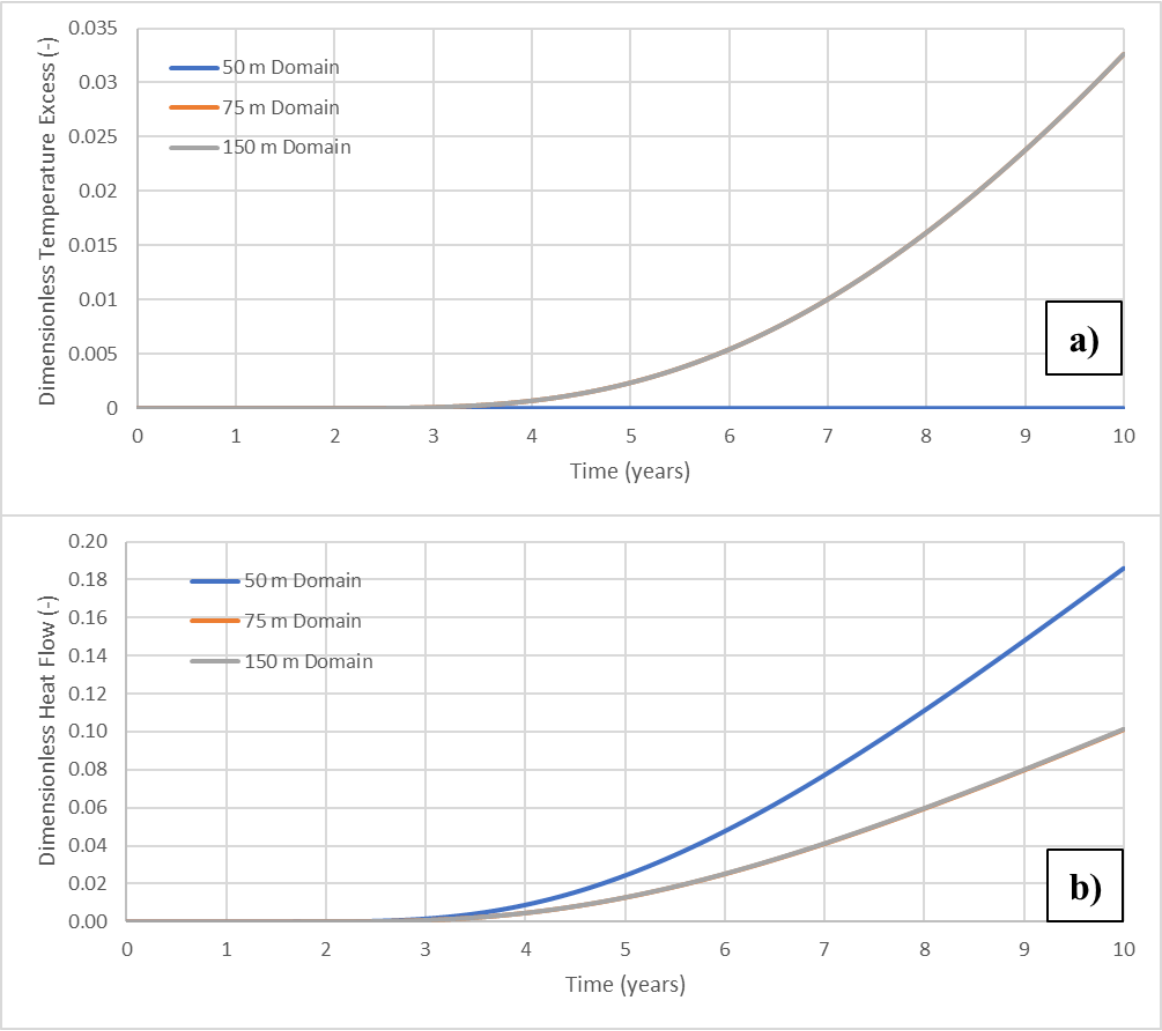

Figure 37: Dimensionless Temperature Excess (a) and Heat Flow (b) at r = 50 m

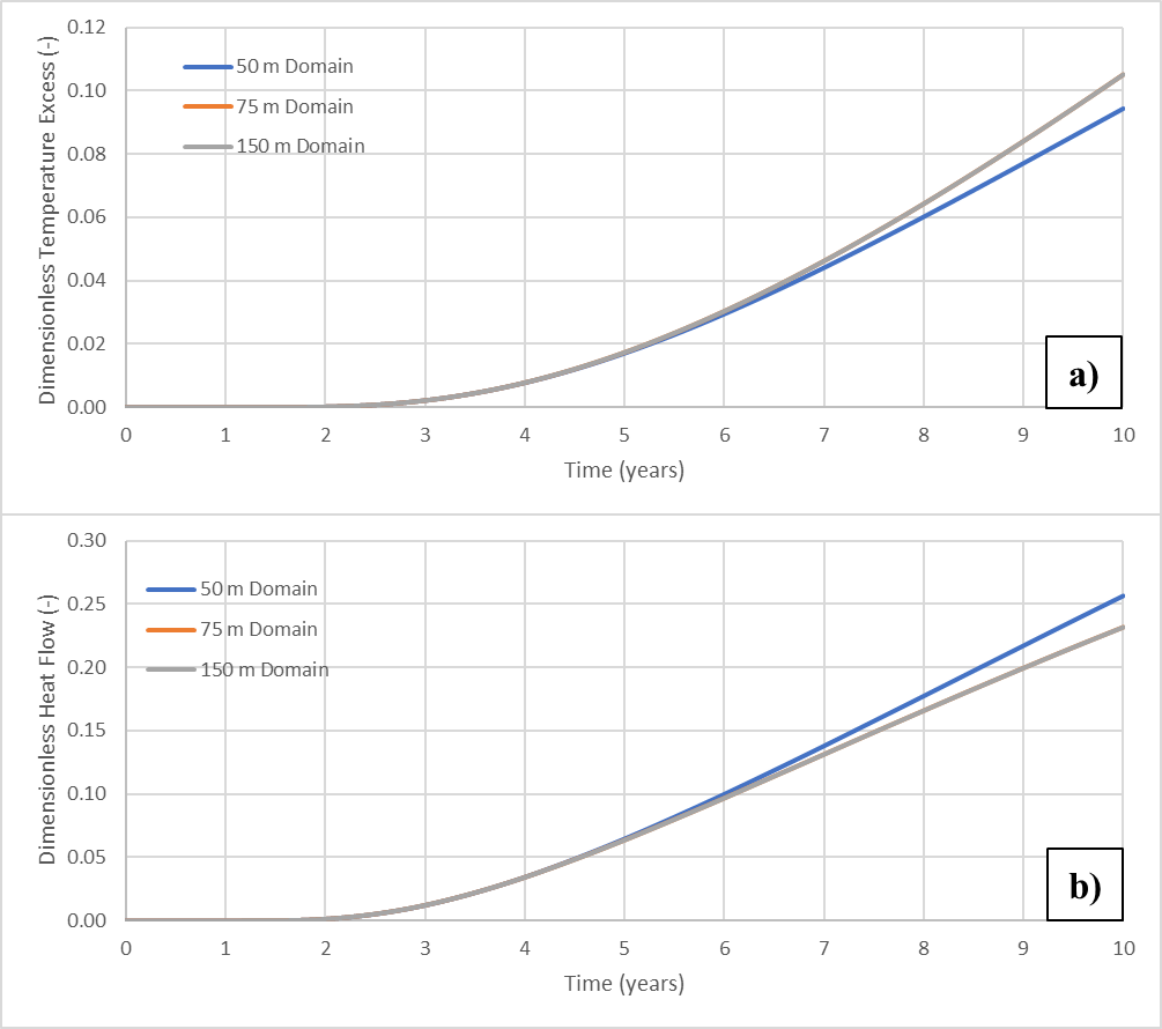

Figure 38: Dimensionless Temperature Excess (a) and Heat Flow (b) at r = 40 m

The effect of the boundary is not limited to the edges of the domain but extends into the interior of the solution as well. Figure 38 shows the results for the location of $r = 40\ m$, which gives additional information due to the lack of a local temperature constraint. The temperature excess is reduced due to the effect of the temperature being fixed at the boundary at $r = 50\ m$, limiting the effect of the soil temperature degradation due to the load thermal imbalance (Figure 38 a)). The error caused by the temperature constraint at

the boundary reflects back into the domain through altered local temperature gradients. The longer that the solution runs, after the heat flow has reached the outer boundary, the farther backwards towards the borehole this altering effect reaches.

These errors present a contradiction in any FEM solutions to the ICSSM. It is well-established that the analytical solution to the mathematical formulation of the ICSSM has no steady-state solution, due to the heat transfer being constrained solely to the radial direction. Depending on the direction of the load at the borehole, the initial condition of the soil temperature excess and the heat flow throughout the ground are both zero, and then a constant dimensionless heat flow of 1.0 is applied at the borehole. As a reminder, the thermal impacting radius is the distance from the borehole wall into the soil domain that is affected by the borehole operation. The TIR of the borehole continually increases with time, and since the outer boundary condition is applied at infinity, this continues indefinitely. Unlike finite source models, there are no axial boundary conditions that can contribute to bringing the solution to a true steady-state.

Most realistic borehole heat exchanger simulations are transient in nature, and as such, there is a limit to the thermal impacting radius. Just as with geometric constraints, FEM solutions are also constrained to a certain time range. Therefore, it is important to properly scale the size of the geometric domain to the solution time range for a boundary independent FEM solution. The result of a solution in which the thermal impacting radius

has reached the outer boundary is an unreliable data set with multiple errors that directly impact system performance.

Firstly, when the domain is too small, the total system energy balance is influenced by heat flow errors at the outer boundary, and this can result in the system reaching a premature system steady-state. For transient simulations, this will result in incorrect soil conditions surrounding the borehole, which will directly impact circulating fluid temperatures, and thus, the heat pump performance. Secondly, when the thermal impacting radius reaches the outer boundary, even during the transient phase of the solution, the heat flow is overestimated by smaller domains due to the undisturbed temperature boundary condition. Although these present as separate errors, the overestimation of the boundary heat flow contributes to reaching a false steady-state.

Finally, smaller domains lack the thermal mass of the far-field, which hinders its ability to properly respond to fluctuating loads. The fluctuating heat flow that occurs at 10 m is significantly higher in magnitude for the 10 m than the three larger domains. These fluctuations naturally reduce in magnitude as the radial position increases, which means this error is only relevant in the soil nearest the borehole.

For any borehole heat exchanger simulation, no matter the complexity, the domain size must be sufficient in order to accommodate not only minimal temperature excesses within the far-field but, just as importantly, to ensure that the boundary conditions do not reflect errors in the heat transfer into the soil domain that surrounds the borehole. As discussed in the section on the development of the radial heat flow variable, in closed

systems such as FEM solutions, the energy balance is highly dependent on the heat transfer in the far-field, which leads to the necessity for greater integration of heat transfer into the definition of the thermal impacting radius.

5.4 New Definition of Thermal Impacting Radius

As previously discussed, the thermal impacting radius as defined by Luo et al. [78] is a function of two determining criteria: the temperature excess, ΔT, and the solution time, t. The TIR is defined as the radial location at which the magnitude of local temperature excess crosses below the value of the determining criteria, ΔT. Although the authors acknowledged the value of the thermal impacting radius is highly dependent on these criteria [78], which are largely determined by the researcher, there are additional concerns with the way in which this radius is calculated.

The location of the thermal impacting radius is solely determined by the local temperature conditions of the soil, and although it is an important physical quantity of the soil, it is not sufficient to accurately describe the heat transfer and overall energy balance within the system. When discussing a value such as the temperature excess, or the change in temperature from the undisturbed value, the temperature is useful in quantifying the amount of heat energy that has been deposited or removed from the soil. As previously discussed in the literature review, the volumetric heat capacity of the soil relates the magnitude of the change in thermal energy to the temperature value, which can be expressed using the equation

$$Q = V\rho C_p \Delta T \tag{41}$$

where Q is the transfer of energy through the surface of a soil control volume, V is the volume, ρC_p is the volumetric heat capacity and ΔT is the change in the control volume's temperature value. For a system wide energy balance, the volume of the soil domain is a function of the TIR since the outer boundary (or radius) of the soil is equivalent to the TIR. For most borehole heat exchanger models, the volumetric heat capacity is a constant throughout the soil domain, however the volume within an axisymmetric context is not. It can be recalled that the radial heat flow variable was developed to determine the heat that passes through a cylinder of the radius, r. In axisymmetric FEM solutions, the volume of a hollow cylinder of the infinitesimal thickness, dr, is not constant but dependent on the value of r itself. This is illustrated in Figure 39, which features a series of connected hollow cylinders that integrate into a single volume of soil, as it would surrounding a borehole heat exchanger. Although the thickness of the cylinders is constant, the volume changes dramatically, increasing with the average radial position itself.

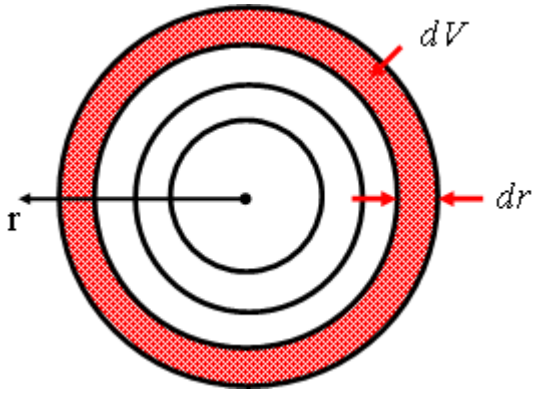

Figure 39: Illustration of the Infinitesimal Volume of Hollow Cylinders

It can be shown that the volume of these hollow cylinders is linearly proportional to the average radial value, and therefore for a series of infinitesimally thin cylinders, the volume is

$$dV = \pi({r_o}^2 - {r_i}^2) \tag{42}$$

$$dV = \pi((r_i + dr)^2 - {r_i}^2) \tag{43}$$

$$dV = \pi(2r_i dr + dr^2) \tag{44}$$

Unlike a square grid of equally consistent grid thickness, dx, which has no locational dependence on the volume, the volume in an axisymmetric context is a function of its radial position itself.

This is of interest to the current work since the current definition for the thermal impacting radius uses a simple temperature excess value to contextualize the entirety of the heat transfer. As it has been shown, the change in heat energy is not only a function of the temperature excess, but also of the soil volume, and as such, an equivalent temperature excess is characteristic of dramatically difference circumstances at different radial positions when viewed through the lens of an energy balance. Therefore, a more appropriate definition of the thermal impacting radius can be made in the context of an energy balance rather than simply the temperature values.

A new definition of the thermal impacting radius can be made which relates the local heat transfer to a heat transfer value that is characteristic of system operation. This illustrates the value of the previously defined radial heat flow variable, which has already

been nondimensionalized within this thesis using the borehole heat load per unit length. As a reminder, this value is calculated using the relationship

$$\sigma = \frac{\dot{Q}_{rad}(r,t)}{q_l} = \frac{-2\pi r k_s \frac{\partial T}{\partial r}}{q_l} \tag{45}$$

Through the following discussion, it can immediately be seen why heat flow is a more appropriate lens through which to determine the thermal impacting radius. Temperature excess, $\Delta T = \theta$, when differentiated will have the exact value of $\frac{\partial T}{\partial r}$, due to the undisturbed temperature being a constant. In the original definition of the TIR, the chosen value of ΔT represented the point where the temperature is beginning to approach the undisturbed value and therefore where the borehole is no longer impacting the surrounding soil. Put in other words, this is the point where the temperature gradient, $\frac{\partial T}{\partial r}$ is beginning to approach a negligible value, without mandating the value must reach exactly zero, where the soil is consistently the undisturbed temperature.

As shown in the discussion surrounding Equations 41-44, the temperature excess, or the gradients of the temperature excess, are not rigorous enough to represent the local energy balances in an axisymmetric problem. Figure 40 displays two curves that are exactly equivalent, except one is shifted by 5 m. As displayed in the figure, since each curve is equivalent, the point at which each crosses the black dotted line has both an equivalent temperature excess and temperature gradient. However, in the case shown below, the location of the TIR would result in a heat flow at the TIR boundary that is 53% higher in the case of Curve 2 than in Curve 1.

Just as the infinitesimal volume of a hollow cylinder is not only a function of dr, but also of r itself, the radial heat flow variable, and its nondimensional form, are functions of both the temperature gradients ($-k_s \frac{\partial T}{\partial r}$) and the radial position ($2\pi r$). This captures an important phenomenon of the thermal impacting radius: an equivalent temperature gradient will result in a variable heat flow that is a function of the radius itself, due to the increasing area of the cylinder that represents the boundary of the thermal impacting radius. Since thermal imbalance, the reason for an ever-increasing thermal impacting radius, is due to an imbalance of energy, the definition of the thermal impacting radius must be based on energy rather than temperature itself.

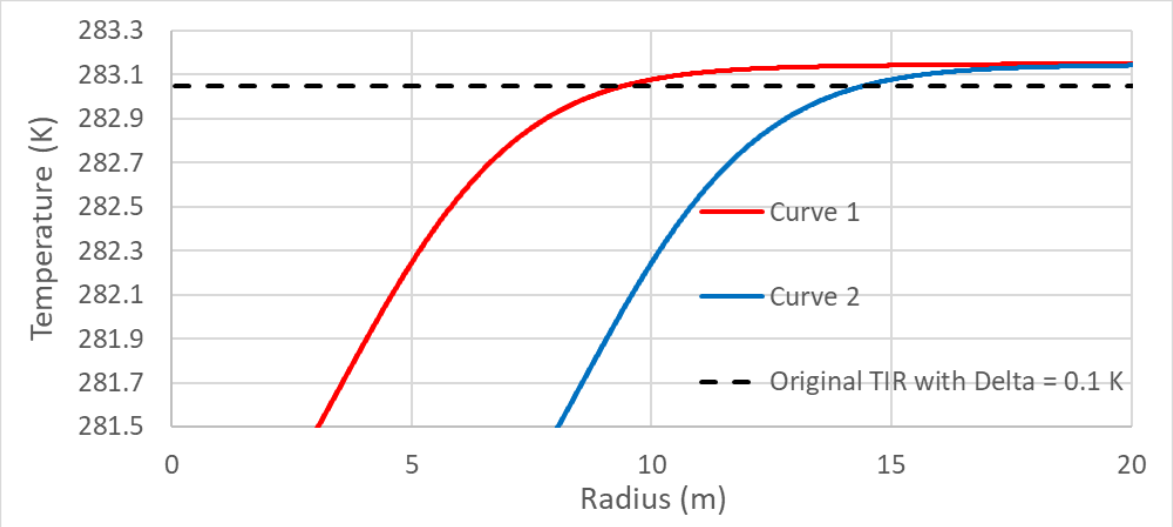

Figure 40: Two Equivalent Curves with Different TIRs

Instead of researchers defining a set value for the factor of temperature excess, ΔT, the determining factor should be designated the dimensionless heat flow, σ, with an appropriate value being low enough to be constituted negligible compared to the borehole heat flow. The value of σ ranges from 0.0 to 1.0, and like the original definition, it is up to

the researcher's discretion to determine a value close enough to 0.0 to be considered appropriate. This allows for a definition of the TIR that is much more consistent with respect to the overall system energy balance. A proof of this improvement follows.

The thermal impacting radius can be calculated for the ICSSM solutions previously discussed. The solution presented here employs a constant borehole heat load, defined by Equation 38 without the fluctuating component, or only the second term. Instead of comparing the dimensionless heat flow at a fixed radius to time, here the data is plotted for fixed timesteps with the radial location as the independent variable. Figure 41 shows that for a constant heat load, the shape of the heat flow vs. radius curve remains constant through time, with the heat flow at each radial position increasing with time and the gradient of the curve decreasing in the thermally impacted region.

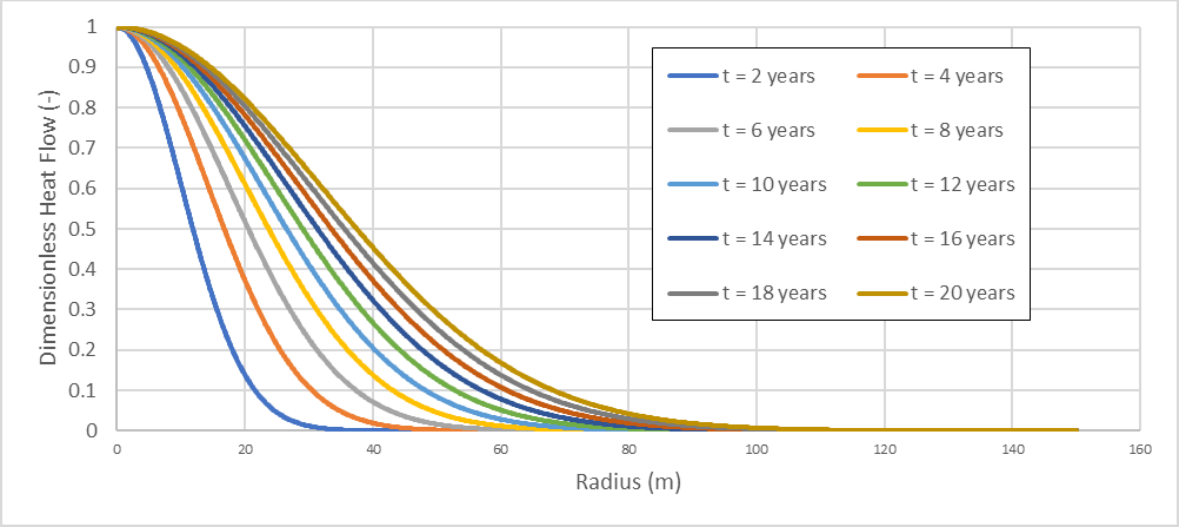

Figure 41: Dimensionless Heat Flow vs. Radial Position for ICSSM

Although the common shape of these curves provides confidence in the ability to determine a relationship between the thermal impacting radius and the dimensionless heat

flow, it is complicated by the time dependence of the curve gradients. Fortunately, the heat flow can be compared to both the time and radius simultaneously, through the use of the dimensionless number, the Fourier Number. There are borehole heat exchanger models that have utilized a constant length scale in order to nondimensionalize the Fourier Number [31], such as the borehole depth or radius. By utilizing the variable radial position, r, and the variable time, t, the Fourier Number can be calculated

$$Fo = \frac{\alpha t}{r^2} \tag{46}$$

where α is the thermal diffusivity of the soil. Calculating the Fourier Number in this way allows the complex relationship between space and time to be represented in a single variable, and determining if the radial heat flow variable, $\dot{Q}_{rad}(r,t)$, is truly a function of multiple variables, or a single variable, $\dot{Q}_{rad}(Fo)$. The ten curves above were re-plotted in Figure 42 for the Fourier Number (Equation 46) instead of the radial position, and it can be seen that it is true that the heat flow is solely a function of the Fourier Number. Each of the ten curves lie exactly along the same path, meaning the heat flow has no dependence on the radial position or time independently of one another.

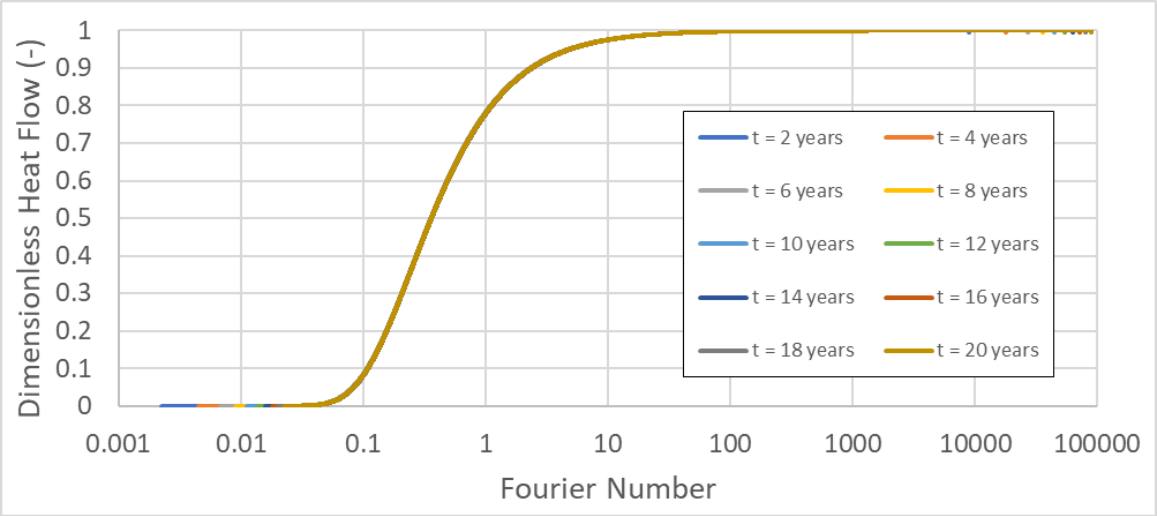

Figure 42: Dimensionless Heat Flow vs. Fourier Number for ICSSM

To ensure this dimensionless curve is independent of a number of model inputs, the solution was repeated while varying the heat flow magnitude, soil thermal conductivity and the soil volumetric heat capacity. These constants represent all the values that are used in nondimensionalizing the heat flow and the Fourier Number. Each curve is labeled with the model input that was adjusted for the solution. Once again, the curve is exactly equivalent for all cases (Figure 43), meaning this curve is the exact solution for the dimensionless heat flow for all solutions to the ICSSM. Therefore, it can be used to define a relationship between the thermal impacting radius and the dimensionless heat flow.

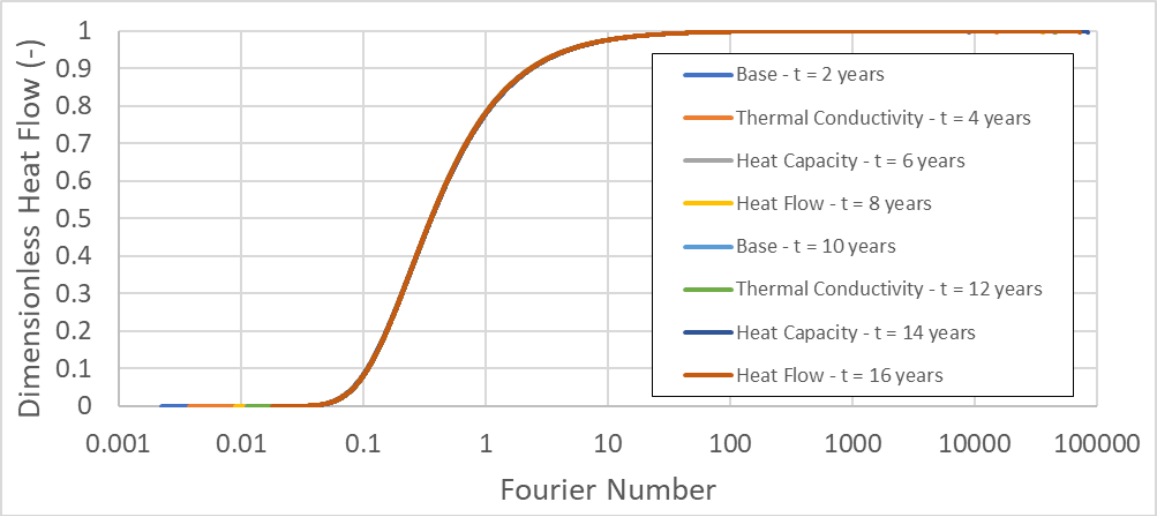

Figure 43: Independence of Dimensionless Heat Flow vs. Fourier Number to Multiple Model Input Conditions

Although the above figures display the dimensionless heat flow as a function of the Fourier Number, the relationship can be reversed for the entire range of dimensionless heat flow values within the limits of, $0 < \sigma < 1$. These limits extend to $-\infty$ and $+\infty$, respectively for the Fourier Numbers, which would ensure the reversed relationship would not be a function, and as such should be limited in the current case. Using these limits, we can define the thermal impacting Fourier Number as a function of the dimensionless heat flow variable, and in turn the thermal impacting radius can be expressed as

$$Fo_{TIR} = f(\sigma) \tag{47}$$

$$TIR = \sqrt{\frac{\alpha t}{Fo_{TIR}(\sigma)}} \tag{48}$$

where the TIR has the units of metres, [m]. Using the curve found in Figure 42, a few possible values for a reasonable dimensionless heat flow to use in the definition of the TIR are presented in Table 5. The table also displays the corresponding Fourier Number.

Table 5: Dimensionless Heat Flow and Fourier Numbers for New TIR

σ (-)	**Value as Percentage** (%)	**Fourier Number**
0.05	5	0.083
0.01	1	0.053
0.005	0.5	0.047
0.001	0.1	0.036

The above figures represent the case of a constant load, but realistic borehole loading includes a fluctuating load with the period of one year. Therefore, to ensure applicability of this definition of the thermal impacting radius, the analysis must be replicated for fluctuating loads. The heat flow must still be nondimensionalized using the average load value, equivalent to a single constant load value, to ensure that the dimensionless heat flow curve fluctuates around the value of $\sigma = 1.0$. In all other ways, the simulations are identical to ensure consistency in the comparison.

Solutions with three different load profiles were prepared, with equal average load values but differing amplitudes of fluctuation to determine the effect this amplitude has on the solution (Figure 44). Figure 45 shows the comparison between the three dimensionless

heat flow curves, including: the constant load profile (a zero amplitude), a nominal dimensionless amplitude of ± 1, and a nominal dimensionless amplitude of ± 5.

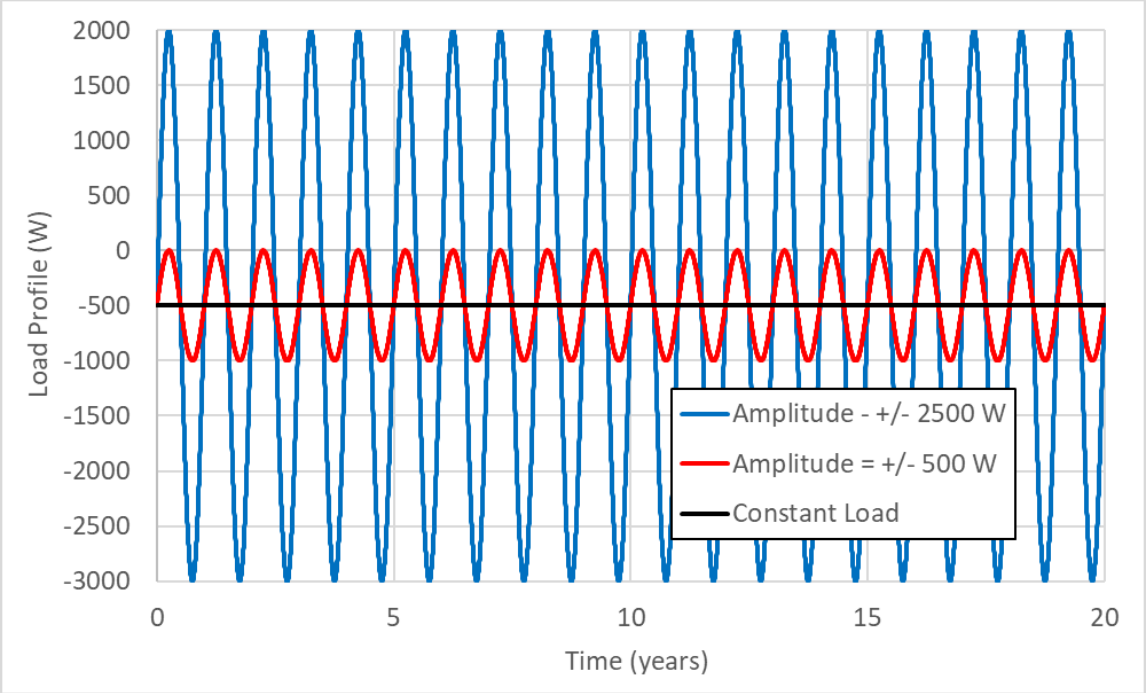

Figure 44: Different Load Profiles used for Investigation of Fluctuation on TIR

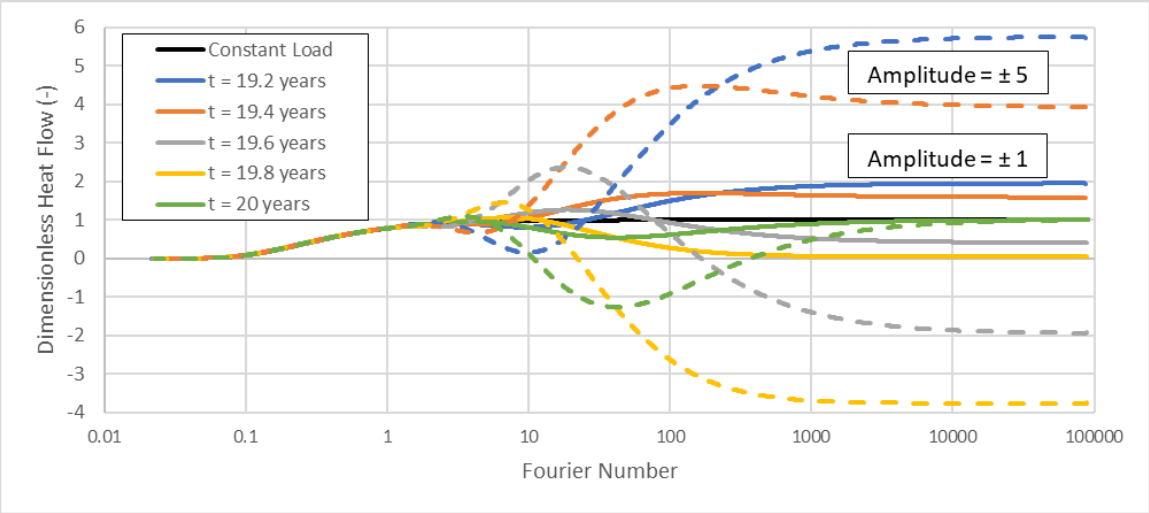

Figure 45: Dimensionless Heat Flow vs. Fourier Number for ICSSM with Fluctuating Load

The amplitude of fluctuation has no effect on the solution at low Fourier Numbers, with heat flows beginning to diverge around the value of $Fo_{TIR} = 0.8$. Figure 46 shows the region of Figure 45 where the divergence occurs. This is very useful for the proposed definition of the thermal impacting Fourier Number, since this means the range of Fourier Numbers, $0 < Fo_{TIR} < 0.8$, which corresponds to the dimensionless heat flow values of $0 < \sigma < 0.78$, is independent of load fluctuations. The fluctuating load only impacts the range of radial values which result in high Fourier Numbers; since the Fourier Number is inversely related to the square of the radial position, this means the fluctuations only impact the domain at low radial positions and high time values. Since the high Fourier Numbers correspond to high dimensionless heat flows, these fluctuations have no effect on the range of values that are appropriate for defining the thermal impacting Fourier Number. Therefore, the edge of the thermally impacted region lies outside the region where fluctuations occur throughout the domain.

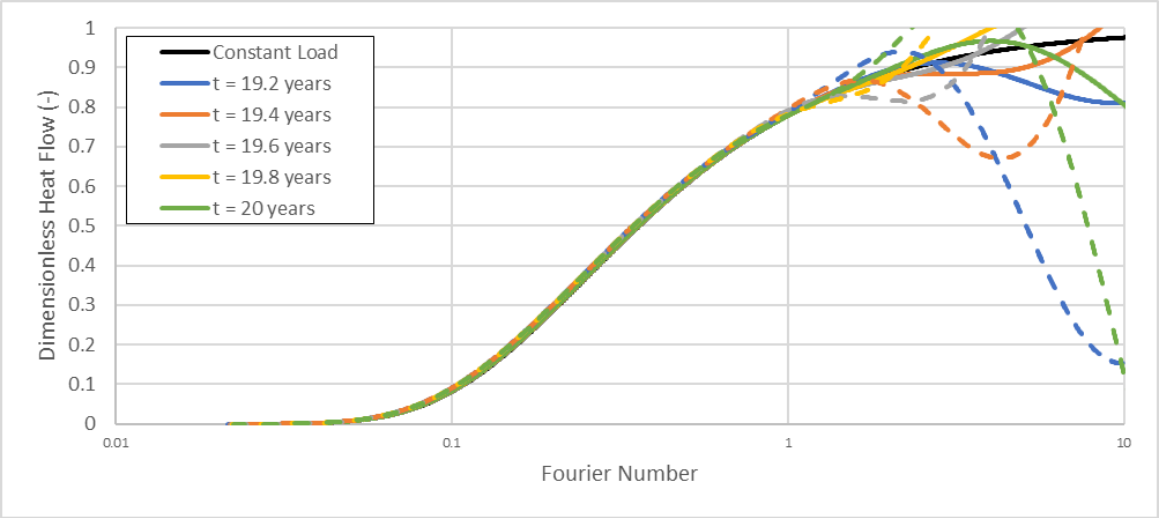

Figure 46: Point of Divergence for Dimensionless Heat Flow of ICSSM with Fluctuating Load

Chapter 6 – Reducing Model Dimensions in Far-Field Soil Domain to Increase Computational Efficiency

6.1 Reducing the Dimensional Dependence in the Far-Field

As it can be seen, both within the literature and within this thesis thus far, three-dimensional FEM solutions are incredibly useful when solving complex problems that require detailed meshes to properly resolve the three-dimensional heat transfer that surrounds a borehole heat exchanger connected to a geothermal heat pump system. The fluid temperature distribution, and thus the efficiency and operation of the heat pump, are highly dependent on the local conditions within the borehole itself and the soil that immediately surrounds it. The difference in the fluid temperature between the inlet and outlet of the borehole heat exchanger, for example, results in a non-uniform distribution in the temperature within the borehole, both in the axial direction and along any plane that acts as a cross-section of the borehole, in other words in the radial and angular directions.

However, as the radial position of the soil increases, the three-dimensional nature of the heat transfer becomes less stark. The axial heat transfer is reduced to negligible levels in the far-field, and therefore the heat transfer essentially becomes only in the radial direction far from the borehole.

Since the fluid enters the borehole from the ground, travels axially along the length, and returns axially to the ground, we know that there will be an axial dependence in the fluid temperatures, and thus the heat transfer from the fluid to the borehole. However, the fluid temperature difference between the inlet and outlet of the borehole heat exchanger is

typically below 10 °C ([14], [18], [70], [71], [89]) depending on pumping factors, such as flow rate and fluid properties. Additionally, the nature of the geometry of a borehole means that the location of the minimum and maximum values of the fluid temperature will lie along the same axial plane, at the ground level. Since the fluid temperature continually changes through the U-tube, as it travels down and then back up the borehole, the average temperature at each axial location does not vary greatly no matter how large the overall temperature difference in the fluid is.

This has been studied extensively ([14], [18], [70], [71], [80], [89]), including in the work of Marcotte and Pasquier [14], who proposed a model to properly resolve the fluid temperature distribution with the borehole based solely on inlet and outlet fluid temperatures. Using a three-dimensional model, which included resolved the fluid domain in three-dimensions, as validation, Marcotte and Pasquier [14] developed an equation known as the *p*-linear average that was able to closely approximate the numerical fluid temperature distribution, a great improvement over the assumption that the temperature changes linearly with relative position along the U-tube length. A figure from Marcotte and Pasquier [14] can be used to illustrate the importance of their findings for the current work presented in this thesis.

It can be seen in Figure 47 that the fluid temperature follows a non-linear distribution, with a higher temperature difference, over total depth, on the supply side than the return. Figure 47 represents a scenario where energy is being extracted from the borehole, and is being used to heat the load, a house in the case of residential systems. This is why the fluid temperature is lowest at the BHE inlet and highest at the BHE outlet.

Although there is a wide range of fluid temperature shown, an overall temperature difference of approximately 7.5 °C, there is only a difference of less than 1.5 °C along the length of the borehole wall. This can be explained by the subsequent figure of the heat flow per unit depth, which shows that the total heat flow at each axial position has remarkable consistency considering the large fluid temperature difference. The heat flow varies from its lowest value of 40 W/m at the lowest depth, at 150 m, up to its higher value of 44 W/m at the ground level, with a slowly increasing rate of change, rather than a strictly linear distribution. Although this heat flow is applied at two distinct local positions for each axial position, both are applied at the centre of the borehole and interact while their thermal effects begin to reach the domain outside of the borehole.

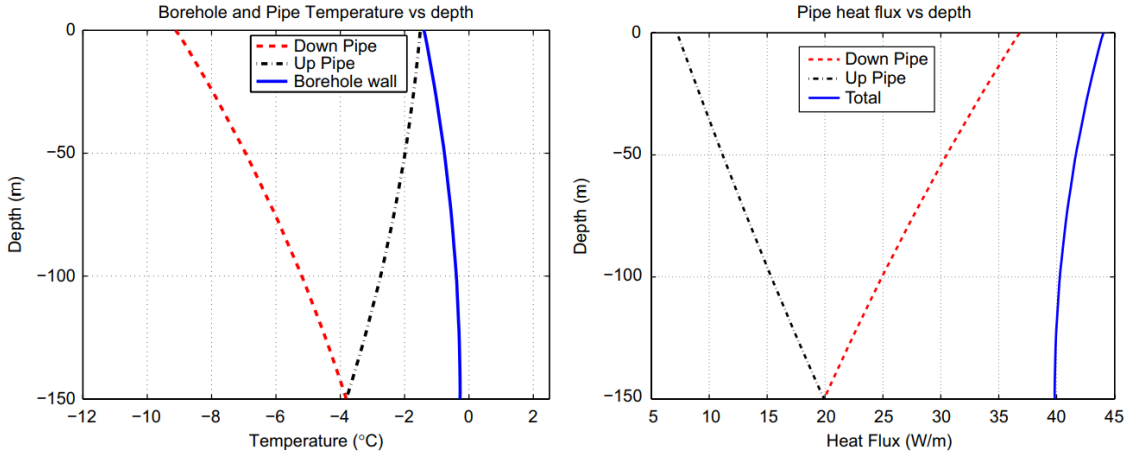

Figure 47: Fluid and Borehole Temperature and Heat Flux vs. Depth [14]

As Marcotte and Pasquier [14] clearly demonstrates, the local heat flux from the fluid to the borehole is extremely dependent on its axial position, or more accurately stated, on its relative position along the length of the entire U-tube, however, when the heat flux is summed at each shared axial position, that is the heat flux of the supply and return legs

of the U-tube, the axial variation is reduced. Therefore, although it is of extreme importance to allow the fluid temperatures and local borehole temperatures to resolve themselves, through three-dimensional FEM in the current case, to ensure accuracy, the domains that surround the heat transfer process within the borehole are not experiencing the vast differences in local heat transfer at the same magnitude.

The angular dependence of borehole heat exchanger operation can be investigated through a validated solution, like the model validation performed in Chapter 4 through a re-creation of Beier et al.'s [17] experimental data set. The radial position and azimuth can be calculated from the geometric position within a cartesian coordinate system using the equation

$$r = \sqrt{x^2 + y^2} \tag{49}$$

$$\theta(^\circ) = \frac{180^\circ}{\pi} \cos^{-1}\left(\frac{x}{\sqrt{x^2 + y^2}}\right) \tag{50}$$

when converting to a cylindrical coordinate system. The temperature as a function of the angular position, for multiple timesteps, is displayed in two figures, Figures 48 and 49. Each figure corresponds to the temperature at a location within and at the outer wall of the borehole, respectively. These radial positions are shown in Figure 50. As expected, the average temperature within and at the outer wall of the borehole increases with time.

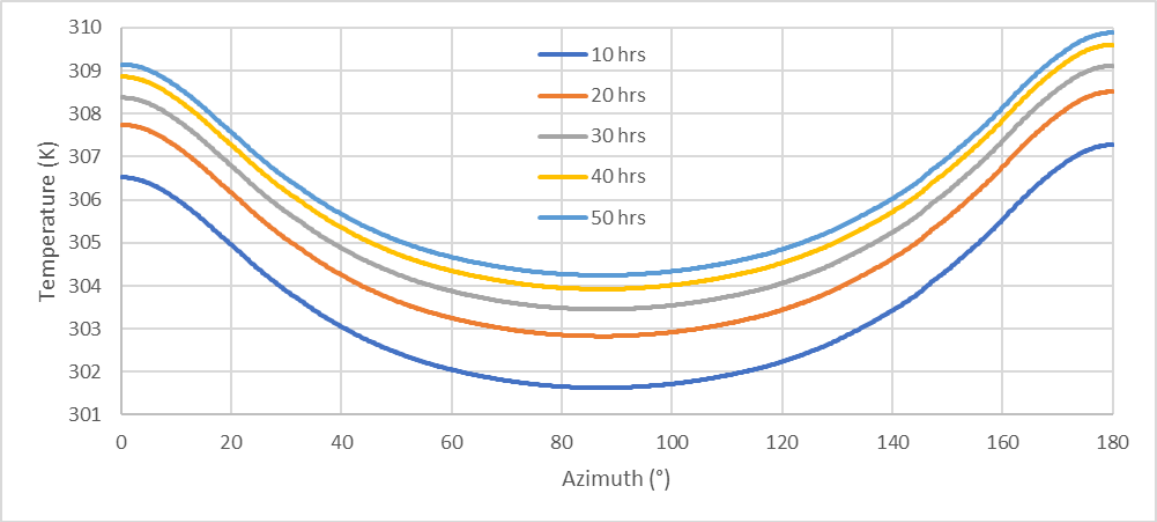

Figure 48: Temperature at r = 4.32 cm or the Outer Edge of the U-Tube Pipes

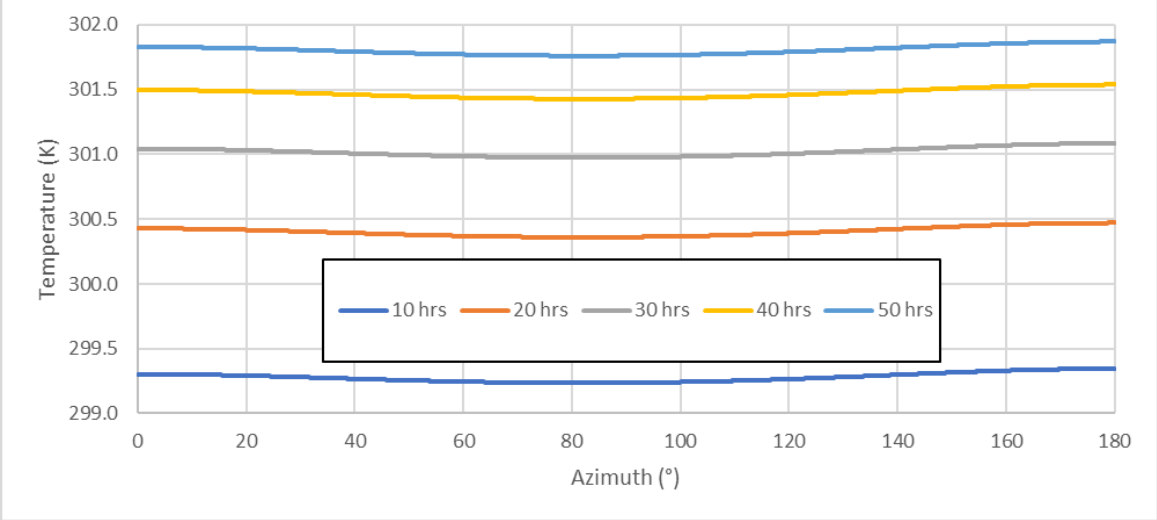

Figure 49: Temperature at r = 6.5 cm or the Borehole Wall

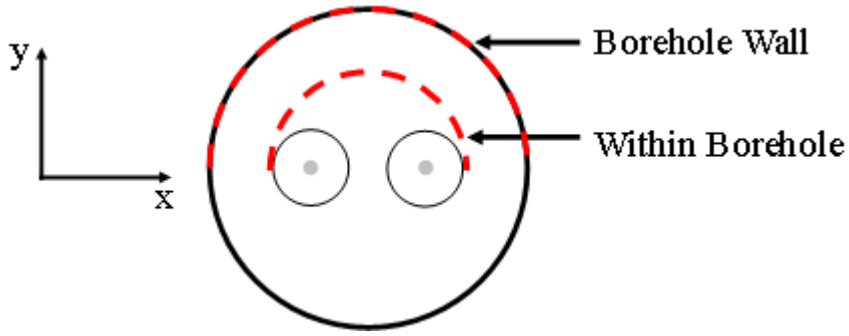

Figure 50: Radial Locations for Angular Dependence Investigation

Although it can be seen that there is greater variation in the temperature within the borehole than at the outer wall, the fact that the temperature increases with time obscures how the angular dependence changes with time. Therefore, the angular dependence can also be investigated by comparing local conditions to an average value at each radial position. A temperature excess ratio can be calculated as

$$Temperature\ Excess\ Ratio = \frac{(T - T_{und})|_{local}}{(T - T_{und})|_{ave}} \tag{51}$$

For a completely angular independent solution, the temperature excess ratio would be exactly 1 for every azimuth value. Figure 51 shows the values of the temperature excess ratio at the radius of 4.32 cm and Figure 52 is the same plot at a radius of 6.5 cm. All figures display the data at the axial location of $z = -0.91\ m$, where the first row of thermistors is located in the experimental work. This is because the greatest fluid temperature difference between the supply and return portions of the U-tube occurs near the surface of the BHE and would represent the location of highest angular dependence.

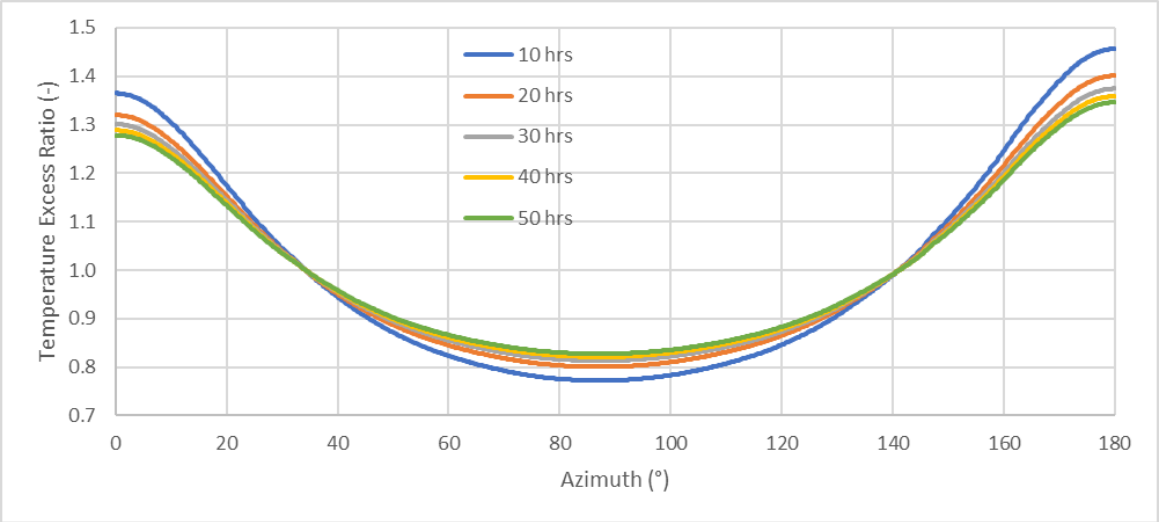

Figure 51: Temperature Excess Ratio at r = 4.32 cm or the Outer Edge of the U-Tube Pipes

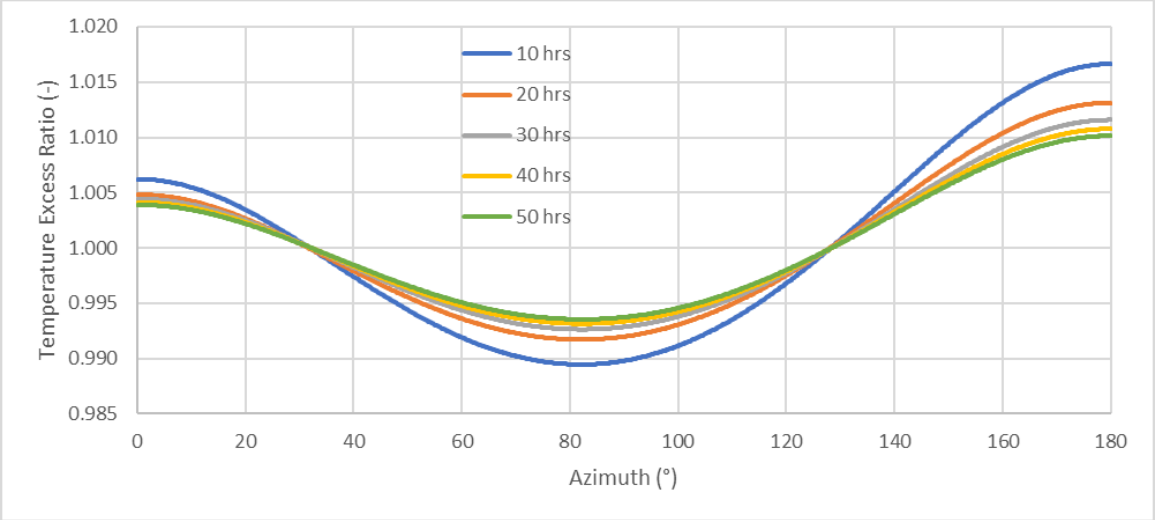

Figure 52: Temperature Excess Ratio at r = 6.5 cm or the Borehole Wall

Within the borehole, where the heat is being injected, the solution is at its most dependent upon the angular position due to the close proximity to the fluid domain. This can be seen in Figure 51, where the temperature excess at angles of 0 and 180°, which correspond to the edge of the return and supply pipes, respectively. This is because these

are the exact locations of heat injection into the solid domain, and the fluid temperature is slightly lower on the return side than the supply side, leading to a skew within the borehole temperature. Between the U-tube pipes, at just below 90° is the temperature excess minimum, once again skewed due to the heat flow difference. Overall, it can be seen that there is a great variation in temperature at a fixed radial position.

The temperature excess ratio is also dependent on the amount of time the load has been applied for. The highest amount of variation, with both the largest maximum and lowest minimum, occurs in the early test time, at 10 hrs, both within the borehole (Figure 51) and on the outer edge of the borehole wall (Figure 52). As time increases, the angular dependence decreases for both locations.

More importantly, the temperature excess ratio decreases dramatically as the radial position increases, which is evident by comparing the values within Figures 51 and 52. Within the borehole, the maximum and minimums values of the temperature excess ratio are 1.456 and 0.772, respectively. At the outer wall of the borehole, these values are reduced to 1.017 and 0.989. From a small radial displacement, of 2.18 cm, the maximum variation in temperature excess goes from nearly 46% to 1.7%, a dramatic reduction in the angular dependence of the solution. Within the soil, as the radial position, and the loading time, continues to increase, the solution continues to approach angular independence.

The typical behaviour, outlined above, of heat transfer around borehole heat exchangers being largely angular independent and with low axial dependence, presents an opportunity for improving the overall model's computational efficiency. The proposed

model will include a finite region of three-dimensional heat transfer to allow for local gradients to resolve themselves until the temperature and heat transfer becomes relatively angularly and axially independent. Angular independence occurs at a much higher radial position, and as such, this section will investigate the effect of eliminating axial heat transfer in the far-field.

Although the density of a fully discretized Finite Element Model is useful for the investigation of the dynamic operation of a borehole heat exchanger, the computational cost is high. The use of FEM models, the likes of which have been previously discussed in this thesis, have largely been restricted to short time-scale studies, typically simulations of Thermal Response Tests (TRT). Not only is this due to the increases in the necessary number of time steps, but also due to the relationship between the borehole operation time and the thermal impacting radius. When there is a constant heat load, or a thermal imbalance within a variable, repeating heat load, the TIR will continually increase with time, as evident in the solution to traditional borehole models like ILS, FLS and ICSS models.

This relationship between time and TIR makes the use of FEM simulations difficult for long-term studies, as the boundary of the cylinder of soil must be large enough to result in a solution that is independent of the outer boundary condition, which is typically set to the far-field temperature. As the length of the study increases, so must the distance of the undisturbed soil boundary, increasing the soil volume of the simulation. If the definition of the TIR based on the ICSSM that was established in Chapter 5.4 is used with a value of $\sigma = 0.01$ and the soil properties used in Chapter 5.1, we can estimate the necessary size of

the soil volume for a variety of study lengths. For 10, 25 and 50 years, the TIR is estimated at 70, 110 and 156 m, respectively. This makes the computational cost increase more rapidly with each additional time step, an impediment to their use.

6.2 1D Axisymmetric Heat Transfer Components

If the results of the last section led us to assume angular and axial independence, the heat transfer within the far-field can be greatly simplified. The heat transfer in a one-dimensional, axisymmetric domain is modeled using a system of equations very similar to the three-dimensional domain [90]. As the solution is axisymmetric, a one-dimensional solution can naturally be extended to a two-dimensional domain in the shape of an annulus. The equations within the model

$$\rho C_p \frac{\partial T}{\partial t} + \nabla \cdot \boldsymbol{q} = 0 \tag{52}$$

$$\boldsymbol{q} = -k\nabla T \tag{53}$$

appear identical to the equations governing the three-dimensional domain but are constrained to solve only in the radial direction.

There is no heat transfer in the axial dimension, and as such the variables solved at each radial position are independent of the axial position. This, in conjunction with the azimuth symmetry, results in a much simpler, one-dimensional problem that reduces the computational effort greatly, for the far-field domain. Although this simplification results in additional inaccuracy within the overall model, it is small due to the temperature

gradients within the soil being much higher in the radial direction than in either the azimuth or axial directions.

Since the one-dimensional domain is to be used in the far-field, the external boundary condition of the undisturbed temperature is applied to the boundary at the largest radial position. It is bounded internally by the three-dimensional domain, which will be shown later to be connected both by a boundary temperature and a common heat flux. A schematic of the complete model is shown in Figure 53. Therefore, it can reasonably be stated that the three-dimensional domain has been connected to a modified Infinite Cylindrical Surface Source Model, with the boundary condition of a heat flux applied at the borehole radius being replaced by a heat flux applied at the radius of the three-dimensional domain. The location of this radius is designated in order to minimize the effect that the axial symmetry in the far-field domain has on the temperature gradients that are in contact with the borehole, while also minimizing the computational effort. At the point where the model transitions from a three-dimensional domain to a one-dimensional domain, there must be a method of system connection that allows for heat transfer between the domains as well as a variable temperature value that does not over constrain the overall model. This connection, designated the Value-Averaging Component in Figure 53, will be established in the following section.

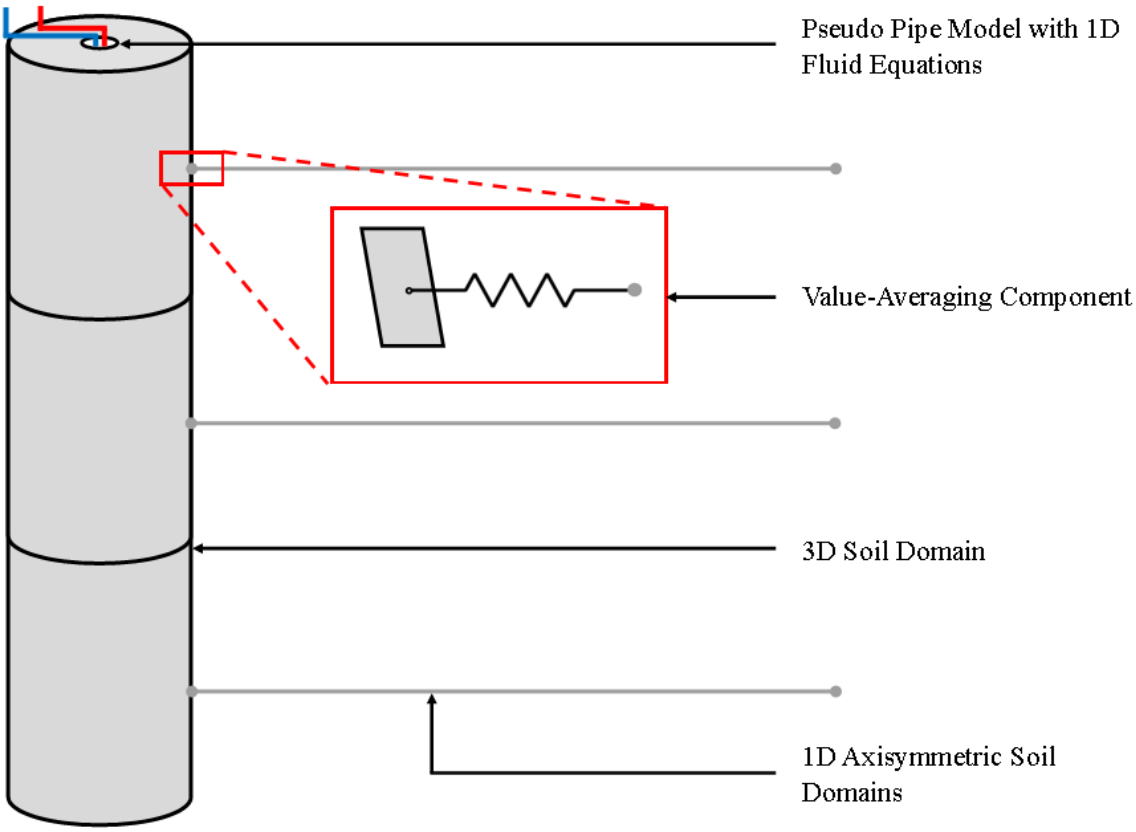

Figure 53: Representative Schematic of Composite Model Domains

6.3 Capacity Resistance Model (CaRM) for Borehole Heat Exchanger Far-Field Behaviour

Although it is necessary to extend the boundary in order to remain independent, the temperature gradients within the far-field soil are much smaller, and as such can still be adequately estimated using simplified physics within the far-field. This allows for an application of a model which provides an approximation of the heat transfer in the far-field with a separate physics than a three-dimensional FEM mesh, that does not overwhelmingly contribute to the computation time. This can be accomplished using a one-dimensional,

axisymmetric heat transfer model connected at the boundary of the three-dimensional domain.

This averaging is made possible through a thermal network method analogous to the Capacity Resistance Model equations, which have been developed as an alternative to FEMs ([20], [91]–[93]). This electrical network analogy does not have any inherent spatial-dimension dependence, which uniquely allows it to connect the boundaries of a three-dimensional and one-dimensional domain. To ensure heat transfer through the thermal network is consistent with the heat transfer resolved within the FEM domains, three components are necessary. Two of these components are described in detail within the definition of CaRM equations, and they correspond to a resistance that models heat conduction and a capacitance that models transient temperature response to thermal energy. The components model the heat transfer using the equations

$$P = -\frac{\Delta T}{R} \tag{54}$$

$$P = -C\frac{\partial T}{\partial t} \tag{55}$$

for thermal resistance and thermal capacitance respectively, where P is the heat rate (W), ΔT is the temperature difference between adjoining nodes (K), R is the conductive thermal resistance (K/W), C is the thermal capacitance (J/K) and $\frac{\partial T}{\partial t}$ is the change in temperature at the node with time. The conductive thermal resistance for each component and the thermal capacitance for each node is calculated using the equations

$$R = \frac{1}{f2\pi kH}\ln\left(\frac{r_o}{r_i}\right) \tag{56}$$

$$C = V\rho C_p \tag{57}$$

where f is the fraction of the cylinder being modeled, k is the thermal conductivity (W/mK), H is the height of the node (m), r_i and r_o are the inner and outer radius respectively (m), V is the node volume (m^3), ρ is the soil density (kg/m^3) and C_p is the soil heat capacity (J/kgK).

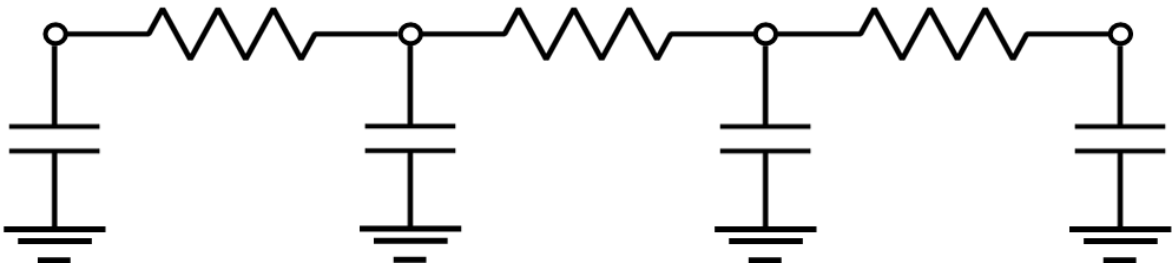

Figure 54: Example pf Electrical Analogy Diagram for CaRM Models

This thermal network connects each node, which is attached to a single thermal capacitance, with a conductive resistance between the node and its adjacent nodes on either side (Figure 54). This allows the conduction of heat from one end of the thermal network to the other, governed by the following equation at each node

$$C(i)\frac{T(i) - T_{\Delta t}(i)}{\Delta t} = \frac{T(i-1) - T(i)}{R(i-1)} + \frac{T(i+1) - T(i)}{R(i)} \tag{58}$$

The final necessary component is the Lumped System Connector. The Lumped Thermal System, in its use as a value averaging component, must be connected to spatially dependent models at two terminal nodes, one at the three-dimensional domain and the other

at the one-dimensional domain. These two terminal nodes are each connected on their internal side to thermal resistances, and on their external side to the FEM solutions. The terminal nodes are governed by model equations that link them to the FEM solutions as equivalent boundary conditions, which ensure continuity in both the temperature and the heat flow between the domains. The two equations average the temperature of the FEM boundary and constrain the node to that average temperature, and the heat rate calculated with the Lumped Thermal System is applied to the FEM solution as an equivalent boundary heat flux. These two conditions can be mathematically expressed as

$$\frac{\oiint T\ ds}{\oiint\ ds} = T_{P_{ext}} \tag{59}$$

$$\oiint -n \cdot q\ ds = P_{ext} \tag{60}$$

where $\oiint ds$ is a surface integral, $T_{P_{ext}}$ is the terminal node temperature and P_{ext} is the terminal node heat rate. Through two terminal nodes, the temperature and heat flow in the three-dimensional domain can be averaged and then applied to the one-dimensional far-field, and vice versa.

In complete CaRM thermal networks, each node is attached to a single thermal capacitance and connected to adjacent nodes with thermal resistances. In its use as a value averaging component, a single internal node is bounded by two Thermal Network Connectors which are externally linked to the corresponding FEM domains, rather than connected to additional nodes through thermal resistances. This ensures consistency in the solution between the average temperature on the three-dimensional boundary and the local

temperature on the one-dimensional boundary, as well as conserving the overall system's heat balance by applying heat rates at each Thermal Network Connector that balance the simply heat flow through the simplified CaRM.

6.4 Finite Line Source Model

Due to the very high ratio between the radius, r_b, and the depth, H, of the borehole H/r_b, and the semi-infinite nature of the surrounding soil, the borehole can be approximated as a line source in certain models. This is the assumption that makes the construction of both the infinite line source [26] and finite line source [31] models possible. As Zeng et al. [31] notes, the ground surface effects are important to properly resolve a steady-state or pseudo steady-state operating condition when there is a thermal imbalance in the annual heating load. In the infinite line source model, the solution will never reach a steady state, even as the time tends to infinity, when there is a lack of a model constraint at Z = 0. Therefore, the finite line source model is more appropriate for use in comparison with the composite model presented here. However, as is demonstrated in Li and Lai [30], the finite-line source model is only accurate at medium- and long-time scales, or Fourier Numbers larger than 0.001.

Short-term responses cannot be captured well by the finite line source model since short-time scale changes in the load will result in high frequency temperature fluctuations. The reason this fails in line source models is that high frequency effects are much more dependent on the heat capacity of the borehole itself, which is ignored in line source models

[30]. As such, the composite model should only be compared to the finite line source model for long-time scales. The steady state solution of the finite line source model is shown here and is compared to a recreation of the model using a modified version of the composite model presented here. As is demonstrated in Zeng et al. [31], the analytical solution to the finite line source model in dimensionless terms is

$$\varphi = \int_0^1 \left\{ \frac{erfc\left(\frac{\sqrt{R^2+(Z-H')^2}}{2\sqrt{Fo}}\right)}{\sqrt{R^2+(Z-H')^2}} - \frac{erfc\left(\frac{\sqrt{R^2+(Z+H')^2}}{2\sqrt{Fo}}\right)}{\sqrt{R^2+(Z+H')^2}} \right\} dH' \qquad (4)$$

where $Z = z/H$, $H' = h'/H$, $R = r/H$, $Fo = \alpha\tau/H^2$, and $\varphi = 4k\pi(T - T_{und})/q_l$. φ is the dimensionless temperature excess, Z and R are the dimensionless coordinates, H' is the dimensionless integrating parameter and Fo is the Fourier Number. As previously stated, the finite line source model is most accurate at long time scales, and so we can compare the steady-state solution to the composite model to determine the maximum uncertainty. We obtain the steady-state analytical solution when time, or the Fourier Number, tends toward infinity in Equation 4, which results in the solution

$$\varphi = \ln\left[\frac{\sqrt{(1-Z)^2+R^2}+1-Z}{\sqrt{(1+Z)^2+R^2}+1+Z} \cdot \frac{2Z^2+2Z\sqrt{R^2+Z^2}+R^2}{R^2}\right] \qquad (61)$$

Equation 61 results in a complete analytical temperature profile that can be compared at multiple locations to the composite model. Before the results are shown, there are a number of factors that must be taken into account when comparing analytical and discretized models.

As mentioned in the Introduction section, the mathematical formulation of the FLS model applies boundary conditions at two infinite boundaries, at $R \to \infty$ and $Z \to \infty$, resulting in a semi-infinite solution domain. This presents a clear problem for discretized models, which rely upon closed systems of finite geometry that are bounded by clear boundary conditions. In the interest of computational efficiency (or more realistically put, viability) the three-dimensional component of the composite model cannot extend multiple borehole depth values ($Z = 1$ being the dimensionless equivalent to a single borehole depth) without creating a discretized mesh of an untenable number of nodes that must be solved. This problem is exacerbated by the fact that it is the steady-state solution that is being compared.

In summary, there are three sources of error that will cause discrepancies between the analytical solution and the results of the composite model. These three sources are:

1. A finite boundary at $r = r_o$, where the temperature is set to the undisturbed soil temperature, instead of at $r \to \infty$.
2. A finite boundary at $z = z_o$, where the temperature is set to the undisturbed soil temperature, instead of at $z \to \infty$.
3. The reduction of the two-dimensional heat transfer problem, in both the radial and axial directions, to a one-dimensional heat transfer problem, *only in the far-field*.

The first two sources of error are only present for a steady-state solution and would not be a concern for the simulation of realistic BHE operation, which occurs over a

specified time period. Evidence for this was presented in the previous section of the thesis, where a method to ensure outer boundary independence was established.

The third source of error is the main point of interest within this section. By comparing the results to a steady-state solution, the maximum possible error caused by the far-field simplification can be determined. Since typical BHE studies are transient, and the error at the start of the test can be assumed to be zero (constant undisturbed soil temperature, no axial heat transfer before the introduction of the thermal impact of the borehole), the model error at any given time for a transient test should be considered to be between zero and the maximum error, increasing as the time of study increases. With these caveats on the sources of error in the numerical solutions to FLS established, a comparison on the results follows.

The numerical models are identical, apart from the number of far-field domains that are resolved. Increasing the number of far-field line domains reduces the axial thickness of each domain, reducing the volume of soil that each domain represents and thus increasing the discretization of the far-field, without the addition of any axial heat transfer to the energy equations. Figure 55 illustrates the geometry of the composite model for each of the three solutions and Figure 56 displays a detailed schematic of the model being solved. It should be noted that these diagrams are representative of the model being solved, but the relative geometries are not to scale and labelled using the dimensionless values of the FLS.

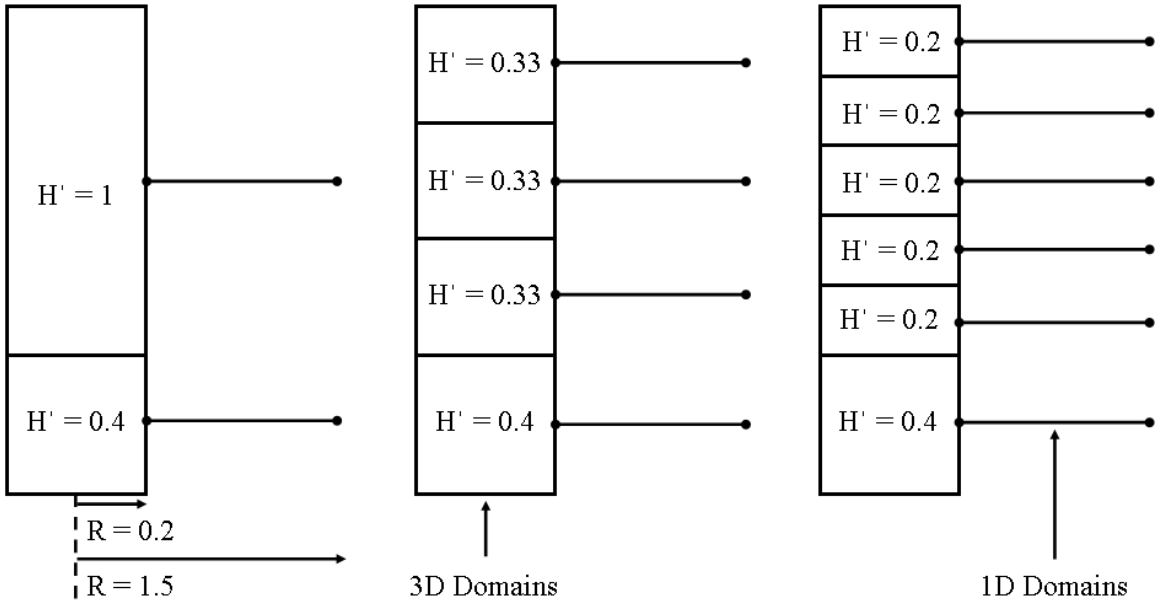

Figure 55: Dimensionless Domain Sizes for 2 Far-Field Domains (left), 4 Far-Field Domains (middle) and 6 Far-Field Domains (right)

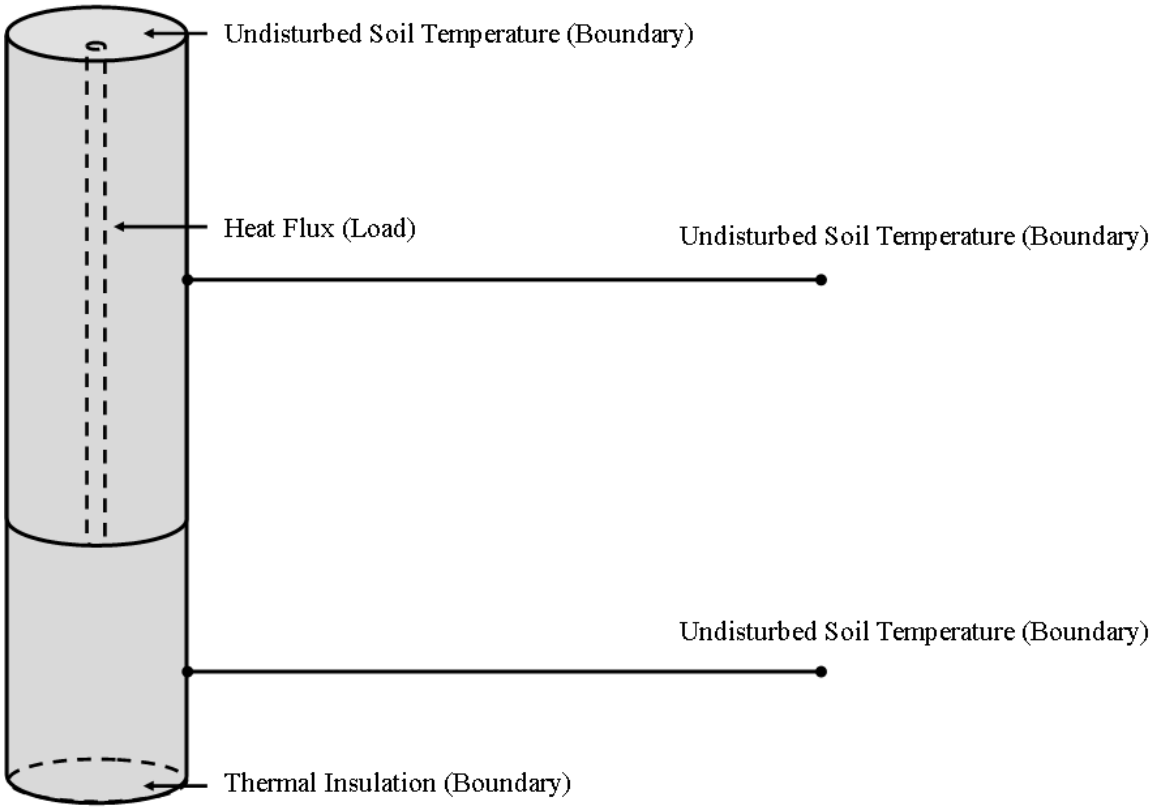

Figure 56: Schematic of Composite Model for Finite Line Source Solution

Since the major assumption made in the composite model is the absence of axial heat transfer in the far-field, the first point of interest is the model's ability to resolve the proper axial temperature distributions near the borehole, where the model is still solving within a three-dimensional domain. The temperatures at the boundaries of this domain, at the radius of the borehole and the outer domain radius, are shown in Figures 57 and 58, respectively.

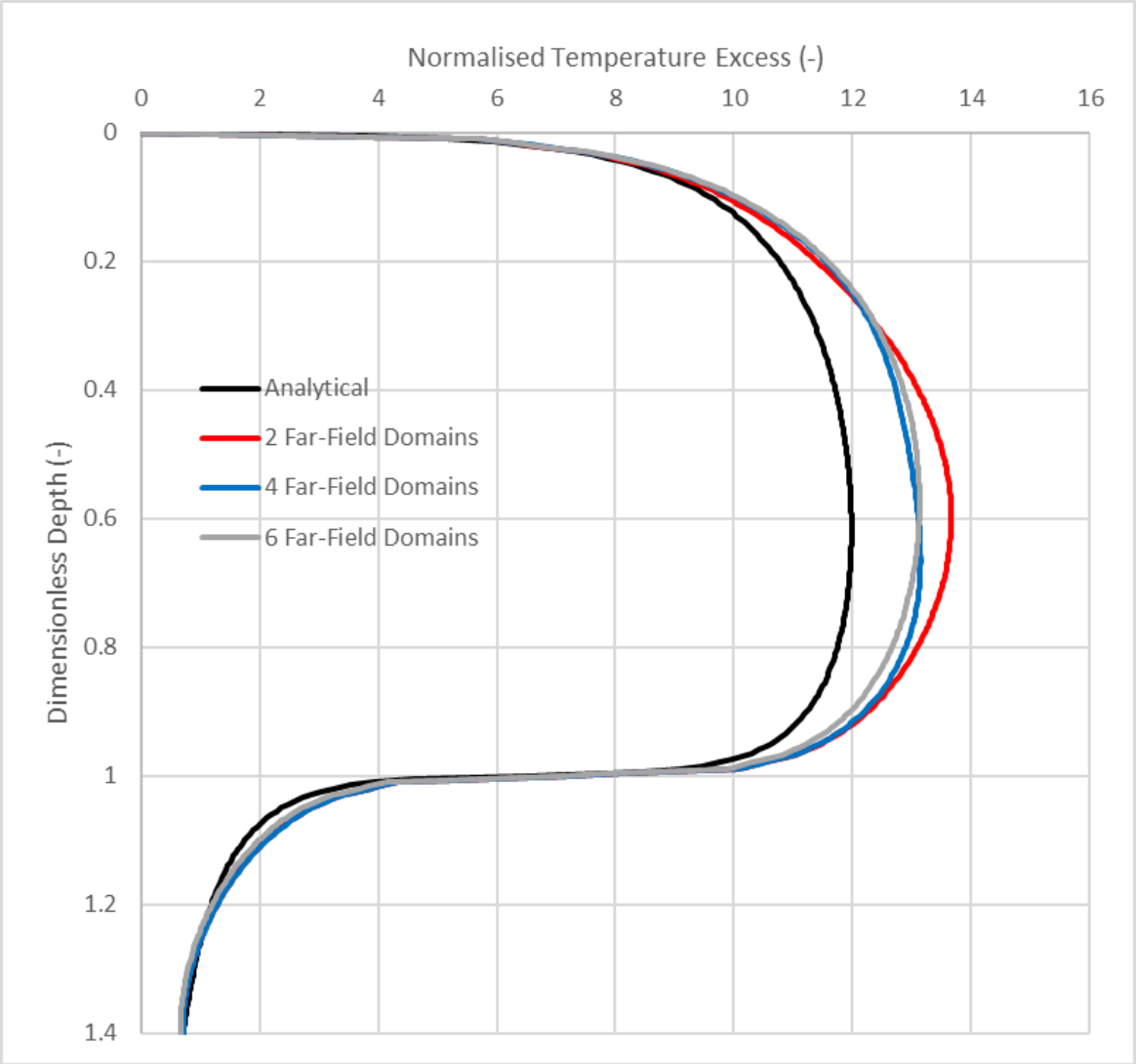

Figure 57: Performance of Composite Model for Axial Temperature Excess Distribution at Borehole Wall

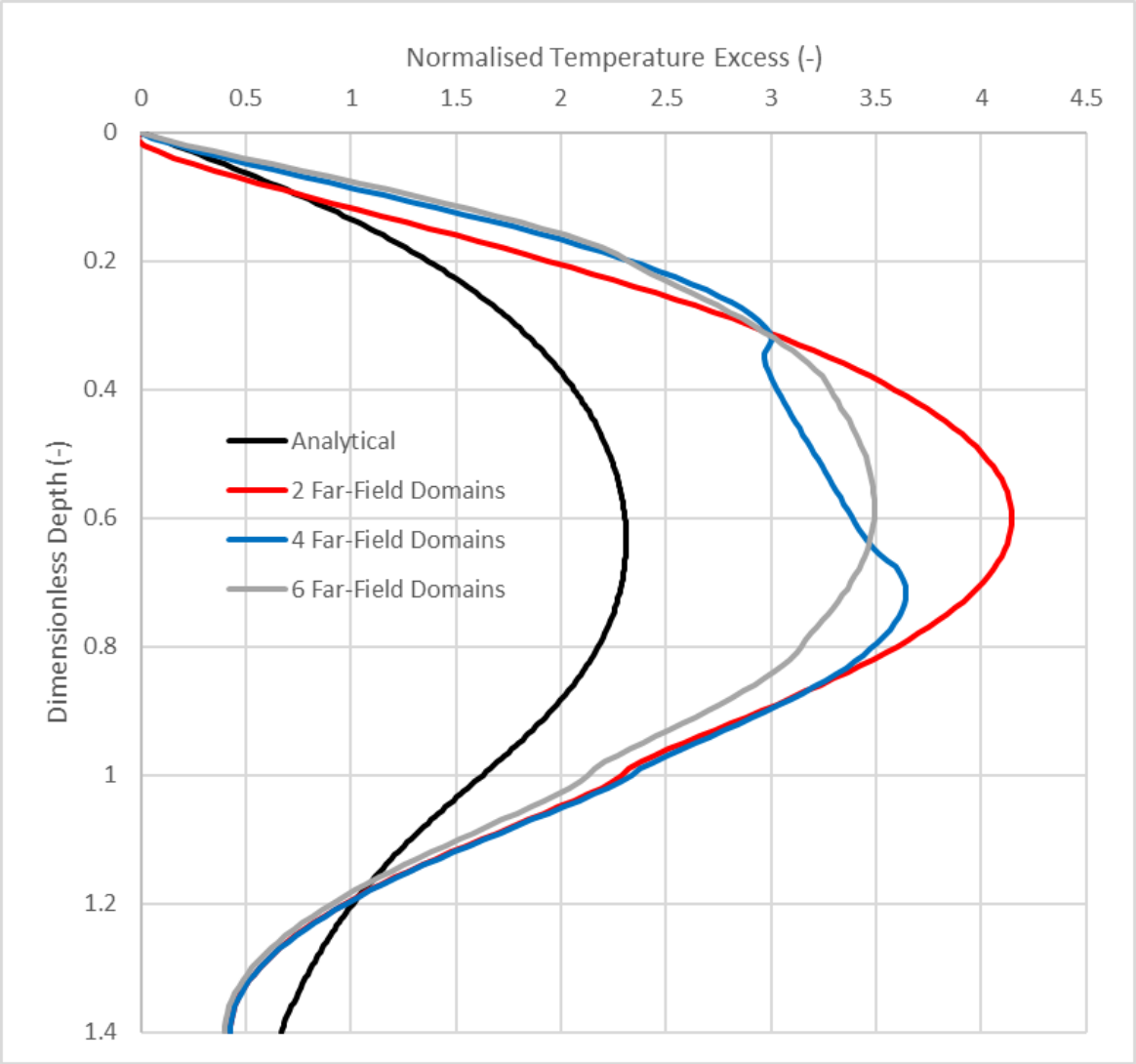

Figure 58: Performance of Composite Model for Axial Temperature Excess Distribution at 3D Domain Boundary

The analytical solutions to Equation 61 that match the two radial positions above, with fixed values of $R = 0.0015$ and $R = 0.2$, respectively, are compared to the solutions of multiple iterations of the composite model.

It is clear that increasing the discretization of the far-field improves the final solution within the near-field, since each far-field node represents a smaller volume of soil and thus is more likely to limit the error caused by the averaging. At both the borehole wall and the outer radius of the three-dimensional domain, the solution with the largest number of far-field domains resolved the most accurate temperature distribution, not only in magnitude but in the shape of the curve compared to the analytical solution. The maximum value of error by magnitude occurs for both radius values at approximately $Z = 0.5$, near the position of the highest normalised temperature excess. At the borehole wall and the outer boundary, the greatest error by percentage is 17.2% and 75.6%, respectively. Focusing on the borehole wall, this value is rather small for an upper limit on the model error that will not be approached outside of incredibly long term studies, which means that the soil temperature that the borehole, and the fluid inside, is interacting with is incredibly close to the value under real operation, which will allow the model to resolve relatively realistic borehole heat transfer and fluid temperatures, which will be reflected in the variable heat pump model.

Figure 59 shows the radial temperature distribution at the dimensionless axial position of $Z = 0.5$, which can be seen from the axial temperature distributions to belong in the region of the highest temperature excesses. For the solutions with a lower number of far-field axial slices, there is a clear discontinuity between the temperatures at the radial position where the model transitions from three- to one-dimensional. This is because the temperature being resolved in the near-field is specifically for $Z = 0.5$ and in the far-field for a range of Z values that is dependent on its location and number of axial slices. With a

small increase in slices, this discontinuity, that still must exist due to the dimension transition, becomes negligible at $Z = 0.5$, which is often used in BHE research as a representative axial location. Similarly to the axial distributions, the solutions with 4 and 6 far-field domains are very similar in magnitude.

The figure also clearly illustrates the amount of error that is introduced due to the geometric constraints of FE modelling. The analytical solution does not reach a normalised temperature excess value of 0.01 (1%) until $R = 3.58$, however due to the application of zero temperature excess at $R = 1.5$ in the numerical solution, it reaches a value of 0.01 at $R = 1.491$. This makes it clear why the numerically determined temperature excesses must be higher than the analytical solution, even without the assumption of no axial heat transfer in the far-field, since the temperature gradients must be higher throughout the domain to reach an undisturbed temperature excess within the smaller affected soil domain.

It is impossible, in FE modelling, to simulate mathematical models that include infinite or semi-infinite domains, which includes the majority of analytical borehole models. Therefore, a significant amount of the maximum error established in this section is due to the axial boundary dependence, not simply the far-field dimension simplification, which disappears for properly sized transient simulations.

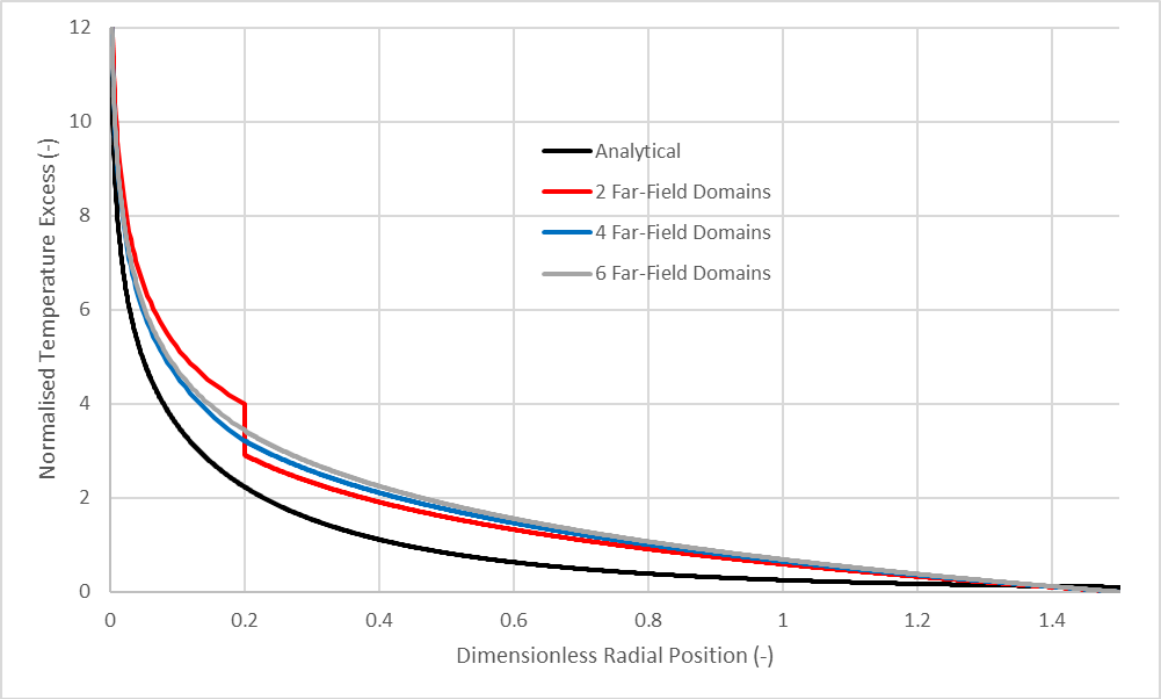

Figure 59: Performance of Composite Model for Radial Temperature Excess Distribution at Z = 0.5

6.5 Infinite Cylindrical Surface Source Model

The infinite cylindrical surface source model is another model presented by Ingersoll et al. [26] that has been influential in the simulation of borehole heat exchangers. Like the infinite line source model, the soil is considered an infinite medium, however the load is applied as a heat flux per unit length at the radius of the borehole, r_b, instead of as a heat source per unit length at the central axis, $r = 0$. Outside of the borehole, the heat transfer is still presumed to be heat conduction in an infinite region, which practically results in conduction solely in the radial direction. Carslaw and Jaeger [27] used the Laplace transform method to solve the problem, which can mathematically be represented by

$$\begin{cases} \rho_s C_{p,s} \dfrac{\partial T_s}{\partial t} = k_s \left(\dfrac{\partial^2 T_s}{\partial r^2} + \dfrac{1}{r} \dfrac{\partial T_s}{\partial r} \right) \\ r = r_b \quad -2\pi r_b k_s \dfrac{\partial T_s}{\partial r} = q_l \\ r \to \infty \quad T_s = T_{und} \\ t = 0 \quad T_s = T_{und} \end{cases} \tag{2}$$

The analytical solution to this problem is complex and must be solved numerically, just as the transient solution to the finite line source model must be. Due to the simplicity of the model's boundary conditions, a close approximation of the solution can be resolved within the COMSOL software, with a sufficiently large external radius replacing the limit of the radius tending towards infinity. This radius can be deemed to be large enough as to not affect the solution if the thermal effect of the borehole has not reached the radius, r_o, at the Fourier Number that corresponds to the end of the transient solution, $t = t_f$. Once again, this relationship is explored in a previous section. To ensure continuity within the composite model, as well as the proper heat transfer between the 3D and 1D domains, the solution to the ICSSM can be compared to the proposed model with corresponding boundary conditions. If the soil domain below the depth of the borehole (Z > 1) is removed, and an insulated boundary condition is set at the top and bottom surfaces of the 3D domain, the proposed model will imitate the conditions of the ICSSM, and the radial temperature distributions can be compared. To ensure the model can resolve a dynamic load, not just a constant load, the annual load of

$$Q_{load} = -\left(\frac{Q_{max} - Q_{min}}{2} \right) \sin\left(\frac{\pi}{182.5} t \right) + \left(\frac{Q_{max} + Q_{min}}{2} \right) \tag{38}$$

was applied to the heat pump model outlined in Appendix A.3, where Q_{max} and Q_{min} are the peak heating and cooling loads, respectively, and t is the time in days. This resulted in a fluctuating heat flux passing through the borehole wall, which was simulated in the full ICSS model to compare the resulting temperature at the boundary between the 1- and 3D domains. The temperatures at radius, $r = 10\ m$, or $R = 0.2$ are shown in Figure 60. It can be seen that the Thermal Network Connectors are properly resolving the heat transfer and radial temperature gradients across the multi-dimensional domains. The radial temperatures are exactly equivalent on the boundary between the domains, as well as within the 3D and 1D domains themselves (Figure 60), since the ICSSM is a problem of radial heat transfer only. This can be further proved by radial temperature distributions, in conjunction with the temporal distributions (Figure 60). Figure 61 shows the radial temperature distributions for multiple timesteps throughout the transient test. It can be seen that the radial temperature distribution across the point of dimensional reduction is properly resolved at each timestep.

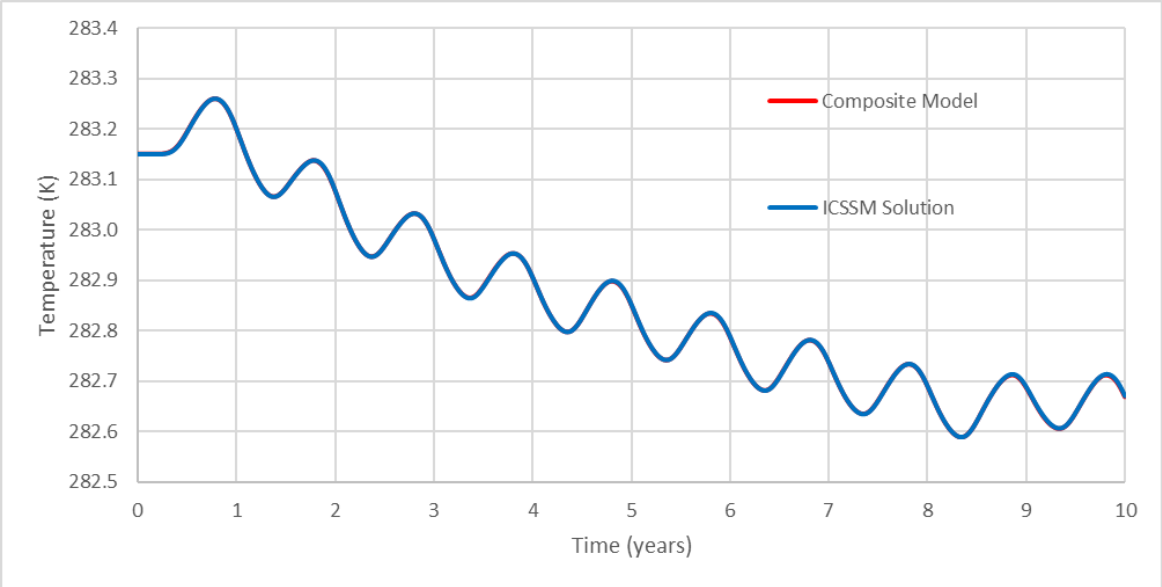

Figure 60: Performance of Composite Model for ICSSM

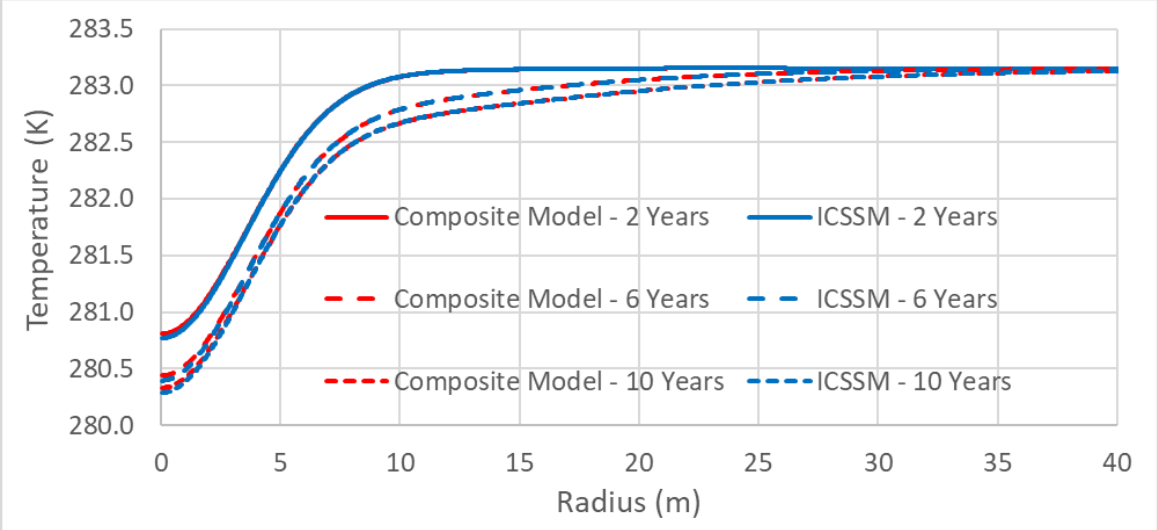

Figure 61: Radial Temperature Distributions of Composite Model and Analytical Solution

6.6 Conclusions

The Finite Line Source and Infinite Cylindrical-Surface Source Models, while very simple in their formulation, are very useful in validating the behaviour of current higher complexity models, such as the model proposed here. Analytical solutions are difficult to attain in complex systems like borehole heat exchangers and, as such, cases with simplified boundary conditions are vital to be able to fully understand the underlying physics of novel models, such as the models proposed here.

It is clear that the radial heat transfer in the far-field is properly resolved, and that the combination of the three-dimensional FEM, simplified CaRM and one-dimensional axisymmetric FEM domains established equivalent effective thermal resistances, temperature gradients, and heat transfer as the mathematical model of the ICSSM. Additionally, although some error is introduced by neglecting the axial heat transfer in the far-field, the majority of the axial heat transfer in actual operation occurs close to the borehole, and thus the proposed model is able to resolve relatively accurate axial temperature distributions within the three-dimensional domain.

The FLS solution is a steady state solution, which would take incredibly long timescales to resolve. The relative error between the analytical solution and the proposed model for a transient case would initially be zero and then increase with time once the heat flow front reached the boundary of the three-dimensional domain. This means the error of the steady-state solution would be the maximum error, with the true error of any transient solution being much lower. In more realistic operating cases than the FLS, the local heat

flow as a function of axial position much more resembles the relationship established in Marcotte and Pasquier [14], which shows fairly weak axial dependence outside of the borehole domain. These axial temperature gradients are lower near the borehole than the radial temperature gradients, and since it is known that axial gradients decrease with radial position, from our solution to the FLS, it can be reasonably concluded that axial heat transfer in the far-field, which is not being resolved within the proposed model and is thus considered to be zero, is negligible in real borehole heat exchanger operation and can be declared so in an effort to improve computational efficiency.

Chapter 7 – Conclusions and Recommended Work

The two objectives of this thesis were:

1. To develop and validate a computationally efficient but robust BHE model which allows for the simulation of realistic, transient behaviour in both the fluid and soil domains.
2. To develop and propose an improved method for determining the thermal impact of the operation of a borehole which contextualizes the impact through system heat transfer rather than local temperature excesses.

The proposed composite BHE model employs a range of physics models in domains of varying dimensions to maximize computational efficiency while allowing for the investigate of long-term transient behaviour within GSHP systems. One of the many benefits of the composite model is the lack of imposed conditions on the model, which allows for the model to resolve system behaviour with inputs limited to values more easily measurable in real circumstances.

First, the pseudo pipe approach developed by Ozudogru et al. [36] was validated and adjusted to allow for the use of a symmetry plane along the axis of the borehole U-tube. In a single borehole, this allows for the size of the discretized mesh to be reduced by a factor of two, reducing the computation time, and could be used to reduce the domain size for a study involving a borehole field, for specific field configurations.

A new method of determining the thermal impact of a borehole in transient operation was developed and validated using the Infinite Cylindrical-Source Surface

Model. The dominant mode of heat transfer, in the radial direction, was used as the basis of the method, which allowed for the new definition of a Thermal Impacting Radius to be devised within the context of the overall system heat balance instead of arbitrary temperature excess values. The new definition is backed up by theoretical and numerically resolved evidence which proves the TIR is a function of the Fourier Number. This new method provides a strong method for determining the necessary size of a simulation domain based on the overall duration of the simulation time period to ensure the model remains independent of the outer boundary.

Using data, provided in highly cited studies as well as this thesis, a justification for the reduction of the model's dimensions in the far-field is made, based on angular independence and low axial dependence in the intermediate soil field. This allowed for the final component of the composite model, one-dimensional axisymmetric heat transfer equations, to be used at the outer edges of the soil domain, a reasonable distance from the borehole. The one-dimensional domains are connected to the three-dimensional domains through the use of value-averaging components that couple two-dimensional boundary planes of the near field to zero-dimensional boundary points of the far-field. This allows for the long-term transient simulation of BHE operation, which will continually cause heat transfer effects with a growing TIR, while maintaining boundary independence without overburdening the necessary computational effort.

Although the composite model has been validated against very commonly used analytical models, like the FLSM and ICSSM, it is recommended that the model be further validated against a set of experimental data. This would require data for soil and fluid

temperatures as well as data that could be used to determine the load profile that was applied to the borehole and could confirm that the simplification in the far-field does not have dramatic effects on the fluid temperatures within the borehole. It is important that that error is not reflected in the fluid temperatures since it drives the COP of the heat pump and therefore the efficiency of the entire GSHP system.

The composite model can be used to introduce system complexities in the near-field for long-term transient studies without increasing the computational effort to levels which are unfeasible. It is also recommended that the model be used to study unique cases of BHE operation, which can include, but are not limited to, angled boreholes, borehole fields and the addition of thermal storage components into the overall GSHP systems.

Angled boreholes, when arranged in borehole fields, allow for the access of a much higher volume of soil for a relatively small cross-sectional area of the borehole field at the ground surface. This is a method currently used in GSHP design in urban areas where much of the land surrounding the BHE is already developed and cannot be accessed at the ground surface. The benefit of increased accessible soil volume makes the modelling of the borehole operation increasingly difficult since the discretized mesh scales with the necessary geometry size, and the computational effort scales with the size of the mesh. However, the use of one-dimensional models in the far-field will allow for modelling of angled borehole fields without increasing the three-dimensional soil domain to unreasonable levels.

The modelling of both angled boreholes and regular borehole fields, could benefit from the proposed composite model since the model resolves the fluid temperatures and extends into the far-field surrounding the borehole field domain without increasing the computational effort to the point of unfeasibility. This composite model allows for the connection of individual boreholes into borehole strings, which more accurately reflects the complex temperature distributions in borehole fields than uniform assumptions.

The proposed definition for a new TIR was initial devised through the theory and numerical solution of the ICSSM. Due to the assumption of an infinite borehole, and an infinite surrounding soil, the analytical model is reduced to a single dimension, the radial direction r. As established in this thesis, radial heat transfer is the dominant mode of heat transfer surrounding a borehole, however axial heat transfer also plays a role on overall system performance. It is recommended that studies be conducted to establish the effect of the dimensionless axial position on the heat flow based TIR. This investigation could include two-dimensional analytical solutions, such as the FLS, or realistic borehole operation which resolve fluid temperatures as a function of the axial position, like the pseudo pipe approach employed within the composite model proposed in this thesis.

Bibliography

[1] NRCAN, “Comprehensive Energy Use Database - Natural Resources Canada.” https://oee.nrcan.gc.ca/corporate/statistics/neud/dpa/menus/trends/comprehensive_tables/list.cfm (accessed Oct. 26, 2022).

[2] H. N. Pollack, S. J. Hurter, and J. R. Johnson, “Heat flow from the Earth’s interior: Analysis of the global data set,” *Rev. Geophys.*, vol. 31, no. 3, pp. 267–280, 1993, doi: 10.1029/93RG01249.

[3] J. Delbeke, A. Runge-Metzger, Y. Slingenberg, and J. Werksman, “Paris Agreement,” 2019. doi: 10.4324/9789276082569-2.

[4] Intergovernmental Panel on Climate Change, “Climate Change 2022 - Mitigation of Climate Change - Summary for Policymakers (SPM),” 2022.

[5] “Global greenhouse gas emissions - Government of Canada.” https://www.canada.ca/en/environment-climate-change/services/environmental-indicators/global-greenhouse-gas-emissions.html (accessed Oct. 26, 2022).

[6] “Climate Action Tracker - Canada.” https://climateactiontracker.org/countries/canada/ (accessed Oct. 26, 2022).

[7] C. L. Rubio, J. L. García-Alcaraz, E. Martínez-Cámara, J. I. Latorre-Biel, E. Jiménez-Macías, and J. Blanco-Fernández, “Replacement of electric resistive space heating by a geothermal heat pump in a residential application – Environmental amortisation,” *Sustain. Energy Technol. Assessments*, vol. 37, no. August 2019, p.

100567, 2020, doi: 10.1016/j.seta.2019.100567.

[8] D. Moya, C. Aldás, and P. Kaparaju, “Geothermal energy: Power plant technology and direct heat applications,” *Renew. Sustain. Energy Rev.*, vol. 94, no. June, pp. 889–901, 2018, doi: 10.1016/j.rser.2018.06.047.

[9] J. Limberger *et al.*, “Geothermal energy in deep aquifers: A global assessment of the resource base for direct heat utilization,” *Renew. Sustain. Energy Rev.*, vol. 82, no. September 2017, pp. 961–975, 2018, doi: 10.1016/j.rser.2017.09.084.

[10] L. Lamarche, “Horizontal ground heat exchangers modelling,” *Appl. Therm. Eng.*, vol. 155, no. February, pp. 534–545, 2019, doi: 10.1016/j.applthermaleng.2019.04.006.

[11] J. Claesson and A. Dunand, *Heat Extraction From the Ground By Horizontal Pipes. a Mathematical Analysis.* 1983.

[12] S. Kavanaugh and K. Rafferty, *Geothermal Heating and Cooling: Design of Ground-Source Heat Pump Systems*. Atlanta: ASHRAE.

[13] M. Bernier, “A review of the cylindrical heat source method for the design and analysis of vertical ground-coupled heat pump systems,” 2000.

[14] D. Marcotte and P. Pasquier, “On the estimation of thermal resistance in borehole thermal conductivity test,” *Renew. Energy*, vol. 33, no. 11, pp. 2407–2415, 2008, doi: 10.1016/j.renene.2008.01.021.

[15] J. Raymond, R. Therrien, L. Gosselin, and R. Lefebvre, “A Review of Thermal

Response Test Analysis Using Pumping Test Concepts," *Ground Water*, vol. 49, no. 6, pp. 932–945, 2011, doi: 10.1111/j.1745-6584.2010.00791.x.

[16] ASHRAE, *ASHRAE handbook: HVAC applications.* Atlanta: ASHRAE, Inc., 2011.

[17] R. A. Beier, M. D. Smith, and J. D. Spitler, "Reference data sets for vertical borehole ground heat exchanger models and thermal response test analysis," *Geothermics*, vol. 40, no. 1, pp. 79–85, 2011, doi: 10.1016/j.geothermics.2010.12.007.

[18] D. Zhang, P. Gao, Y. Zhou, Y. Wang, and G. Zhou, "An experimental and numerical investigation on temperature profile of underground soil in the process of heat storage," *Renew. Energy*, vol. 148, pp. 1–21, 2020, doi: 10.1016/j.renene.2019.11.123.

[19] S. H. Baek, M. S. Yeo, and K. W. Kim, "Effects of the geothermal load on the ground temperature recovery in a ground heat exchanger," *Energy Build.*, vol. 136, pp. 63–72, 2017, doi: 10.1016/j.enbuild.2016.11.056.

[20] P. Pasquier and D. Marcotte, "Joint use of quasi-3D response model and spectral method to simulate borehole heat exchanger," *Geothermics*, vol. 51, pp. 281–299, 2014, doi: 10.1016/j.geothermics.2014.02.001.

[21] Y. L. E. Law and S. B. Dworkin, "Characterization of the effects of borehole configuration and interference with long term ground temperature modelling of

ground source heat pumps," *Appl. Energy*, vol. 179, pp. 1032–1047, 2016, doi: 10.1016/j.apenergy.2016.07.048.

[22] A. Aljabr, A. Chiasson, and A. Alhajjaji, "Numerical Modeling of The Effects of Micro-Encapsulated Phase Change Materials Intermixed with Grout in Vertical Borehole Heat Exchangers," *Geothermics*, vol. 96, pp. 1–10, 2021, doi: 10.1016/j.geothermics.2021.102197.

[23] J. Lund, B. Sanner, L. Rybach, R. Curtis, and G. Hellström, "Geothermal (ground-source) heat pums A world review," *Geo-Heat Cent. Q. Bull.*, pp. 1–10, 2004.

[24] J. W. Lund and A. N. Toth, "Direct utilization of geothermal energy 2020 worldwide review," *Geothermics*, vol. 90, pp. 1–39, 2021, doi: 10.1016/j.geothermics.2020.101915.

[25] S. E. Grasby *et al.*, "Geothermal energy resource potential of Canada, Open File 6914 (revised)," *Geol. Surv. Canada*, vol. Open File, p. 322 p., 2012, [Online]. Available: http://geoscan.nrcan.gc.ca/starweb/geoscan/servlet.starweb?path=geoscan/fulle.web&search1=R=291488%0APembina

[26] A. C. Ingersoll, L.R. Zobol, O.J. Ingersoll, *Heat Conduction with Engineering, Geological, and Other Applications, revised edition*. Madison, WI, USA: University of Wisconsin Press, 1954.

[27] H. S. Carslaw and J. C. Jaeger, "Carslaw and Jaeger, Conduction of Heat in

Solids.pdf." p. 517, 1959.

[28] S. Bertagnolio, M. Bernier, and M. Kummert, "Comparing vertical ground heat exchanger models," *J. Build. Perform. Simul.*, vol. 5, no. 6, pp. 369–383, 2012, doi: 10.1080/19401493.2011.652175.

[29] Y. Cui, J. Zhu, S. Twaha, and S. Riffat, "A comprehensive review on 2D and 3D models of vertical ground heat exchangers," *Renew. Sustain. Energy Rev.*, vol. 94, no. May 2017, pp. 84–114, 2018, doi: 10.1016/j.rser.2018.05.063.

[30] M. Li and A. C. K. Lai, "Review of analytical models for heat transfer by vertical ground heat exchangers (GHEs): A perspective of time and space scales," *Appl. Energy*, vol. 151, pp. 178–191, 2015, doi: 10.1016/j.apenergy.2015.04.070.

[31] H. Y. Zeng, N. R. Diao, and Z. H. Fang, "A finite line-source model for boreholes in geothermal heat exchangers," *Heat Transf. - Asian Res.*, vol. 31, no. 7, pp. 558–567, 2002, doi: 10.1002/htj.10057.

[32] L. Lamarche and B. Beauchamp, "A new contribution to the finite line-source model for geothermal boreholes," *Energy Build.*, vol. 39, no. 2, pp. 188–198, 2007, doi: 10.1016/j.enbuild.2006.06.003.

[33] R. Al-Khoury, P. G. Bonnier, and R. B. J. Brinkgreve, "Efficient finite element formulation for geothermal heating systems. Part I: Steady state," *Int. J. Numer. Methods Eng.*, vol. 63, no. 7, pp. 988–1013, 2005, doi: 10.1002/nme.1313.

[34] R. Al-Khoury and P. G. Bonnier, "Efficient finite element formulation for

geothermal heating systems. Part II: Transient," *Int. J. Numer. Methods Eng.*, vol. 67, no. 5, pp. 725–745, 2006, doi: 10.1002/nme.1662.

[35] L. Lamarche, S. Kajl, and B. Beauchamp, "A review of methods to evaluate borehole thermal resistances in geothermal heat-pump systems," *Geothermics*, vol. 39, no. 2, pp. 187–200, Jun. 2010, doi: 10.1016/J.GEOTHERMICS.2010.03.003.

[36] T. Y. Ozudogru, C. G. Olgun, and A. Senol, "3D numerical modeling of vertical geothermal heat exchangers," *Geothermics*, vol. 51, pp. 312–324, Jul. 2014, doi: 10.1016/j.geothermics.2014.02.005.

[37] P. Kandiah and M. F. Lightstone, "Modelling of the thermal performance of a borehole field containing a large buried tank," *Geothermics*, vol. 60, pp. 94–104, 2016, doi: 10.1016/j.geothermics.2015.12.001.

[38] M. Z. Olfman, A. D. Woodbury, and J. Bartley, "Effects of depth and material property variations on the ground temperature response to heating by a deep vertical ground heat exchanger in purely conductive media," *Geothermics*, vol. 51, pp. 9–30, Jul. 2014, doi: 10.1016/j.geothermics.2013.10.002.

[39] S. Koohi-Fayegh and M. A. Rosen, "Examination of thermal interaction of multiple vertical ground heat exchangers," *Appl. Energy*, vol. 97, pp. 962–969, 2012, doi: 10.1016/j.apenergy.2012.02.018.

[40] M. Ahmadfard and M. Bernier, "A review of vertical ground heat exchanger sizing tools including an inter-model comparison," *Renew. Sustain. Energy Rev.*, vol.

110, no. January 2018, pp. 247–265, 2019, doi: 10.1016/j.rser.2019.04.045.

[41] A. Chiasson, *Geothermal heat pump and heat engine systems: theory and practice*. ASME Press and John Wiley & Sons, Ltd., 2016.

[42] J. Claesson and P. Eskilson, "Conductive heat extraction to a deep borehole: Thermal analyses and dimensioning rules," *Energy*, vol. 13, no. 6, pp. 509–527, 1988, doi: 10.1016/0360-5442(88)90005-9.

[43] C. Naldi and E. Zanchini, "Effects of the total borehole length and of the heat pump inverter on the performance of a ground-coupled heat pump system," *Appl. Therm. Eng.*, vol. 128, pp. 306–319, 2018, doi: 10.1016/j.applthermaleng.2017.09.025.

[44] T. You, W. Wu, W. Shi, B. Wang, and X. Li, "An overview of the problems and solutions of soil thermal imbalance of ground-coupled heat pumps in cold regions," *Appl. Energy*, vol. 177, pp. 515–536, 2016, doi: 10.1016/j.apenergy.2016.05.115.

[45] N. Batini, A. F. Rotta Loria, P. Conti, D. Testi, W. Grassi, and L. Laloui, "Energy and geotechnical behaviour of energy piles for different design solutions," *Appl. Therm. Eng.*, vol. 86, pp. 199–213, 2015, doi: 10.1016/j.applthermaleng.2015.04.050.

[46] J. Chen, L. Xia, B. Li, and D. Mmereki, "Simulation and experimental analysis of optimal buried depth of the vertical U-tube ground heat exchanger for a ground-coupled heat pump system," *Renew. Energy*, no. 73, pp. 46–54, 2015.

[47] K. Zhou, J. Mao, Y. Li, and J. Xiang, “Parameters optimization of borehole and internal thermal resistance for single U-tube ground heat exchangers using Taguchi method,” *Energy Convers. Manag.*, vol. 201, no. October, p. 112177, 2019, doi: 10.1016/j.enconman.2019.112177.

[48] C. K. Lee, “Effects of multiple ground layers on thermal response test analysis and ground-source heat pump simulation,” *Appl. Energy*, vol. 88, no. 12, pp. 4405–4410, 2011, doi: 10.1016/j.apenergy.2011.05.023.

[49] A. K. Tiwari and P. Basu, “Interpretation of TRT data in the presence of natural convection and groundwater flow in saturated ground,” *Comput. Geotech.*, vol. 140, no. August, p. 104426, 2021, doi: 10.1016/j.compgeo.2021.104426.

[50] R. Fan, Y. Jiang, Y. Yao, D. Shiming, and Z. Ma, “A study on the performance of a geothermal heat exchanger under coupled heat conduction and groundwater advection,” *Energy*, vol. 32, no. 11, pp. 2199–2209, 2007, doi: 10.1016/j.energy.2007.05.001.

[51] Y. Guo, X. Hu, J. Banks, and W. V. Liu, “Considering buried depth in the moving finite line source model for vertical borehole heat exchangers—A new solution,” *Energy Build.*, vol. 214, 2020, doi: 10.1016/j.enbuild.2020.109859.

[52] S. Lazzari, A. Priarone, and E. Zanchini, “Long-term performance of BHE (borehole heat exchanger) fields with negligible groundwater movement,” *Energy*, vol. 35, no. 12, pp. 4966–4974, 2010, doi: 10.1016/j.energy.2010.08.028.

[53] M. Li, P. Li, V. Chan, and A. C. K. Lai, "Full-scale temperature response function (G-function) for heat transfer by borehole ground heat exchangers (GHEs) from sub-hour to decades," *Appl. Energy*, vol. 136, pp. 197–205, 2014, doi: 10.1016/j.apenergy.2014.09.013.

[54] Y. Noorollahi, P. Bigdelou, F. Pourfayaz, and H. Yousefi, "Numerical modeling and economic analysis of a ground source heat pump for supplying energy for a greenhouse in Alborz province, Iran," *J. Clean. Prod.*, vol. 131, pp. 145–154, 2016, doi: 10.1016/j.jclepro.2016.05.059.

[55] D. Kim, G. Kim, D. Kim, and H. Baek, "Experimental and numerical investigation of thermal properties of cement-based grouts used for vertical ground heat exchanger," *Renew. Energy*, vol. 112, pp. 260–267, 2017, doi: 10.1016/j.renene.2017.05.045.

[56] D. Qi, L. Pu, F. Sun, and Y. Li, "Numerical investigation on thermal performance of ground heat exchangers using phase change materials as grout for ground source heat pump system," *Applied Thermal Engineering*, vol. 106. pp. 1023–1032, 2016. doi: 10.1016/j.applthermaleng.2016.06.048.

[57] A. Aljabr, A. Chiasson, and A. Alhajjaji, "Numerical Modeling of The Effects of Micro-Encapsulated Phase Change Materials Intermixed with Grout in Vertical Borehole Heat Exchangers," *Geothermics*, vol. 96, 2021, doi: 10.1016/j.geothermics.2021.102197.

[58] M. Longeon, A. Soupart, J. F. Fourmigué, A. Bruch, and P. Marty, "Experimental

and numerical study of annular PCM storage in the presence of natural convection," *Appl. Energy*, vol. 112, pp. 175–184, 2013, doi: 10.1016/j.apenergy.2013.06.007.

[59] W. Wu, B. Wang, T. You, W. Shi, and X. Li, "A potential solution for thermal imbalance of ground source heat pump systems in cold regions: Ground source absorption heat pump," *Renew. Energy*, vol. 59, pp. 39–48, 2013, doi: 10.1016/j.renene.2013.03.020.

[60] W. Retkowski, G. Ziefle, and J. Thöming, "Evaluation of different heat extraction strategies for shallow vertical ground-source heat pump systems," *Appl. Energy*, vol. 149, pp. 259–271, 2015, doi: 10.1016/j.apenergy.2015.03.004.

[61] J. Xi, Y. Li, M. Liu, and R. Z. Wang, "Study on the thermal effect of the ground heat exchanger of GSHP in the eastern China area," *Energy*, vol. 141, pp. 56–65, 2017, doi: 10.1016/j.energy.2017.09.060.

[62] W. Li, X. Li, Y. Wang, and J. Tu, "An integrated predictive model of the long-term performance of ground source heat pump (GSHP) systems," *Energy Build.*, vol. 159, pp. 309–318, 2018, doi: 10.1016/j.enbuild.2017.11.012.

[63] M. Lee, D. Cha, S. Yun, S.-M. Yoon, and Y. Kim, "Comparative heating performance evalutation of hybrid ground-source heat pumps using serial and parallel configurations with the application of ground heat exchangers," *Energy Convers. Manag.*, no. 229, p. 113743, 2021.

[64] F. Chen *et al.*, "Numerical assessment on the thermal imbalance of multiple ground heat exchangers connected in parallel," *Geothermics*, vol. 96, no. May, p. 102191, 2021, doi: 10.1016/j.geothermics.2021.102191.

[65] Z. Liu, W. Xu, C. Qian, X. Chen, and G. Jin, "Investigation on the feasibility and performance of ground source heat pump (GSHP) in three cities in cold climate zone, China," *Renew. Energy*, vol. 84, pp. 89–96, 2015, doi: 10.1016/j.renene.2015.06.019.

[66] S. Shukla, A. M. Bayomy, S. Antoun, A. Mwesigye, W. H. Leong, and S. B. Dworkin, "Performance characterization of novel caisson-based thermal storage for ground source heat pumps," *Renew. Energy*, vol. 174, pp. 43–54, 2021, doi: 10.1016/j.renene.2021.04.075.

[67] D. Bauer, W. Heidemann, and H. J. G. Diersch, "Transient 3D analysis of borehole heat exchanger modeling," *Geothermics*, vol. 40, no. 4, pp. 250–260, 2011, doi: 10.1016/j.geothermics.2011.08.001.

[68] B. Cerfontaine, G. Radioti, F. Collin, and R. Charlier, "Formulation of a 1D finite element of heat exchanger for accurate modelling of the grouting behaviour: Application to cyclic thermal loading," *Renew. Energy*, vol. 96, pp. 65–79, 2016, doi: 10.1016/j.renene.2016.04.034.

[69] D. Gordon, T. Bolisetti, D. S. K. Ting, and S. Reitsma, "Short-term fluid temperature variations in either a coaxial or U-tube borehole heat exchanger," *Geothermics*, vol. 67, pp. 29–39, 2017, doi: 10.1016/j.geothermics.2016.12.001.

[70] L. Zhang, Q. Zhang, G. Huang, and Y. Du, "A p(t)-linear average method to estimate the thermal parameters of the borehole heat exchangers for in situ thermal response test," *Appl. Energy*, vol. 131, pp. 211–221, 2014, doi: 10.1016/j.apenergy.2014.06.031.

[71] L. Zhang, Q. Zhang, J. Acuña, and X. Ma, "Improved p(t)-linear Average Method for Ground Thermal Properties Estimation during in-situ Thermal Response Test," *Procedia Eng.*, vol. 121, pp. 726–734, 2015, doi: 10.1016/j.proeng.2015.09.020.

[72] Y. Noorollahi, R. Saeidi, M. Mohammadi, A. Amiri, and M. Hosseinzadeh, "The effects of ground heat exchanger parameters changes on geothermal heat pump performance – A review," *Appl. Therm. Eng.*, vol. 129, pp. 1645–1658, 2018, doi: 10.1016/j.applthermaleng.2017.10.111.

[73] N. Pandey, K. Murugesan, and H. R. Thomas, "Optimization of ground heat exchangers for space heating and cooling applications using Taguchi method and utility concept," *Appl. Energy*, vol. 190, pp. 421–438, 2017, doi: 10.1016/j.apenergy.2016.12.154.

[74] M. Z. Lukawski, R. L. Silverman, and J. W. Tester, "Uncertainty analysis of geothermal well drilling and completion costs," *Geothermics*, vol. 64, pp. 382–391, 2016, doi: 10.1016/j.geothermics.2016.06.017.

[75] N. Batini, A. F. Rotta Loria, P. Conti, D. Testi, W. Grassi, and L. Laloui, "Energy and geotechnical behaviour of energy piles for different design solutions," *Appl. Therm. Eng.*, vol. 86, pp. 199–213, Jul. 2015, doi:

10.1016/J.APPLTHERMALENG.2015.04.050.

[76] P. Eskilson and J. Claesson, “Simulation model for thermally interacting heat extraction boreholes,” *Numer. Heat Transf.*, vol. 13, no. 2, pp. 149–165, 1988, doi: 10.1080/10407788808913609.

[77] C. Li, J. Mao, Z. Xing, J. Zhou, and Y. Li, “Analysis of geo-temperature restoration performance under intermittent operation of borehole heat exchanger fields,” *Sustain.*, vol. 8, no. 1, pp. 1–14, 2016, doi: 10.3390/su8010035.

[78] Y. Luo, G. Xu, and N. Cheng, “Proposing stratified segmented finite line source (SS-FLS) method for dynamic simulation of medium-deep coaxial borehole heat exchanger in multiple ground layers,” *Renew. Energy*, vol. 179, pp. 604–624, 2021, doi: 10.1016/j.renene.2021.07.086.

[79] Y. Huang, Y. Zhang, Y. Xie, Y. Zhang, and X. Gao, “Thermal performance analysis on the composition attributes of deep coaxial borehole heat exchanger for building heating,” *Energy Build.*, vol. 221, p. 110019, 2020, doi: 10.1016/j.enbuild.2020.110019.

[80] Y. Huang, Y. Zhang, Y. Xie, Y. Zhang, X. Gao, and J. Ma, “Long-term thermal performance analysis of deep coaxial borehole heat exchanger based on field test,” *J. Clean. Prod.*, vol. 278, p. 123396, 2021, doi: 10.1016/j.jclepro.2020.123396.

[81] J. Liu, F. Wang, W. Cai, Z. Wang, and C. Li, “Numerical investigation on the effects of geological parameters and layered subsurface on the thermal

performance of medium-deep borehole heat exchanger," *Renew. Energy*, vol. 149, pp. 384–399, 2020, doi: 10.1016/j.renene.2019.11.158.

[82] COMSOL Multiphysics 5.3, "Pipe flow module," *Manual*, pp. 1–6, 2017.

[83] V. Gnielinski, "New equations for heat and mass transfer in turbulent pipe and channel flow," *Int. J. Chem. Eng.*, vol. 16, pp. 359–268, 1976.

[84] S. W. Churchill, "Friction factor equations spans all fluid-flow regimes," *Chem. Eng.*, vol. 84, pp. 91–92, 1997.

[85] R. A. Beier, "Deconvolution and convolution methods for thermal response tests on borehole heat exchangers," *Geothermics*, vol. 86, no. December 2019, p. 101786, 2020, doi: 10.1016/j.geothermics.2019.101786.

[86] R. A. Beier, "Personal Communication." 2021.

[87] R. A. Beier, J. Acuña, P. Mogensen, and B. Palm, "Vertical temperature profiles and borehole resistance in a U-tube borehole heat exchanger," *Geothermics*, vol. 44, pp. 23–32, 2012, doi: 10.1016/j.geothermics.2012.06.001.

[88] R. A. Beier, J. Acuña, P. Mogensen, and B. Palm, "Borehole resistance and vertical temperature profiles in coaxial borehole heat exchangers," *Appl. Energy*, vol. 102, pp. 665–675, 2013, doi: 10.1016/j.apenergy.2012.08.007.

[89] R. A. Beier, "Transient heat transfer in a U-tube borehole heat exchanger," *Appl. Therm. Eng.*, vol. 62, no. 1, pp. 256–266, 2014, doi: 10.1016/j.applthermaleng.2013.09.014.

[90] "COMSOL Multiphysics v.5.4." COMSOL AB, Stockholm, Sweden. [Online]. Available: www.comsol.com

[91] P. Pasquier and D. Marcotte, "Short-term simulation of ground heat exchanger with an improved TRCM," *Renew. Energy*, vol. 46, pp. 92–99, 2012, doi: 10.1016/j.renene.2012.03.014.

[92] A. Zarrella, M. Scarpa, and M. De Carli, "Short time step analysis of vertical ground-coupled heat exchangers: The approach of CaRM," *Renew. Energy*, vol. 36, no. 9, pp. 2357–2367, 2011, doi: 10.1016/j.renene.2011.01.032.

[93] M. De Carli, M. Tonon, A. Zarrella, and R. Zecchin, "A computational capacity resistance model (CaRM) for vertical ground-coupled heat exchangers," *Renew. Energy*, vol. 35, no. 7, pp. 1537–1550, 2010, doi: 10.1016/j.renene.2009.11.034.

[94] G. Radioti, B. Cerfontaine, R. Charlier, and F. Nguyen, "Experimental and numerical investigation of a long-duration Thermal Response Test: Borehole Heat Exchanger behaviour and thermal plume in the heterogeneous rock mass," *Geothermics*, vol. 71, no. October 2017, pp. 245–258, 2018, doi: 10.1016/j.geothermics.2017.10.001.

[95] W. Choi and R. Ooka, "Effect of disturbance on thermal response test, part 2: Numerical study of applicability and limitation of infinite line source model for interpretation under disturbance from outdoor environment," *Renew. Energy*, vol. 85, pp. 1090–1105, 2016, doi: 10.1016/j.renene.2015.07.049.

[96] S. Morchio, M. Fossa, and R. A. Beier, “Study on the best heat transfer rate in thermal response test experiments with coaxial and U-pipe borehole heat exchangers,” *Appl. Therm. Eng.*, vol. 200, no. September 2021, p. 117621, 2022, doi: 10.1016/j.applthermaleng.2021.117621.

[97] A. M. Bayomy, J. Wang, and S. B. Dworkin, “Numerical and analytical study of a geo-exchange borehole using conventional grout and bentonite-based backfilling material,” *Int. J. Energy Res.*, vol. 45, no. 9, pp. 13545–13562, 2021, doi: 10.1002/er.6684.

[98] SCL, “TRNSYS 18,” 2018. [Online]. Available: http://www.trnsys.com/

[99] University of Wisconsin-Madison. Solar Energy Laboratory, “Volume 8: Weather Data. TRNSYS 18 A Transient System Simulation Program.,” 2017. [Online]. Available: http://www.trnsys.com/index.html

[100] H. M. Teamah and M. F. Lightstone, “Numerical study of the electrical load shift capability of a ground source heat pump system with phase change thermal storage,” *Energy Build.*, vol. 199, pp. 235–246, 2019, doi: 10.1016/j.enbuild.2019.06.056.

Appendix

A.1 Verifications of COMSOL's Heat Transfer in Pipes

Constant Heat Rate

COMSOL

For this verification, the COMSOL model is simplified to a steady-state solution without pipe roughness, wall heat transfer or the pressure work term. The 1D energy equation is, practically, simplified from the general equation

$$\rho A C_p \frac{\partial T_f}{\partial t} + \rho A C_p \boldsymbol{u} \cdot \nabla T_f = \nabla \cdot Ak \nabla T_f + f_D \frac{\rho A}{2 d_h} |\boldsymbol{u}|^3 + Q + Q_{wall} + Q_p \qquad (A.1)$$

to

$$\rho A C_p \boldsymbol{u} \cdot \nabla T_f = \nabla \cdot Ak \nabla T_f + Q \qquad (A.2)$$

The model input variables are discussed later in the section.

Analytical

The general energy equation developed for axisymmetric flow in a circular pipe yields

$$\rho C_p u \left(\frac{dT_f}{dz}\right) + \rho C_p \vartheta \left(\frac{dT_f}{dr}\right) = u \frac{dP}{dz} + \frac{1}{r} \frac{\partial}{\partial r} \left(rk \frac{\partial T_f}{\partial r}\right) + \mu \left(\frac{\partial u}{\partial r}\right)^2 \qquad (A.3)$$

which can be simplified for the purpose of this verification. For laminar flow, the energy equation for axisymmetric flow in a pipe with axisymmetric heating can be expressed as

$$\frac{u}{\alpha}\left(\frac{dT_f}{dz}\right) = \frac{1}{r}\frac{\partial}{\partial r}\left(r\frac{\partial T_f}{\partial r}\right) \tag{A.4}$$

for fully developed flow without viscous dissipation. These terms represent the first and second terms in the COMSOL model, respectively, with the Q term acting as the analytical solutions boundary condition. For 3D flow, a bulk temperature, T_b, can be defined as the adiabatic mixing of a moving fluid at any given cross-section to reflect an average temperature. This definition is useful for a 1D solver such as COMSOL's *Heat Transfer in Pipes*. The non-dimensional temperature is defined in terms of the bulk temperature and the wall temperature, T_o, and it is constant in the z-direction for a fully developed temperature profile

$$\left[\frac{\partial}{\partial r}\left(\frac{T_{f,o} - T_f}{T_{f,o} - T_{f,b}}\right)\right]_{r=r_o} = Constant \tag{A.5}$$

If the heat transfer coefficient is introduced in terms of the bulk temperature and we apply the Fourier conduction law to the fluid, then

$$q_o'' = h\left(T_{f,o} - T_{f,b}\right) \tag{A.6}$$

$$q_o'' = -k\left(\frac{\partial T_f}{\partial r}\right)_{r=r_o} \tag{A.7}$$

$$\frac{q_o''/k}{q_o''/h} = \frac{h}{k} = Constant \qquad (A.8)$$

which is approximately true away from the pipe entrance for certain boundary conditions. Once again, this is useful for our case of solving a 1D energy equation, which ignores the radial development of temperature and velocity profiles. The non-dimensional temperature profile is commonly seen to be invariant in the *z*-direction as well, which is expressed as

$$\frac{\partial}{\partial z}\left(\frac{T_{f,o} - T_f}{T_{f,o} - T_{f,b}}\right) = 0 \qquad (A.9)$$

and can be differentiated to show that

$$\frac{\partial T_f}{\partial z} = \frac{dT_{f,o}}{dz} - \frac{T_{f,o} - T_f}{T_{f,o} - T_{f,b}}\frac{dT_o}{dz} + \frac{T_{f,o} - T_f}{T_{f,o} - T_{f,b}}\frac{dT_{f,b}}{dz} \qquad (A.10)$$

If the heat rate per unit length is constant, then $dT_{f,o}/dz = dT_{f,b}/dz$, since the temperature difference must be constant, which simplifies the above to $dT_{f,o}/dz = dT_{f,b}/dz = Constant$. This can be substituted into the original energy equation for axisymmetric flow

$$\frac{u}{\alpha}\left(\frac{dT_{f,b}}{dz}\right) = \frac{1}{r}\frac{\partial}{\partial r}\left(r\frac{\partial T_f}{\partial r}\right) \qquad (A.11)$$

This provides justification for using the bulk temperature for certain boundary conditions, including constant heat rate and a constant surface temperature (in the next verification), in relation to the fluid's position *in the flow direction*. Now that this has been

justified, the conservation of energy is applied to an elemental control volume, which encapsulates the entire cross-sectional area of the pipe, and yields

$$\rho\pi r_o^2 u C_p T_b + 2\pi r_o dz q_o'' = \rho\pi r_o^2 u C_p \left(T_{f,b} + \frac{dT_{f,b}}{dz} dz\right) \quad (A.12)$$

$$q_o'' = \frac{1}{2}\rho r_o u C_p \left(\frac{dT_{f,b}}{dz}\right) \quad (A.13)$$

which can be integrated to get

$$dT_{f,b} = \frac{2q_o''}{\rho r_o u C_p} dz \quad (A.14)$$

$$T_{f,b}(z) = \frac{2q_o''}{\rho r_o u C_p} \cdot z + T_{in} \quad (A.15)$$

It should be noted, that COMSOL uses a heat rate per unit length (W/m) due to solving a 1D solver, so it must be converted to an equivalent constant surface heat rate (W/m^2). This is calculated using the following formula

$$q_o'' = \frac{q_o'}{2\pi r_o} \quad (A.16)$$

With a general solution, properties can be introduced to create a specific analytical solution. The following table summarizes the properties used for the verification, in both the COMSOL model and the analytical equation.

Table 6: Properties for Constant Heat Rate Verification

Property	**Value**
$\boldsymbol{q_o'}$	$20{,}000\ W/m$
$\boldsymbol{q_o''}$	$63{,}661.98\ W/m^2$
$\boldsymbol{\rho}$	$997\ kg/m^3$
$\boldsymbol{r_o}$	$0.05\ m$
$\boldsymbol{u}$	$0.5\ m/s$
$\boldsymbol{C_p}$	$4184\ J/kg \cdot K$
$\boldsymbol{T_{in}}$	$20(℃)$

This results in the analytical solution

$$T_{f,b}(℃) = 1.220908946 \cdot z(m) + 20(℃) \qquad (A.17)$$

A comparison of the analytical and COMSOL solutions is seen in Figure 62 below.

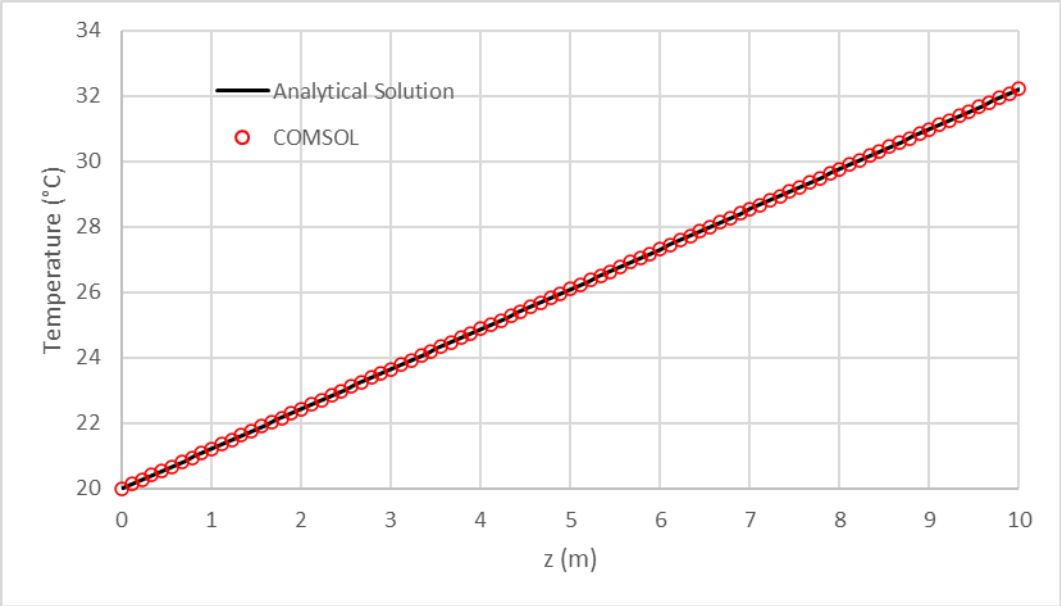

Figure 62: Results of the Constant Heat Rate Test Validation

With a constant heat rate, constant density and constant specific heat capacity we can see that the analytical temperature profile is linear as the fluid passes through the pipe from inlet to outlet. It should be noted that COMSOL uses a temperature dependent model for the density and specific heat capacity of water, however in this small temperature range the variation is negligible. The COMSOL model agrees well with the analytical solution.

Constant Heat Transfer Coefficient and Wall Temperature

COMSOL

For this verification, the COMSOL model is simplified to a steady-state solution without pipe roughness, general heat source or the pressure work term. The 1D energy equation is, practically, simplified from

$$\rho A C_p \frac{\partial T_f}{\partial t} + \rho A C_p \boldsymbol{u} \cdot \nabla T_f = \nabla \cdot Ak \nabla T_f + f_D \frac{\rho A}{2 d_h} |\boldsymbol{u}|^3 + Q + Q_{wall} + Q_p \qquad (A.1)$$

to

$$\rho A C_p \boldsymbol{u} \cdot \nabla T_f = \nabla \cdot Ak \nabla T_f + Q_{wall} \qquad (A.18)$$

The model input variables are discussed later in the section.

Analytical

In the previous section, justification was provided for substituting the bulk temperature into the energy equation for a constant wall temperature. The energy balance for a simple heat exchanger with an isothermal wall and constant heat transfer coefficient is

$$\dot{m} C_p dT_f = h P_o \left(T_{ext} - T_f\right) dz \qquad (A.19)$$

when diffusion is negligible. This can be solved to get the exact solution:

$$\frac{T_{ext} - T_{f,b}(z)}{T_{ext} - T_{in}} = e^{\left(-\frac{hP_o}{\dot{m}C_p} \cdot z\right)} \quad (A.20)$$

$$T_{f,b}(z) = (T_{in} - T_{ext})e^{\left(-\frac{hP_o z}{\dot{m}C_p}\right)} + T_{ext} \quad (A.21)$$

Once again, real property values are introduced to establish an analytical equation. The following table summarizes the properties used for the verification, in both the COMSOL model and the analytical equation.

Table 7: Properties for Constant Heat Transfer Coefficient Verification

Property	**Value**
h	$10{,}000\ W/m^2 \cdot K$
$\boldsymbol{\rho}$	$997\ kg/m^3$
$\boldsymbol{r_o}$	$0.05\ m$
$\boldsymbol{u}$	$0.5\ m/s$
$\boldsymbol{\dot{m}}$	$3.915\ kg/s$
$\boldsymbol{P_o}$	$0.31416\ m$
$\boldsymbol{C_p}$	$4184\ J/kg \cdot K$
$\boldsymbol{k}$	$0.598\ W/m \cdot K$
$\boldsymbol{T_{in}}$	20 ℃
$\boldsymbol{T_{ext}}$	50 ℃

This results in the analytical solution

$$T_{f,b}(℃) = 30\left(1 - e^{-0.1918 \cdot z(m)}\right) + 20(℃) \qquad (A.22)$$

A comparison of the analytical and COMSOL solutions is seen in Figure 63 below.

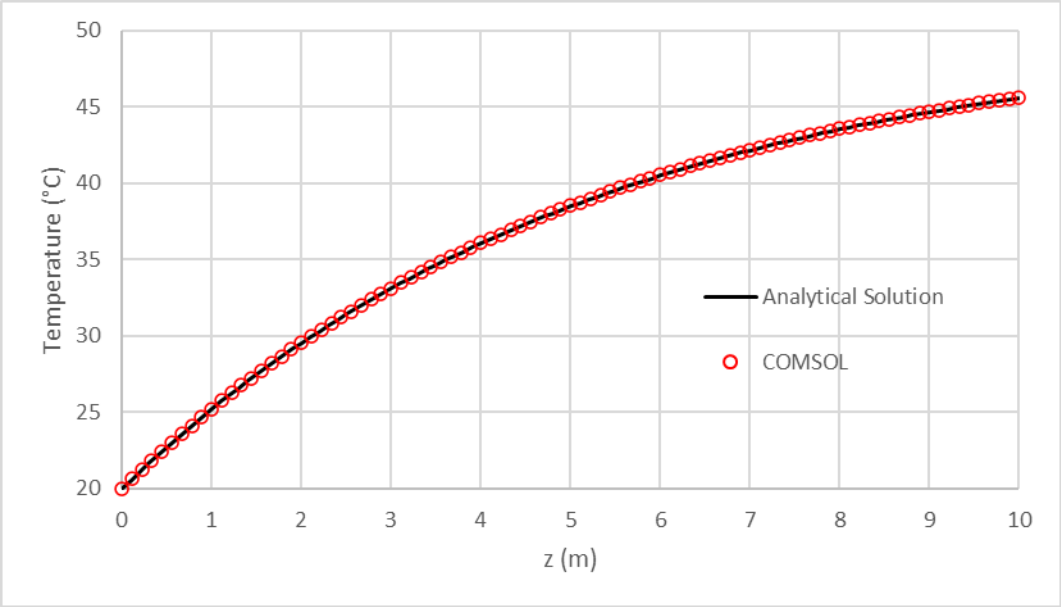

Figure 63: Results of the Constant Heat Transfer Coefficient and Wall Temperature Validation

Both solutions clearly follow an exponential trend with the same shape factors. Again, in this small temperature range the variation of the water's properties is negligible. It is also verified for this simple case that diffusion is minimal. This is expected when we observe the Péclet Number for our verification case

$$Pe_D = \frac{Du}{\alpha} \tag{A.23}$$

$$\alpha = \frac{k}{\rho C_p} \tag{A.24}$$

$$Pe_D = 348{,}783 \tag{A.25}$$

The Péclet Number is a ratio of the advective transport rate to the diffusive transport rate, which provides theoretical confidence for the simplification.

Transient Heat Accumulation

COMSOL

Finally, it is important to ensure that the transient term behaves as expected for the 1D pipe elements. To do so, the transient term and wall heat transfer are isolated by solving a case without flow ($\boldsymbol{u} = \mathbf{0}$) to solve an analytical solution. By setting the velocity to zero, this also eliminates the temperature gradient in the pipe, which also nullifies the conduction term. To simplify, the general heat source term and the pressure work term are also removed. This makes the 1D energy equation simplify from

$$\rho A C_p \frac{\partial T_f}{\partial t} + \rho A C_p \boldsymbol{u} \cdot \nabla T_f = \nabla \cdot Ak \nabla T_f + f_D \frac{\rho A}{2 d_h} |\boldsymbol{u}|^3 + Q + Q_{wall} + Q_p \tag{A.1}$$

to

$$\rho A C_p \frac{\partial T_f}{\partial t} = (hZ)_{eff} \left(T_{ext} - T_f\right) \tag{A.26}$$

The model input variables are discussed later in the section.

Analytical

If it is assumed that there is a high ratio of surface area to fluid volume, as in a thin pipe, the transient temperature of a control can be solved for from the general energy equation, through a 1D energy equation. Without convection heat transfer ($\boldsymbol{u} = \mathbf{0}$) or a general heat source, the governing equation is

$$MC_p dT_f = hA\left(T_{ext} - T_f\right) \tag{A.27}$$

For consistency, this is called the bulk temperature. The equation is rearranged to be able to solve the differential equation

$$MC_p \frac{\partial T_{f,b}}{\partial t} = hA\left(T_{ext} - T_{f,b}\right) \tag{A.28}$$

$$MC_p \frac{\partial T_{f,b}}{\partial t} + hAT_{f,b} = hAT_{ext} \tag{A.29}$$

This differential equation is simple to solve with the knowledge of the initial temperature, T_{in}. This results in the equation

$$T_{f,b}(t) = (T_{in} - T_{ext})e^{-\frac{hA}{MC_p}t} + T_{ext} \tag{A.30}$$

Once again, real property values are introduced to establish an analytical equation. The following table summarizes the properties used for the verification, in both the COMSOL model and the analytical equation.

Table 8: Properties for Transient Accumulation Verification

Property	**Value**
h	$1{,}000\ W/m^2 \cdot K$
$\boldsymbol{\rho}$	$997\ kg/m^3$
$\boldsymbol{r_o}$	$0.05\ m$
$\boldsymbol{L}$	$10\ m$
$\boldsymbol{M}$	$78.304\ kg$
$\boldsymbol{C_p}$	$4184\ J/kg \cdot K$
$\boldsymbol{T_{in}}$	20 ℃
$\boldsymbol{T_{ext}}$	50 ℃

This results in the analytical solution

$$T_{f,b}(℃) = 50 - 30e^{-0.009589 \cdot t(s)} \qquad (A.31)$$

A comparison of the analytical and COMSOL solutions is seen in Figure 64 below.

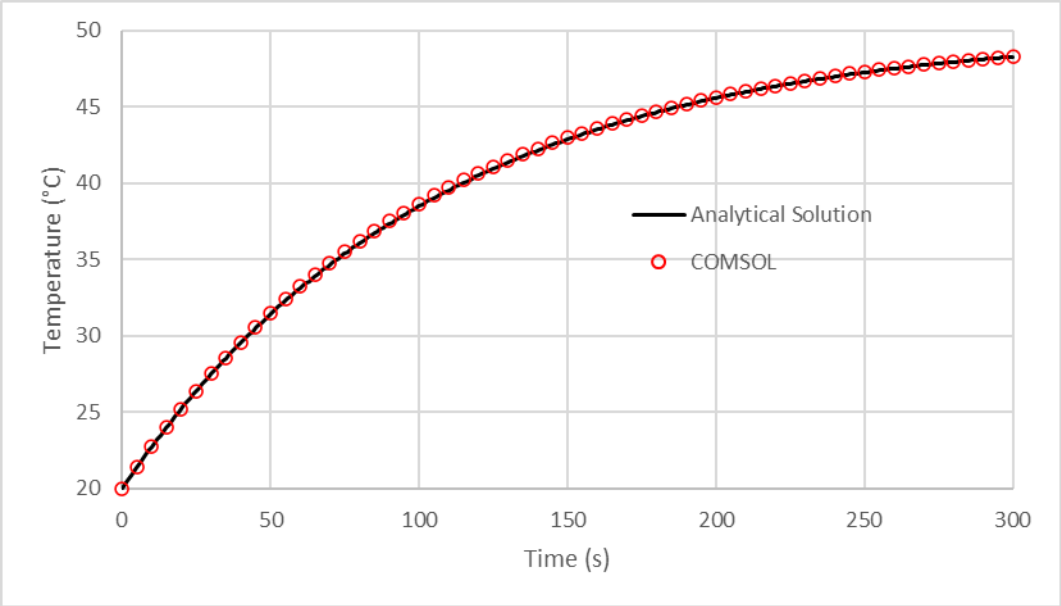

Figure 64: Results of the Transient Heat Accumulation Validation

Pseudo Pipe Conduction

When using COMSOL's *Heat Transfer in Pipes*, the 3D geometry of fluid *and* the surrounding pipe is represented by 1D line segments that are drawn in 3D space, at the centre axis of the true pipe geometry. This results in a number of potential sources of error when incorporated into larger 3D models, such as those necessary for modelling borehole heat exchangers. These include a temperature coupling error, as the solid domain must be extended to the centre axis of the pipe which creates an error in the radial temperature distribution, and the lack of thermal mass of the pipes in the 1D model. To overcome these challenges, the 'Pseudo Pipe' approach was developed by Ozudogru et al. [36]. The reader is referred to Ozudogru et al. [36] for a more detailed description. To verify this approach,

a simple radial conduction model is compared to an analytical solution based on the thermal resistance analogy.

COMSOL

Although COMSOL must solve the temperature distribution in three-dimensional space, when studying the radial heat transfer from a 1D pipe element, simplifications can be made to match a resolvable analytical solution. As always, the governing equation of the pipe domain can simplify from

$$\rho A C_p \frac{\partial T_f}{\partial t} + \rho A C_p \boldsymbol{u} \cdot \nabla T_f = \nabla \cdot Ak \nabla T_f + f_D \frac{\rho A}{2 d_h} |\boldsymbol{u}|^3 + Q + Q_{wall} + Q_p \qquad (A.1)$$

to

$$\rho A C_p \boldsymbol{u} \cdot \nabla T_f = Q_{wall} \qquad (A.32)$$

for an incompressible, steady state flow without friction or a heat source. With low enough heat extraction from the solid domain, as is set up in this verification, the temperature variation in the fluid is enough to disregard the conduction term as well. This 1D solution is coupled to the real soil domain by a solid cylinder representing the pipe wall geometry, in actuality a *hollow* cylinder, to conduct the 1D temperature distribution to a 3D physical space, as a boundary to the soil domain, which the pipe would be in an actual 3D environment. To do this successfully, the real pipe thermal conductivity is attributed to the *Wall Heat Transfer* node in the *Heat Transfer in Pipes* interface, which governs the Q_{wall} term of the energy equation, and the thermal conductivity of the pseudo pipe domain is set to a highly conductive *radial* value. This allows for the temperature of the pseudo

pipe to match the 1D pipe element in the flow direction without adding non-physical conduction in the flow direction, while still creating a 'bulk' temperature distribution in 3D space. The *Heat Transfer in Solids* interface, which controls all the solid domains, is governed by the equation

$$\rho C_p \frac{\partial T_s}{\partial t} + \rho C_p \boldsymbol{u} \cdot \nabla T_s + \nabla \cdot \boldsymbol{q} = Q + Q_{ted} \qquad (A.33)$$

$$\boldsymbol{q} = -k \nabla T_s \qquad (A.34)$$

which can be simplified to

$$-\nabla \cdot k \nabla T_s = Q \qquad (A.35)$$

for a steady state solution, without translational motion or thermoelastic damping. For the purposes of the verification, the thermal conductivity, k, will be set to only be radial, $\{k_{mat}, k_{mat}, 0\}$, in all solid domains, however, in a true borehole heat exchanger model, this is only applied to the pseudo pipe domain.

The model input variables are discussed later in the section.

Analytical

The thermal resistance analogy follows the equation

$$Q = qA_o = \frac{\left(T_f - T_{ext}\right)}{R_{Total}} \qquad (A.36)$$

where the total resistance is

$$R_{Total} = \sum \frac{1}{h_j A_j} + \sum \frac{\ln(d_o/d_i)}{2\pi k_j L} \qquad (A.37)$$

For this case, there is one fluid and two solid layers, the copper wall and the soil cylinder. The resistance is therefore

$$R_{Total} = \frac{1}{hA_{p,i}} + \frac{\ln\left(d_{w,o}/d_{w,i}\right)}{2\pi k_w L} + \frac{\ln\left(d_{s,o}/d_{s,i}\right)}{2\pi k_s L} \qquad (A.38)$$

If conduction is constrained to be entirely radial in the solid domain, and the heat flux at the outer boundary of the solid domain is constant, this means at any point, the temperature difference between the fluid and the external temperature is a constant represented by the equation

$$\Delta T(z) = qA_o R_{Total} = qA_o \left(\frac{1}{hA_{p,i}} + \frac{\ln\left(d_{w,o}/d_{w,i}\right)}{2\pi k_w L} + \frac{\ln\left(d_{s,o}/d_{s,i}\right)}{2\pi k_s L} \right) \qquad (A.39)$$

Real property values are introduced, for our final case, to establish an analytical equation. The following table summarizes the properties used for the verification, in both the COMSOL model and the analytical equation. Since the thermal resistance analogy assumes a unidirectional flow of heat, thermal properties are applied as scalars, whereas in COMSOL the thermal conductivity is applied as a vector in three-dimensional space.

Table 9: Properties for Pseudo Pipe Conduction Verification

Property	**Value**
$\boldsymbol{q}$	$-100\ W/m$
h	$1{,}067\ W/m^2 \cdot K$
$\boldsymbol{d_{w,i}}$	$0.098\ m$
$\boldsymbol{d_{w,o}}$	$0.1\ m$
$\boldsymbol{d_{s,i}}$	$0.1\ m$
$\boldsymbol{d_{s,o}}$	$1\ m$
$\boldsymbol{L}$	$10\ m$
$\boldsymbol{k_w}$	$0.39\ W/m \cdot K$
$\boldsymbol{k_{w,pseudo}}$	$\{1000, 1000, 0\}\ W/m \cdot K$
$\boldsymbol{k_s}$	$\{2.82, 2.82, 0\}\ W/m \cdot K$
$\boldsymbol{A_{p,i}}$	$3.0788\ m^2$
$\boldsymbol{A_o}$	$31.4159\ m^2$
$\boldsymbol{u}$	$0.5\ m/s$

This results in the constant analytical solution

$$\Delta T(z) = \ 44.3686\ (℃) \qquad (A.40)$$

A comparison of the analytical and COMSOL solutions is seen in Figure 65 below.

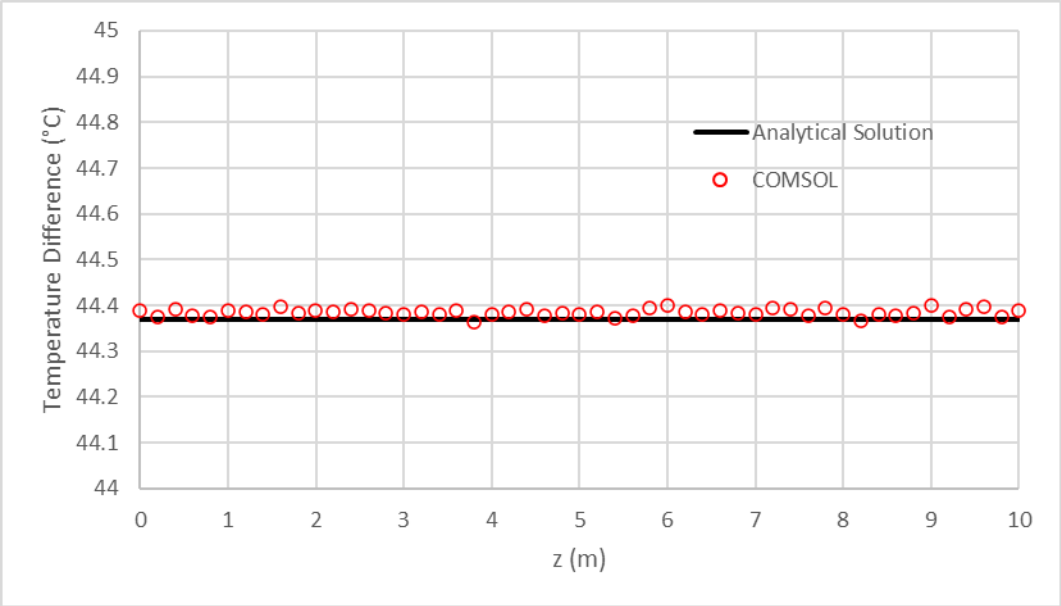

Figure 65: Results of the Pseudo Pipe Conduction Validation

The maximum difference between the Analytical and COMSOL solutions at any point along the pipe length is 0.0299972 °C, which can be accounted for in slight changes in temperature dependent fluid properties and mesh dependence at the outer boundary (see Figure 66, for reference). In a perfectly mesh independent solution, the temperature at the boundary would be a smooth gradient. Figure 67 is the radial temperature distribution at halfway through the pipe ($z = 5\,m$) and shows the solution to the temperature coupling error, as the radial gradient is moved to its correct position at the true pipe geometry's outer radius. Figure 67 also provides additional evidence of mesh dependence on the small differences between the COMSOL and analytical solution, as we can see the space between the edge element and the next internal node. This validates the 'pseudo pipe' method, as it

properly couples the 1D fluid flow to the 3D domain without the radial temperature error that arises without the presence of the pseudo pipe.

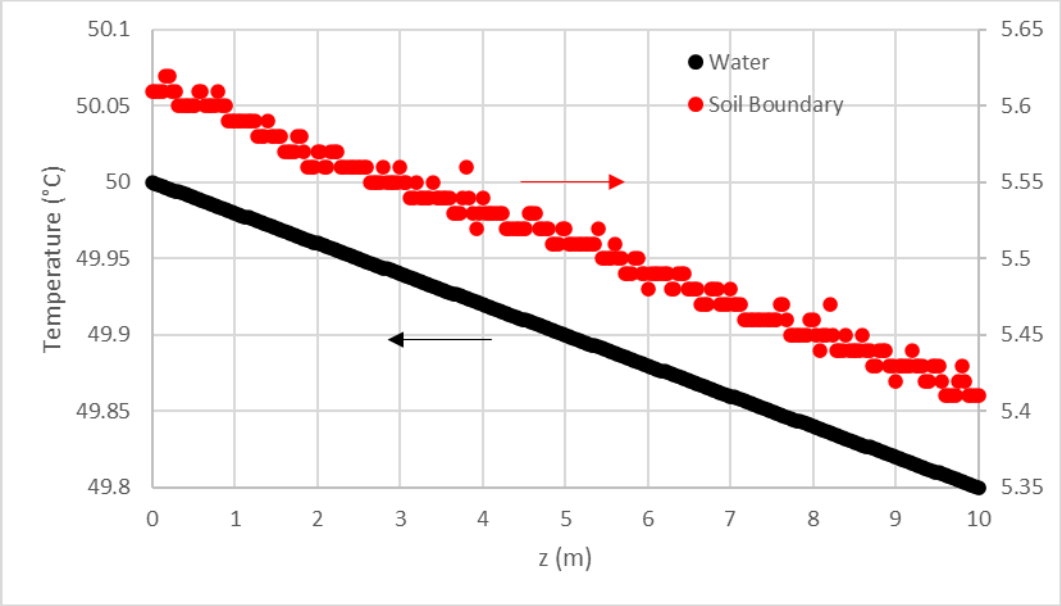

Figure 66: Axial Temperature Distribution of 1D Fluid Element and Soil at r = 0.5 m

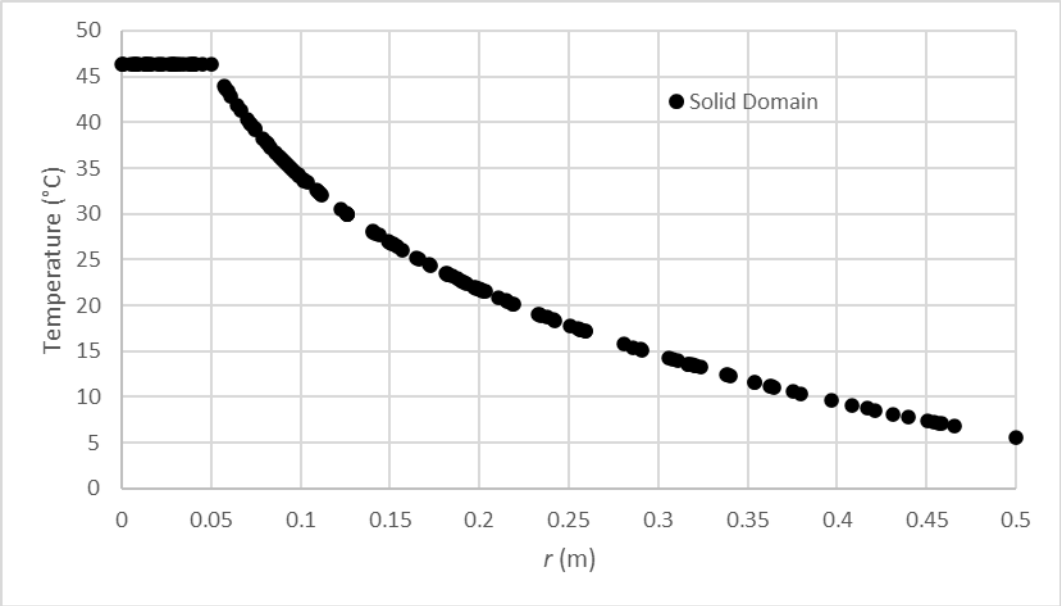

Figure 67: Radial Temperature Distribution at z = 5 m

A.2 Details of the Symmetrical Adjustments

The *Heat Transfer in Pipes* physics employs heat transfer correlations that govern the model, since it cannot rely upon traditional FEM methods resolved on a 3D discretized mesh. These correlations are dependent on the hydraulic diameter, which also determines the calculated surface area for heat transfer between the 1D element and the 3D domain, which presents the problem of needing to reduce the surface area without changing the hydraulic diameter. Therefore, the Wall Heat Transfer is instead manually adjusted, by a factor of 0.5, so the magnitude of heat transfer between the fluid and solid domain's is

exactly half for an identical hydraulic diameter. The old variable equation, shown on left of the arrow and the new equation, shown on the right, are expressed as

$$htp.Qwall = htp.hZeff * (htp.wht1.Text - T)\ to\ htp.Qwall \rightarrow htp.hZeff * (htp.wht1.Text - T)/2 \quad (A.41)$$

Each of the four addition terms of the 1D Energy Equation need to be equally adjusted, to assure that the change in the Wall Heat Transfer does not alter the fluid temperature gradients. The variable common between each term is the cross-sectional area of the pipe, which should be reduced to reflect the geometry of the half-circular cross-section. To ensure the hydraulic diameter stays constant, the wetted perimeters of the internal and external pipe faces are also reduced by a factor of 0.5. The old and new variable definitions, once again, are

$$htp.A = 0.25 * pi * (2.733[cm])^2\ to\ htp.A \rightarrow 0.125 * pi * (2.733[cm])^2 \quad (A.42)$$

$$htp.Z = pi * 2.733[cm]\ to\ htp.Z \rightarrow pi * 2.733[cm]/2 \quad (A.43)$$

$$htp.Zww = pi * htp.dhww\ to\ htp.Zww \rightarrow pi * htp.dhww/2 \quad (A.44)$$

These adjustments can be made within the relevant component equations in the COMSOL software interface prior to resolving the simulation.

A.3 Developing and Integrating a Variable COP Heat Pump Model

*A.*3.1 Inspiration for External Heat Pump Calculation

In order to assess not only the performance of the BHE, but also the performance of the GSHP system itself, some type of model for the heat pump is needed. Instead of applying a variable, specified temperature at the inlet, the circulating fluid loop is closed and a model for the fluid temperatures external to the BHE is added. There are multiple reasons why this is more appropriate for long-term system simulation.

Firstly, there is much less experimental data available for long timescale operation of borehole heat exchangers, and as such the scenarios in which the model can be used has often been limited to short timescale operations, namely in simulating Thermal Response Tests ([49], [94]–[96]). This has been useful in the development of these models and the investigation of TRT's accuracy and effectiveness, but the scenario of a constant load is rather limited in its real-world application. Secondly, it may be of interest to use the discussed model to study the effect that a model parameter may have on the fluid temperatures. This may include any model input, but the example can be taken of the thermal diffusivity of the soil, α_s.

The thermal diffusivity of the soil will influence the effective thermal resistance of the soil domain in relation to the borehole. This will affect the overall heat transfer, and therefore the fluid temperature distribution within the GSHP system. If the inlet temperature to the BHE is fixed as a boundary condition, the simulation can not properly respond to the overall system's effects on the circulating fluid temperatures. Without

communication between the outlet temperature from one timestep and the inlet temperature of the next timestep, the model is missing an important component of the model's ability to predict long timescale operation and its efficiency.

As such, the domain of the model must be extended to include the portion of the fluid's heat transfer that occurs externally to the borehole heat exchanger within the geothermal heat pump. Extending the domain of the model will ultimately make the boundary conditions set to the inlet and outlet of the fluid domain obsolete, as will be seen in this section, and allow for much greater flexibility of the scenarios that can be simulated using the proposed model. This section highlights and explains two important contributions to the model that must be made to apply the proposed model accurately. First, an example of a variable housing heat load is developed, as the transient fluid temperature input is replaced by a load that is applied to the fluid at the geothermal heat pump. Secondly, the method with which this load is applied to the fluid is outlined and its implementation is explained in detail. Figure 68 illustrates this energy balance, which surrounds the GSHP and governs how it connects the house load to the BHE. In order to make the proposed model as independent as possible, communication between simulation timesteps was employed, to ensure the history of the previously resolved solutions continued to affect the solutions to follow, as is realistic to true borehole heat exchanger operation.

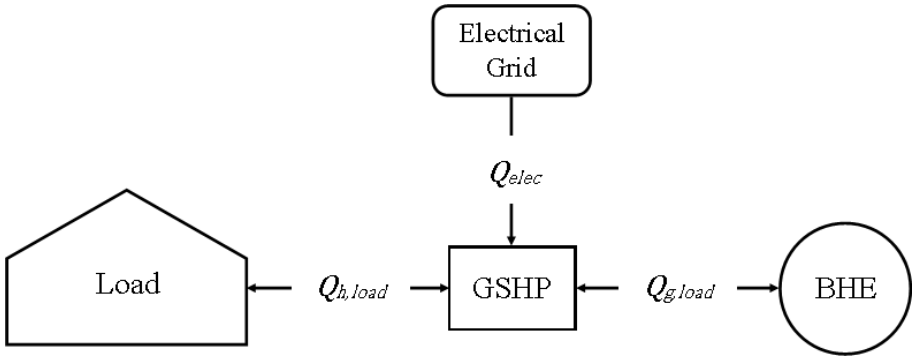

Figure 68: Illustration of Energy Balance on a Ground-Source Heat Pump within a Geoexchange System

A.3.2 Applying the Heat Load to the Model

In order to create a realistic long-term simulation of a borehole heat exchanger in use in a residential setting, an equally realistic building load profile needs to be employed. This can be achieved in a variety of ways, with varying levels of complexity. A method treating the house as a lumped thermal capacitance is used as an example in Appendix A.3.3, to illustrate a variable load that accounts for the seasonal conditions in Southern Ontario.

No matter the method of load generation, the result must be a load, in watts, W, as a function of the time, with the period of a year, to capture the full seasonal effects. Although this load profile represents the realistic behaviour of a dynamic house, the load applied to a borehole heat exchanger is dependent on the efficiency of the ground-source heat pump, and as such, dependent on the temperatures leaving and entering the borehole heat exchanger itself. Additionally, the fluid boundary conditions applied to the previously

developed borehole heat exchanger model, which are a set inlet temperature and a heat outflow condition at the outlet, will act as the basis for the heat load approach but will be adjusted to accommodate a wider range of operation scenarios.

In order to integrate this load profile into a long-term dynamic study of a borehole heat exchanger, an algorithm for the calculations of fluid boundary conditions was developed. The algorithm is presented in Figure 69 and was inspired by a number of sources taken from literature ([62], [66], [97]). Several assumptions were made on the load side (house load) to simplify the algorithm's integration as the house side temperatures were not pertinent to this study.

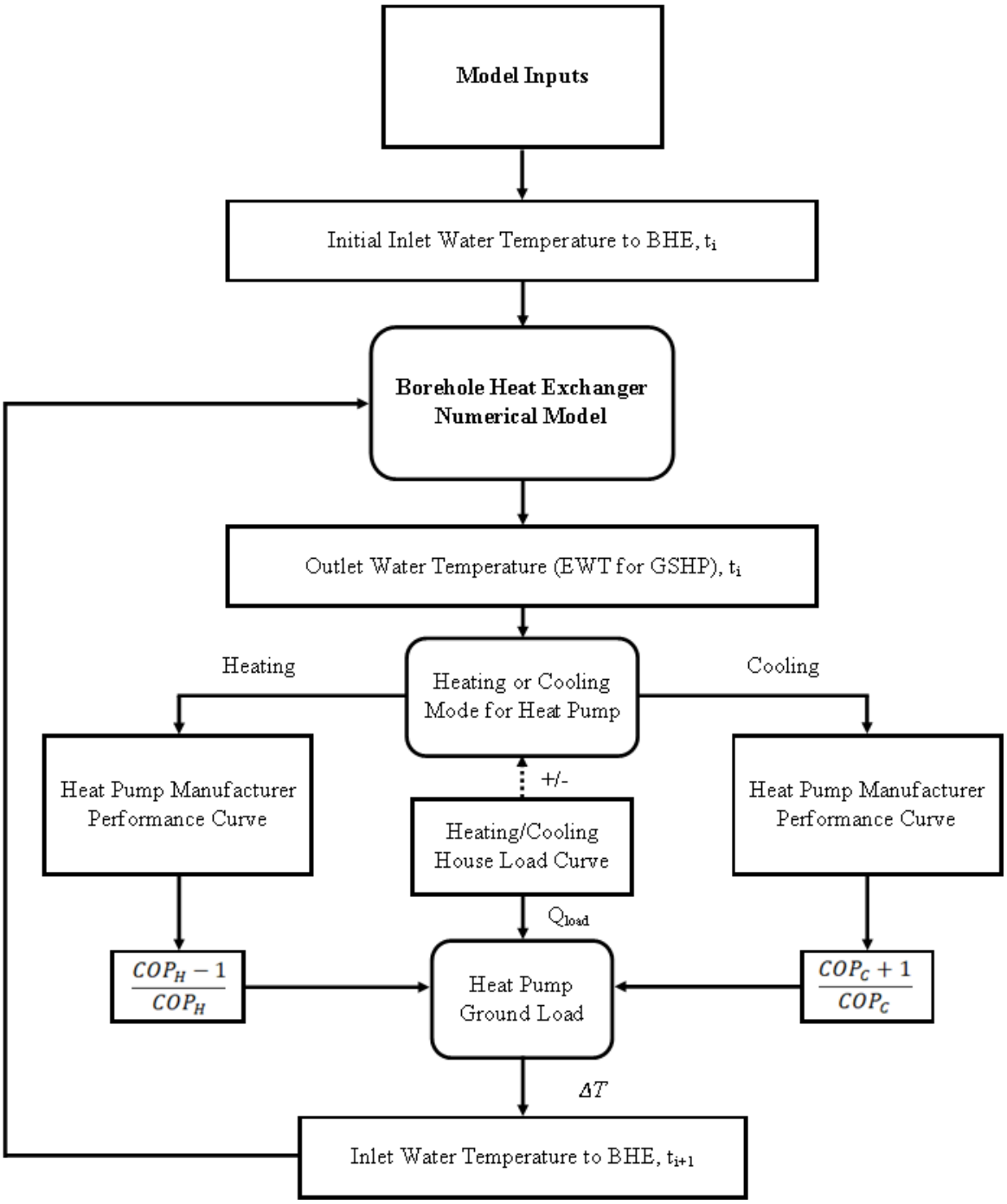

Figure 69: Algorithm for Integrating Variable Heat Pump Equations with Borehole Heat Exchanger Model

As seen in Figure 69, the initial water temperature is applied to the numerical model, and the fluid temperature distribution, along with the surrounding soil temperatures are solved by the COMSOL model. The resulting outlet water temperature at the first timestep is stored and used to determine the heat pump performance and necessary ground load to satisfy the house's heating or cooling needs for the following timestep. The BHE outlet temperature is considered to be equivalent to the entering water temperature (EWT) for the heat pump. This temperature is used to calculate the relevant COP for the GSHP, for either heating or cooling, based upon a performance curve which calculates COP as a function of the EWT. The manufacturer's COP curves (Figure 70) were used for this study, however no independent authentication of these heat pump of efficiencies were carried out for the purposes of this study.

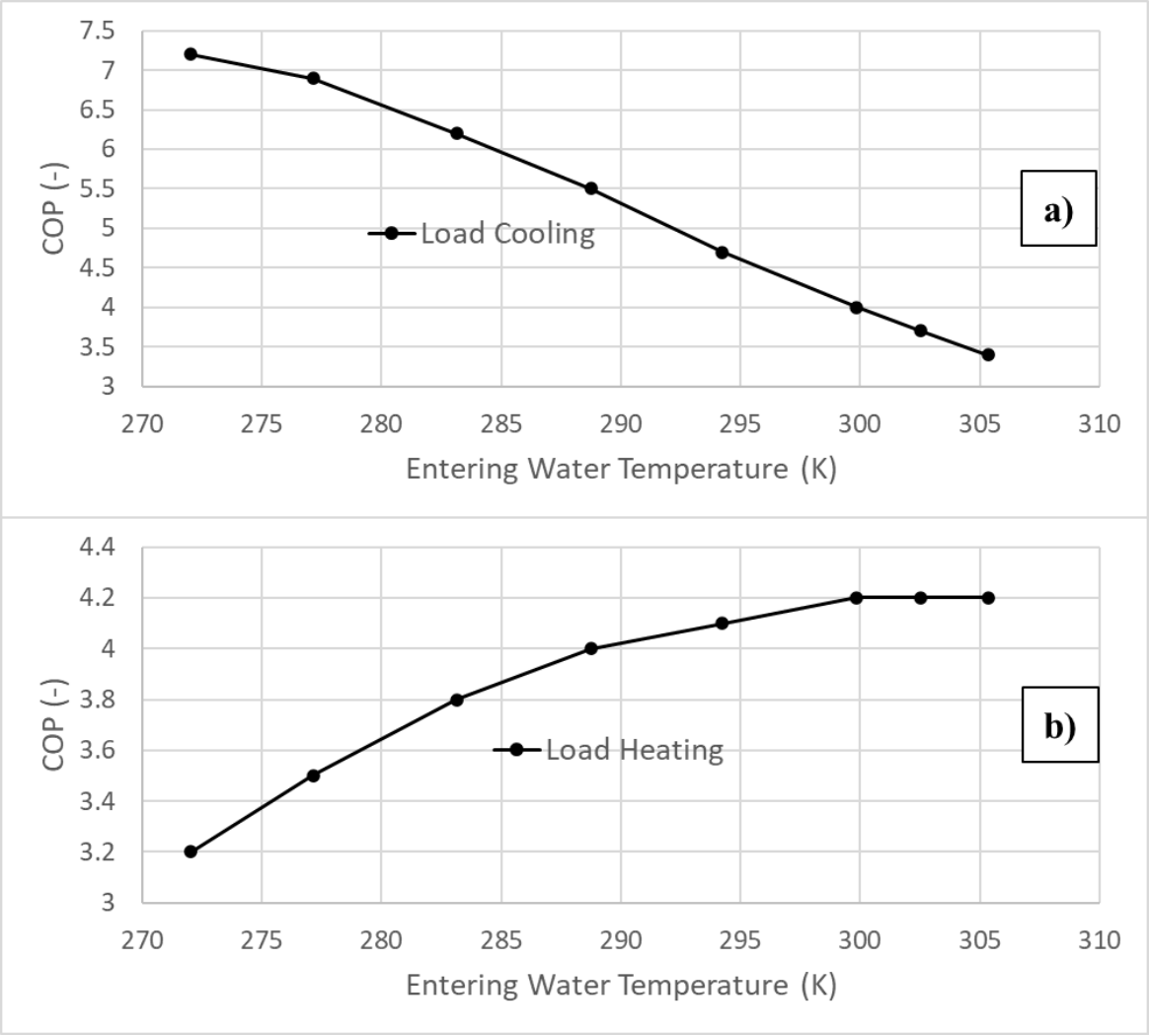

Figure 70: Manufacturer's Curve for Heat Pump COP of a) Cooling Mode and b) Heating Mode

For this model, the COP is only a function of the EWT, however, in reality the COP is a function of a great number of factors, which includes the flow rates and temperatures on either side of the heat pump, both the load and source sides. The COP can be used to adjust the house load to the appropriate ground load, using the equations

$$Q_{extracted} = -\left(\frac{COP_H - 1}{COP_H}\right) Q_{h,load} \qquad (A.45)$$

$$Q_{injected} = -\left(\frac{COP_C + 1}{COP_C}\right) Q_{h,load} \quad (A.46)$$

for the heating and cooling seasons, respectively. It should be noted that the addition of the negative sign results in negative values for heat extraction, and positive values for heat injection, and as such the ground load will subsequently be added to the fluid energy later in the algorithm. The value of $Q_{extracted}$ or $Q_{injected}$ that is relevant to each timestep is equivalent to the ground load, or $Q_{g,load}$ and is applied to the outlet temperature from the previous timestep, to determine the inlet temperature for the current timestep

$$T_{in,t_{i+1}} = T_{out,t_i} + \frac{Q_{g,load,t_{i+1}}}{C_p \dot{m}_f} \quad (A.47)$$

where $C_p \dot{m}_f$ is the product of the heat capacity and the mass flow rate of the circulating fluid. This ensures that the ground load calculated as a power value with the units Watts [W] is converted to a change in temperature, ΔT [K], by dividing by the fluid's thermal capacitance [W/K]. Although Equation A.47 suggests that the algorithm applies a future ground load, this calculation occurs at timestep t_{i+1}, by storing the BHE outlet temperature from the previous timestep as a variable, T_{old}, and calculating the BHE inlet temperature at the beginning of each current timestep.

The integration of this algorithm into the BHE model allows for the model to dynamically calculate the fluid temperatures based on the previous fluid temperatures within the borehole, the efficiency of the heat pump and the temperatures within the borehole and surrounding soil, creating a transient simulation with as little restraint on the solution as possible. The monitoring of a number of these values, which include the heat

pump COP, the borehole and soil temperatures, can be used to determine the long-term performance of the system.

A.3.3 Housing Heat Load

The following is an example load profile determined by the software TRNSYS [98], through the use of a lumped capacitance model and a thermostat temperature controller. The home was assumed to be in the Greater Toronto Area, and as such weather data for Toronto was used to estimate the ambient temperature of the air surrounding the house. This data was supplied by Meteonorm and is made up of hourly data that in aggregate represents a typical year [99]. The thermostat controller was set to have the lower and upper temperature limits of 18 and 24 °C, respectively.

When the temperature of the house in the lumped capacitance model attempts to go above or below these values due to heat transfer with the surroundings, cooling or heating loads are triggered. These loads are calculated using the equation

$$Q_{h,load} = UA\left(T_{h,load} - T_{amb}\right) - Q_{int} \qquad (A.48)$$

where $Q_{h,load}$ is the load provided by the heat pump, UA is the loss coefficient between the house and the ambient, $T_h \; and \; T_{amb}$ are the house and ambient temperatures respectively and Q_{int} are the internal gains within the house. Internal gains represent the energy produced within an operating house, including waste energy produced by inhabitants, lighting and appliances. It should be noted in this equation that a positive $Q_{h,load}$ value corresponds to a heating load and a negative value corresponds to a cooling load. The thermal capacitance of the house determines the amount of energy it takes to raise or lower

the average temperature by 1 °C (or K). This limits the change in the house temperature per timestep and results in a dynamic, transient load profile. The ratio between the thermal capacitance and the loss coefficient is known as the thermal time constant of the home and is relevant to lumped system analysis. The temperature of the house without any heat sources can be modelled by the equation

$$MC_p \frac{dT_{h,load}}{dt} = -UA\left(T_{h,load}(t) - T_{amb}\right) \quad (A.49)$$

$$\frac{dT_{h,load}}{dt} + \frac{1}{\tau} T_{h,load} = \frac{1}{\tau} T_{amb} \quad (A.50)$$

$$\tau = \frac{MC_P}{UA} \quad (A.51)$$

in systems with a constant ambient temperature, the solution to this first-order equation is

$$T_{h,load}(t) = \left(T_{h,load}(0) - T_{amb}\right)e^{-\frac{t}{\tau}} + T_{amb} \quad (A.52)$$

This equation gives a general estimate to the decay of the house temperature but fails due to a variety of factors. The variable ambient temperature, the internal gains and the heating or cooling being applied to the house changes the decay (or growth) of the house temperature after hitting the upper or lower limits of the controller temperatures, respectively. These complexities are the reason that the model must be solved as a coupled system, and the TRNSYS software is employed. The relevant inputs for the model are shown in Table 10 below, and the resulting load profile and temperatures can be seen in Figures 71 and 72.

Table 10: TRNSYS Lumped Capacitance Model Inputs

Input	Value
House Floor Area	180 m^2
Building Loss Coefficient	0.15 kW/K [100]
Internal Gains	1,087.133 W
House Temperature, Upper Limit	24 °C
House Temperature, Lower Limit	18 °C
Temperature Deadband Region	20-22 °C
House Thermal Capacitance	50,000 kJ/K

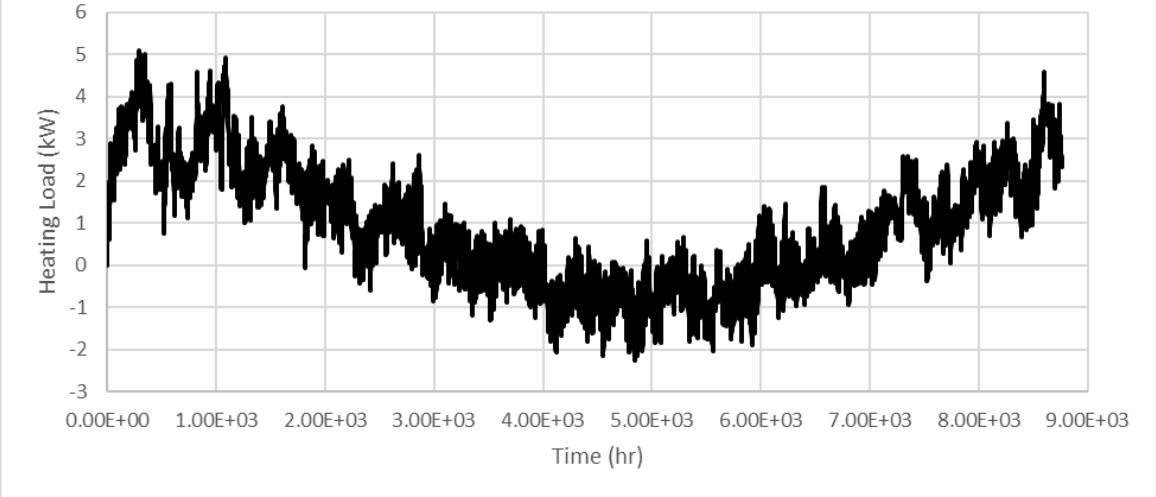

Figure 71: Heating Load Profile Produced by TRNSYS Lumped Capacitance Model

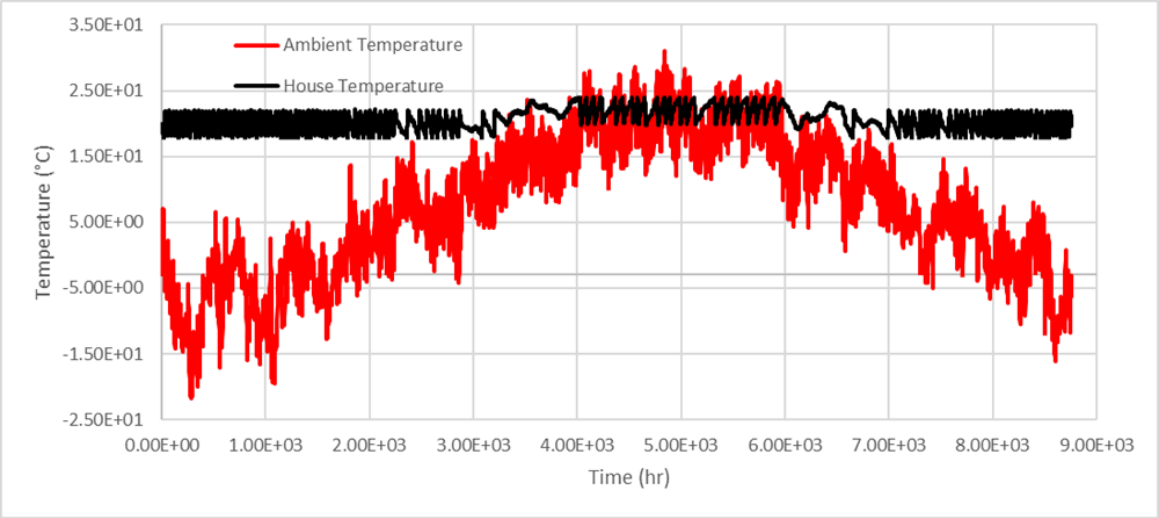

Figure 72: Ambient Temperature Used and House Temperature Calculated by TRNSYS Lumped Capacitance Model

Due to the limitations of the simple lumped capacitance model, the heating load has a high degree of fluctuation in magnitude which, if used directly, would result in unrealistic system behaviour for the heating and cooling of a residential home. More specifically, during the spring and autumn months, when loads are much smaller in magnitude and often jump from heating to cooling loads multiple times within a single day, a real GSHP system would be turned off, and climate control would be fulfilled by other means, including natural ventilation and other power-saving methods. As such, the heating load was artificially adjusted to include shutdown times from April 1 to June 30, and September 16 to November 15. Although these shutdown dates may shift slightly from year-to-year, they represent realistic times of temperature recovery within both the fluid and soil domains that are of interest in the current study. This updated load profile is shown in Figure 73.

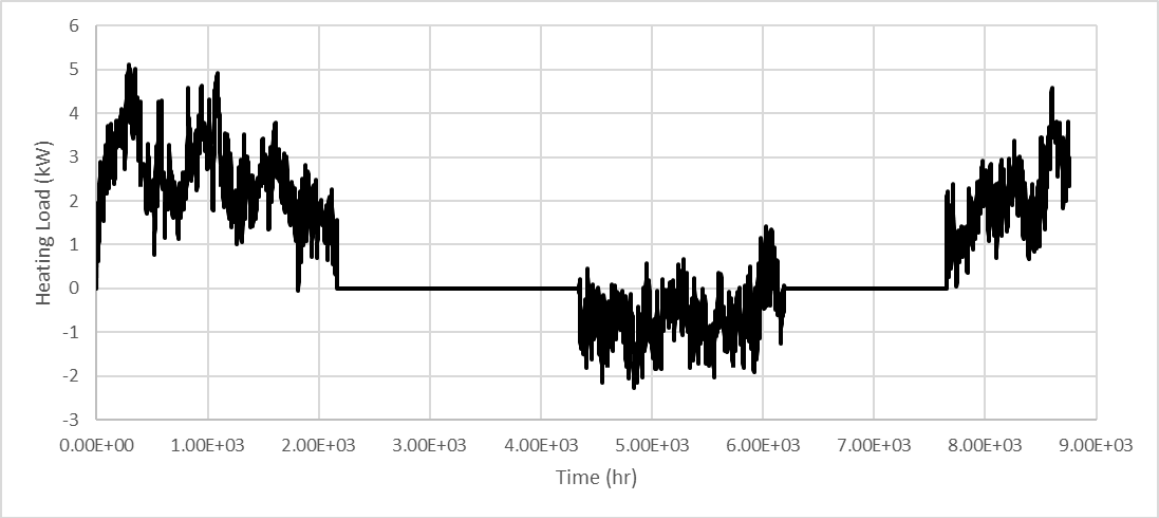

Figure 73: Heating Load Profile with Applied Shutdown Periods

The previously mentioned thermal imbalance ratio, IR, for this load profile is -82.71%, which represents a heavily heating dominated building. It should be noted that the artificially applied shutdown time did little to change the IR value of the load, which was -80.19% for the unadjusted load profile. This is consistent with the location and utility of a residential building in the Toronto region. The effect of this thermal imbalance will be investigated during the long-term study.

In addition to the shutdown times applied to the load profile, the same on/off behaviour was applied to the fluid velocity within the 1D pipe elements. In a real GSHP system, the fluid would not be circulated without a corresponding load on the heat pump, and as such this mimics system behaviour more realistically then a constant flow rate.